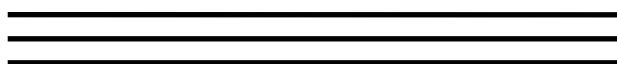# МОДЕЛИРОВАНИЕ

В ПРИКЛАДНОЙ ЭЛЕКТРОДИНАМИКЕ

И ЭЛЕКТРОНИКЕ

МОДЕЛИРОВАНИЕ В ПРИКЛАДНОЙ ЭЛЕКТРОДИНАМИКЕ
И ЭЛЕКТРОНИКЕ

MODELING

IN APPLIED ELECTROMAGNETICS

AND ELECTRONICS

Collected scientific papers

Issue 10

МОДЕЛИРОВАНИЕ
В ПРИКЛАДНОЙ ЭЛЕКТРОДИНАМИКЕ
И ЭЛЕКТРОНИКЕ

Сборник научных трудов

Выпуск 10

Издательство Саратовского университета
2010

Моделирование в прикладной электродинамике и электронике: Сб.
М38   науч. тр. – Саратов: Изд-во Сарат. ун-та, 2010. – Вып. 10. – ** с.: ил.

Сборник содержит научные работы, представленные на проведенном и организованном в рамках международной конференции Saratov Fall Meeting (SFM'2009) в сентябре 2009 г. в Саратовском государственном университете тринадцатом семинаре IEEE Saratov-Penza Chapter «Electromagnetics of Microwaves, Submillimeter and Optic Waves». Семинар организован Саратовской и Пензенской первичной ячейкой «Микроволновая теория и техника / Электронные приборы / Антенны и распространение радиоволн / Компоненты, упаковка и технология изготовления/Науки о плазме» (IEEE MTT/ED/AP/CPMT/PS Saratov–Penza Chapter), входящей в международную научную организацию Institute of Electrical and Electronic Engineers. Работы, выполненные саратовскими членами IEEE, учеными и молодыми специалистами, представляют оригинальные результаты по компьютерному моделированию в электродинамике, электронике СВЧ, акустоэлектронике, СВЧ технике, оптике.

Для работников научных учреждений, вузов, инженеров–разработчиков, может быть полезен аспирантам и студентам старших курсов факультетов: радиофизических, радиотехнических, электротехнических, энергетических.

Издание осуществлено при поддержке обществ ED-S, MTT-S, AP-S, PS, IEEE

Издано в авторской редакции

В В Е Д Е Н И Е

Компьютерное моделирование является основным мощнейшим инструментом исследования сложных систем и структур. Использование строгих компьютерных моделей позволяет адекватно производить их анализ, синтез или оптимизацию и зачастую вытесняет натурный эксперимент. Для большого числа рассматриваемых задач проведение натурного эксперимента чрезвычайно сложно или невозможно вовсе, поэтому развитие методов математического моделирования является чрезвычайно важным и актуальным.

В прикладной электронике и электродинамике, включая и оптику, использование строгих методов анализа и синтеза при моделировании означает применение алгоритмов на основе уравнений Максвелла и строгих решений уравнений движения. Важным элементом, влияющим на адекватность моделирования, служит корректное введение материальных уравнений и уравнений движения частиц, а также учет нелинейных свойств.

В последнее время все большее значение приобретают автоматизированные системы анализа и проектирования приборов, устройств и структур СВЧ, КВЧ и оптических диапазонов. Применение электродинамических методов происходит для всех частот используемых электромагнитных волн, включая и оптический диапазон, причем в оптике традиционные методы анализа вытесняются строгим электродинамическим рассмотрением. Наряду с традиционными частотными подходами к моделированию развиваются и пространственно-временные методы, что характеризует бурный прогресс прикладной нестационарной электродинамики и оптики. Другими актуальными современными направлениями, представленными в сборнике, являются моделирование наноструктур (включая квазипериодические структуры) и применение электродинамических методов к нелинейным задачам.

Десятый выпуск сборника продолжает серию публикаций трудов научных семинаров объединенной первичной ячейки (IEEE MTT/ED/AP/CPMT.PS Saratov–Penza Chapter) входящей в международную научную организацию Institute of Electrical and Electronic Engineers. Указанная ячейка создана летом 1995 г. в Саратове и Пензе. В сборник вошли труды, представленные в 2009 г. на очередном тринадцатом семинаре (Saratov–Penza Chapter Workshops), который являлся седьмым семинаром данной первичной ячейки под названием «Workshop on Electromagnetics of microwaves, submillimeter and optic waves». С 2003 года семинары под указанным названием проводятся ежегодно в сентябре в рамках международной конференции «Saratov Fall Meeting» в Саратовском государственном университете.

I N T R O D U C T I O N

In recent time there was an increasing development of Computer Aid Design (CAD) methods and rigorous approaches for microwave electron devices, units and elements all over the world and in Russia particularly. These methods have been applied both for linear and nonlinear systems and structures in time and spectrum domains. There is growing interest in electromagnetic and optics to nanostructures and metamaterials.

The correct introduction of material and motion equations and using of strict electrodynamic models play important role in adequate numerical simulation of structures. Recently the nonstationary approach for electromagnetics and electronics stays more desirable and applicable. The nanostructures such as photonic crystals and metamaterials play the important role in modern science and cause the different methods of its simulation. These directions of modeling is also have mirrored in the present 9-th issue.

In 1995 on July 11 the IEEE Joint MTT/ED Chapter has been formed in Saratov and Penza under the sponsorship and help of Electron Devices and Microwave Theory and Techniques Societies (ED–S and MTT–S). Then it has been supported by Antennas and Propagation, Components, Packaging, and Manufacturing Technology and Nuclear and Plasma Science Societies (APS, CPMTS and NPSS), and now it is named as IEEE MTT/ED/AP/CPMT/NPSS Saratov–Penza Chapter included into the IEEE Russian Section.

This issue contains the papers presented at the 13-th IEEE MTT/ED/AP/CPMT Saratov–Penza Chapter Workshop named as "Electromagnetics of Microwaves, Submillimeter and Optic Waves". This Workshop has been held in conjunction with the Saratov Fall Meeting at the Saratov State University in September 2009.

WHY THE REFRACTIVE INDEX CAN NOT BE NEGATIVE

M.V. Davidovich, *Senior Member IEEE*

Saratov State University, 410012, Saratov, Russia

E-mail *DavidovichMV@info.sgu.ru*

Abstract − It has been shown that for left-handed metamaterials and generally for negative refraction media the refraction index cannot be entered unequivocally and cannot be considered as real, and especially as negative. This index for above referred media is not expedient.

The refractive index (RI) n (or retardation coefficient) was initially introduced in optics long before Maxwell has formulated the electrodynamics which interprets the optics as its own part. So, it has been transferred from the scalar optic problems to vector electromagnetic ones. At that time the dispersion was not considered. Recently the so-called left-handed media (LHM) or metamaterials with negative refractions (NR) are under the intensive investigation. The widespread opinion dominates in literature that LHMs have the negative refraction index (NRI). In 1967 V.G. Veselago has published the paper [1], where he considered the medium (which he called left) with scalar real and simultaneously negative permittivity ε and permeability μ. He investigated the geometric (ray) diffraction theory for infinite in two directions (x,y) and finite in z-direction plate of thickness d with such LHM and has discovered the anomalous refraction Snell law. Also he has discovered some anomalous effects: Doppler effect, Vavilov-Cherenkov effect, negative light pressure. These effects are connected with NR phenomena (excepting negative pressure). It was well-known long before the Veselago's paper and considered in several publications (see references in the papers [2–9]). These considerations proceed from earlier Lamb (1904), Laue (1905), Mandelstam (1940) and others, from the papers corresponding with backward wave tubes and antennas. The history of this question one may find in Russian [2–9] and English [9] papers. The doubtless Veselago's merit is that he drew attention of scientific community to necessity of search possible artificial media (AM) with such unusual properties. Since 80-th to 90-th the research direction of AM investigations is expansive developing. The researches have been begun early in 40 and 50th years and then was named as investigation of artificial dielectrics [9–12]. Next the more general name "metamaterials" was assigned to these AM later. Next the periodic AM with different forms of wire inclusions (wire media) began to be studied intensively in the beginning of 90th and were then are named as metallic photonic crystals (PC).

In 2000 J. Pendry has published the article [13] in which he claimed that the Veselago lens (further in literature named as ideal Pendry lens) is overcoming the diffraction limit. But the Pendry's consideration was based on gross errors (see, for example, the articles [3–6,14–22] and the discussion there). After the publication [13] and similar, including the experimental work [23], the such conceptions as Veselago medium, double negative materials (DNM, DNG), backward media, LHM, wire PCs, complex media, negative group velocity media (NGV), negative refraction index media and some others finally have been approved. And the number of publications on these questions increases avalanche-like. Although the term "negative refraction " is the most general and it was well-known long before the paper [1], and this phenomenon takes place also in slow wave systems, nature crystals, dielectric PC, generally in optics when the energy transfer direction of monochromatic wave may constitute the obtuse angle with the direction of phase motion, the term "negative refraction index" on our opinion is not correct. We will

show further why the RI couldn't be negative, can not be such, and why it is not appropriate for NR media. Authors of some works (apparently, realising it) instead of NRI use the terms "negative refraction" [6] or "negative media" [8] along with NR. The big number of above abbreviations also indicates on the problem. In several such papers the NRI is not considered altogether, but in most of publications the NRI $n < 0$ nevertheless is considered. Thus, the NRI is the sufficiently established term (especially in English scientific literature), and the number of papers with its usage is highly large. The goal of this paper is to show that the question here is not only in terminology: the introduction of NRI $n < 0$ in the relations, in which it evidently couldn't be introduced, often leads to incorrect physical results.

There is prevailing common opinion in literature that for LHM with $\varepsilon < 0$ and $\mu < 0$ one must extract the root as follow: $n = -\sqrt{\varepsilon\mu} < 0$. And in the normalized impedance it is need to take the root branch as $\rho = \sqrt{\mu/\varepsilon} > 0$ [24]. These values one can insert in spectral form of Maxwell equations for harmonic plan wave (the equations (5) from [1]), that is indirectly assumed under such determination [24]. The energy flow and phase motion directions then are opposite, i.e. the wave is backward. The values n and ρ are introduced in such manner in optics, But they there both positive (also together with positive ε and μ). To choose the branch of root one must set some physical condition. In optics there is the dissipation according to which $\text{Im}(\tilde{n}) < 0$ and $\text{Re}(\tilde{\rho}) > 0$ (for complex values with the time dependence $\exp(i\omega t)$). It may seem that by introducing the complex RI, impedance, permittivity $\tilde{\varepsilon} = -\varepsilon - i\varepsilon''$ and permeability $\tilde{\mu} = -\mu - i\mu''$, where all quantities are positive, one can from the conditions $\text{Im}(\tilde{n}) < 0$ and $\text{Re}(\tilde{\rho}) > 0$ get the unambiguously: $\tilde{n} = n' - in''$, $n' = -\sqrt{\varepsilon\mu} < 0$, $n'' = (\varepsilon''\mu + \varepsilon\mu'')/\sqrt{\varepsilon\mu} > 0$, $\tilde{\rho} = \sqrt{\mu/\varepsilon}[1 + i(\mu''/\mu - \varepsilon''/\varepsilon)/2]$. But the problem here that it is impossible to take the limits $\varepsilon'' \to 0$ and $\mu'' \to 0$. It will be shown further. Furthermore, the value $\sqrt{\varepsilon\mu}$ is polysemantic. Imposing these estimates and binding two roots (either of the two is double-valued), we use only backward wave. But in the PC both backward and forward waves are possible for each dispersion branch. Let's consider the simplest case of propagation along z-axis. For such wave the transition from forward to backward ones occurs under the replacement $k_z \to -k_z \pm 2m\pi/a_z$ (a_z is the period along z), and also by going over the passage from one dispersion branch (hypersurface) to another through any bandgap by changing the k_0. These propagation branches (bands) are separated by the bandgaps, and the waves in different directions are differed (for anisotropic or bianisotropic AM). The effective permittivity and permeability (and RI) are the even functions of k_z (and others components if any). Hence, the transfer from forward wave to backward one takes place not due to sign of n, but owing to sign of k_z (under $|k_z a_z| < \pi$), or due to sign of dk_0/dk_z (here we propose the absence of loss). In low frequency limit $k_0 \to 0$ and for $|\mathbf{k}| \to 0$ (in our case for $k_z > 0$) the wave is forward-directed, i.e. the NR corresponds with the characteristic Bragg spatial $|\mathbf{k}| \cdot |\mathbf{a}| \sim 1$ ($\mathbf{a}$ is the translation vector) and frequency $k_0 n_{ef}(0)|\mathbf{a}| \sim 1$ resonances (scales). Here $n_{ef}(0)$ is the effective RI in the low frequency limit which is produced by the homogenization. The exclusion here is the physically unrealizable and similar ideal plasma wire medium with infinite parallel wires, which has the low-frequency cutoff. Accordingly all the RI n_{ef}, ε_{ef} and μ_{ef} (without dependence from that tensors they or scalars) are depending of ω and $\mathbf{k}$. Usually the homogenization in optics (excepting crystal optics) leads to the isotropic RI, as the wavelength is sufficiently greater

than the typical dimensions of natural substance. In the hard ultraviolet and in the X-ray diapasons it is not so.

It is already well known from optics that in the regions with strong anomalous dispersion it may be negative i.e. the inverse waves may exist. In particular, under the large oscillator forces the NR in narrow band may exist (that runs up to this seldom), but $n'(\omega) = \mathrm{Re}(n(\omega)) > 0$ (see formula 83.13 from [25]). In this case the phase and the energy move in opposite directions, and the losses are highly large, i.e. $n''(\omega) = -\mathrm{Im}(\widetilde{n}(\omega))$ may be of $n'(\omega)$ order. The group velocity does not characterize here anything. Usually in periodic waveguides (say, for microwaves) the losses are negligible small, therefore the NR is described by positive retardation n and negative group velocity [26]. These are the one-dimensional-periodic (1-D-P) structures, therefore n is scalar. The losses lead to negative influence on NR media properties (in particular, they destruct the focusing capability of Pendry lens (PL) and Veselago-Pendry lens (VPL)), and the sufficiently big papers are devoted to that. But, as it is surprising, some losses are necessary are necessary for existence of NR. Namely, in the paper [27] it has been shown that in isotropic media with NR there is lower limit of electric and magnetic losses, and the NR does not exist lower this limit. The Kramers-Kronig relations [25] for $n^2(\omega)$ have been used to proof this and the criterion has been obtained [27]:

$$\frac{2}{\pi}\int_0^\infty \frac{\varepsilon''(\widetilde{\omega})\mu'(\widetilde{\omega}) + \mu''(\widetilde{\omega})\varepsilon'(\widetilde{\omega})}{(\widetilde{\omega}^2 - \omega^2)}\widetilde{\omega}^3 d\widetilde{\omega} \le -1 \,.$$

At that the value $n^2(\omega)$ (but not $n(\omega)$) is the analytical functions in one of ω semiplanes (depending on the sign choice in the $\exp(\pm i\omega t)$). Nevertheless, to reduce the losses the several metamaterials different from DNG wire media are investigated in a number of papers [28–30]. In these papers the 1-D-P PCs with high-temperature superconductive and magnetic films [28], with superconductive and dielectric films [29], and also with additional inclusions of structures like "magnetic atom" in form of MgF_2 film with golden plate [30] have been considered. Such superconductive magnetic structures are the uniaxial PCs. Thus, in [29] the transverse $\varepsilon_\parallel$ and longitudinal $\varepsilon_\perp$ components of permittivity are introduced, and it is shown that even for superconductive state there are sufficiently considerable losses. They suppress the increase of damping (evanescent) mode amplitudes and put obstacles for superresolution, but, nevertheless, the NRI is introduced in [29] and the references to experiments concerning the figure of merit (FOM) in form $|n'|/|n''|$ are given. This FOM for LHM in infra-red and optical diapasons lies in the region $0.1 - 3.5$. But such anisotropic or bianisotropic structures couldn't be described by one scalar RI. Moreover, the magnetic inclusions need the magnetic field which is proposed to control their properties [28]. Such PCs in magnetic field are the gyrotropic media.

It is useful to remember how the n is introduced in optics. For transparent isotropic media in the disregard of dispersion (and therefore, neglecting of losses) we have $\varepsilon(\mathbf{r}) > 1$, and it is possible to determine the RI $n = \sqrt{\varepsilon}$. In this case it is a simple constant for homogeneous medium. The taking into account of frequency dispersion for monochromatic waves already leads to complex frequency depended values $\varepsilon(\mathbf{r},\omega)$ и $n(\mathbf{r},\omega) = n'(\mathbf{r},\omega) - jn''(\mathbf{r},\omega)$, where $\varepsilon''(\mathbf{r},\omega) \ge 0$, $n''(\mathbf{r},\omega) \ge 0$, in which connection the equality is possible only if $\omega = 0$ or $\omega \to \infty$ [25]. That is justly in any dissipative medium, and the complex number can't be negative. In his paper [1] V.G. Veselago at first proceeds from the dispersion equation (DE) for anisotropic medium without dissipation [1]:

$$\det A = 0, \qquad A_{ik} = k_0^2 \hat{\varepsilon}_{il}\hat{\mu}_{lk} - k^2 \delta_{ik} + k_i k_k \,, \qquad (1)$$

8

where $k_0^2 = \omega^2 / c^2$ and $k^2 = \mathbf{k}^2$. Besides the equation (1) one may, as a matter of fact, use also the equation

$$\det B = 0, \qquad B_{ik} = k_0^2 \hat{\mu}_{il} \hat{\varepsilon}_{lk} - k^2 \delta_{ik} + k_i k_k, \tag{2}$$

i.e. the DE and n are ambiguously determined and introduced. Further in proposal of isotropy the equation (1) is rewrote in [1] as

$$k^2 - k_0^2 n^2 = 0, \; n^2 = \varepsilon\mu. \tag{3}$$

That, as a matter of fact, means the scalarization of Maxwell equations, that generally it is not necessary to do and anyone shouldn't to do, because of only the values $\hat{\varepsilon}$ and $\hat{\mu}$ are initially in these equations (or in the more complicated material equations which must be used there). The DE (1) and (2) are the equations to determine the dispersion, i.e. the dependence $\mathbf{k} = \mathbf{k}(k_0)$ or inverse dependence $k_0 = k_0(\mathbf{k})$. If plane wave spreads along z-axis, i.e. $\mathbf{k} = \mathbf{z}_0 k_z$, then the equation (3) gives two solutions $k_z^2 = k_0^2 \varepsilon\mu$ and $k_z = \pm k_0 \sqrt{\varepsilon\mu}$, that corresponds to forward and backward waves, in which connection one may take the arithmetic value for the root, i.e. if $\varepsilon < 0$ and $\mu < 0$ then $n = \sqrt{\varepsilon\mu} > 0$. As it will be shown further, the values $\varepsilon < 0$ and $\mu < 0$ is the exactly unrealizable abstraction. So, the choice of forward or backward waves is determined by the sign of k_z, but not of n. This sign in general case of dissipative media must be chosen from the condition $\mathrm{Im}(k_z) < 0$ [8], i.e. the wave with the dependence $\exp(i\omega t - ik_z z)$ must damp in media along the direction z of energy transfer. This direction in dissipative media must be determined by the Pointing vector direction [8,31,32], but not by the group velocity vector (as it is made in the majority of works). Such root choice gives the backward wave if $\varepsilon' < 0$ and $\mu' < 0$: $\mathrm{Re}(k_z) < 0$. Both considerations: the present form and the form from [1] are equivalent in isotropic case, but everyone should have in view and remember that the initial for DE is the dependence $\mathbf{k} = \mathbf{k}(k_0)$, but not the $n = n(k_0)$.

All real known LHM are bianisotropic with periodic metallic inclusions of complicated form (usually these elements are pins and split ring resonators, or Ω-elements, spirals, helixes and some similar configurations). The electrophysical (electromagnetic) parameters of metamaterials must be obtained by homogenization [6,33–48]. It is fulfilled by inverse problem solutions and averaging based on full-wave analysis of periodic structure. It is necessary for this to solve many times the direct problems for dispersion and field determination using the rigorous methods (for example, integral equation method, or plane wave expansion method) [48]. The homogenization is also based on the models of media, for example, in the form [45–47]

$$\mathbf{P}^e = \varepsilon_0 \left(\hat{\varepsilon} - \hat{I} \right) \overline{\mathbf{E}} + c^{-1} \hat{\zeta} \overline{\mathbf{H}} = \varepsilon_0 \left[\left(\hat{\varepsilon} - \hat{I} \right) \overline{\mathbf{E}} + Z_0 \hat{\zeta} \overline{\mathbf{H}} \right],$$

$$\mathbf{P}^m = \mu_0 \left(\hat{\mu} - \hat{I} \right) \overline{\mathbf{H}} + c^{-1} \hat{\zeta} \overline{\mathbf{E}} = \mu_0 \left[\left(\hat{\mu} - \hat{I} \right) \overline{\mathbf{H}} + Z_0^{-1} \hat{\zeta} \overline{\mathbf{E}} \right],$$

and then on the determination of parameters of such models by strict or approximate fitting to the boundary problem solution [45,47]. Here $Z_0 = \sqrt{\mu_0 / \varepsilon_0}$ is the vacuum impedance, $\mathbf{P}^e$ and $\mathbf{P}^m$ are averaged over the periodic cell dipole moments (electric and magnetic), the upper line means the field averaging. The higher averaged multipole moments in principle also must be included in polarization. The effective medium tensors $\hat{\varepsilon}, \hat{\mu}, \hat{\zeta}, \hat{\xi}$ are resulted from the homogenization are dependent on averaging method and determined, at least, for wave length $\lambda > D$, where D is the characteristic dimension connected with the region of averaging (for example, the cell period). The homogenization procedure in addition to calculation of averaged cell dipole moments may be based on least-square analysis (minimization) of rigorous (full-wave) and model DE solutions, or least-square analysis (minimization) for corresponding plane wave diffraction results for structure vacuum-

metamaterial with different angles of hade and polarizations to boundary [10,45,48]. It is so as the Ewald-Oseen extinction theorem [43] in this case may be proven. One of the first such publication in which the effective permittivity was determined by plane wave normal fall on plane boundary of media with periodically included small ferrite and metallic balls, and also air-bladders (halls) in dielectric was the monograph [10]. The effective parameters in general case must be fitted so that the least-square discrepancy has the minimum [45,48]. Let's write down the averaged fields (denoted by the upper line) as

$$\overline{\mathbf{E}} = \mathbf{A}\exp(i\omega t \mp i\mathbf{kr}), \qquad \overline{\mathbf{H}} = \mathbf{C}\exp(i\omega t \mp i\mathbf{kr}). \qquad (4)$$

In general case one can extract from Maxwell equations not the relation (1) but the following matrix equation [47]

$$\begin{bmatrix} \hat{\varepsilon} & \hat{k}/k_0 + \hat{\xi} \\ \hat{\varsigma} - \hat{k}/k_0 & \hat{\mu} \end{bmatrix} \cdot \begin{pmatrix} \mathbf{A} \\ Z_0\mathbf{C} \end{pmatrix} = \begin{pmatrix} \mathbf{0} \\ \mathbf{0} \end{pmatrix},$$

which is equivalent to two DEs in the forms

$$\left[\left(k_0^{-1}\hat{k} + \hat{\xi}\right)\hat{\mu}^{-1}\left(k_0^{-1}\hat{k} - \hat{\varsigma}\right) + \hat{\varepsilon}\right]\mathbf{A} = 0, \qquad \left[\left(k_0^{-1}\hat{k} - \hat{\varsigma}\right)\hat{\varepsilon}_e^{-1}\left(k_0^{-1}\hat{k} + \hat{\xi}\right) + \hat{\mu}_e\right]\mathbf{C} = 0 \qquad (5)$$

and to two DEs in the forms

$$\det\left(\left(k_0^{-1}\hat{k} + \hat{\xi}\right)\hat{\mu}^{-1}\left(k_0^{-1}\hat{k} - \hat{\varsigma}\right) + \hat{\varepsilon}\right) = 0, \qquad \det\left(\left(k_0^{-1}\hat{k} - \hat{\varsigma}\right)\hat{\varepsilon}^{-1}\left(k_0^{-1}\hat{k} + \hat{\xi}\right) + \hat{\mu}\right) = 0. \qquad (6)$$

Here we introduce the cross-polarization tensors $\hat{\xi}, \hat{\varsigma}$ and the matrixes:

$$\hat{k} = \begin{bmatrix} 0 & -k_z & k_y \\ k_z & 0 & -k_x \\ -k_y & k_x & 0 \end{bmatrix}, \qquad \hat{k}^2 = \begin{bmatrix} -k_z^2 - k_y^2 & k_x k_y & k_z k_z \\ k_x k_y & -k_z^2 - k_x^2 & k_x k_y \\ k_z k_z & k_x k_y & -k_y^2 - k_x^2 \end{bmatrix}. \qquad (7)$$

From these equations after the homogenization one should determine the dispersion relation $k_0 = f(\mathbf{k})$. The metamaterials in general are possessed of spatial dispersion, i.e. their effective spatial-depended parameters are not local and in the $\mathbf{k}$-space they are the functions of $\mathbf{k}$. Let us summarize the essence of homogenization. Many times setting the different values and directions of $\mathbf{k}$ (the wave properties differ in different directions) and determining the corresponding values of k_0 from boundary problem solutions and from model of DE we are calculating the polarization and fitting the material parameters so that the wave properties in inhomogeneous structures would be on average equivalent to the plane wave properties in the model homogeneous anisotropic or bianisotropic medium. Correspondingly the material equations are equivalent on average to media particles motions under the wave influence. If there are two sorts of inclusions, and the first give the input mainly into electric polarization and the second ones for the most part into magnetic one, and in which connection they have weak electromagnetic correlations, that one may neglect the cross-polarization tensors: $\hat{\xi} = \hat{\varsigma} = 0$. Then $\left[\hat{k}\hat{\mu}^{-1}\hat{k} + k_0^2\hat{\varepsilon}\right]\mathbf{A} = 0$, $\left[\hat{k}\hat{\varepsilon}^{-1}\hat{k} + k_0^2\hat{\mu}\right]\mathbf{C} = 0$. If the matrixes (7) commute with the inverse tensor $\hat{\mu}^{-1}$, that there is $\left[\hat{k}^2 + k_0^2\hat{\mu}\hat{\varepsilon}\right]\mathbf{A} = \left[\hat{k}^2 + k_0^2\hat{n}^2\right]\mathbf{A} = 0$, where

$$\hat{n} = (\hat{\mu}\hat{\varepsilon})^{1/2} = \hat{n}' - i\hat{n}'' = \left[(\hat{\mu}'\hat{\varepsilon}' - \hat{\mu}''\hat{\varepsilon}'') - i(\hat{\mu}''\hat{\varepsilon}' + \hat{\mu}'\hat{\varepsilon}'')\right]^{1/2}. \qquad (8)$$

In the small loss case we have $\hat{n} = \hat{n}'\left[\hat{I} - i(\hat{\mu}''\hat{\varepsilon}' + \hat{\mu}'\hat{\varepsilon}'') \cdot \hat{n}'^{-2}/2\right]$, and

$$\hat{n}' = \mathrm{Re}(\hat{n}) = (\hat{\mu}'\hat{\varepsilon}')^{1/2}, \qquad \hat{n}'' = -\mathrm{Im}(\hat{n}) = (\hat{\mu}''\hat{\varepsilon}' + \hat{\mu}'\hat{\varepsilon}'') \cdot (2\hat{n}')^{-1}. \qquad (9)$$

The problem arises here how one must extract the roots from matrixes. If $\hat{\varepsilon}'$ and $\hat{\mu}'$ are the diagonal tensors with all negative (or positive) components, then $\hat{n}'$ is the positive definite matrix. But the components may have different signs. One may also to use the tensor $\tilde{\hat{n}} = (\hat{\varepsilon}\hat{\mu})^{1/2}$. The permittivity must commutate with permeability for coincidence of these two definitions. Generally we must introduce several impedances, propagation constants

and several constructions like RI in the considered bianisotropic media. The first two kinds of terms are possible and necessary. But for RI it is possible and it is better not to do this, otherwise it is connected with the troubles of root extraction from matrixes. If one directly uses the Maxwell equations (but not the wave equations) the similar problems are absent, and the different impedances and propagation constants (also several kinds) are turning out in correct forms. But the RI does not quite arise instead of this. If the Cartesian axis directions coincide with the cubic periodic cell verge directions and the metallic inclusions are symmetrically located, then we have the simplifications $\hat{\varepsilon} = \varepsilon \hat{I}$, $\hat{\mu} = \mu \hat{I}$, $\varepsilon = \varepsilon' - i\varepsilon''$, $\mu = \mu' - i\mu''$, $\varepsilon'' > 0$, $\mu'' > 0$. In general case one must take the sign in (4) in such a way that the fields damp along the direction $\mathbf{n}_0 = (\mathbf{\Pi} + \mathbf{\Pi}^*)/|\mathbf{\Pi} + \mathbf{\Pi}^*|$ of energy movement. Here the $\mathbf{\Pi} = \overline{\mathbf{E}} \times \overline{\mathbf{H}}^* / 2$ is the Pointing vector. If the tensor $\hat{n}$ is diagonal and one puts $k_x = k_y = 0$, then there are two solutions: $k_z = \pm k_0 \hat{n}_x$ and $k_z = \pm k_0 \hat{n}_y$. Here the sign in dissipative media must be taken in such manner that there was the damping along the energy propagation direction. For hypothetical medium $\varepsilon = \mu = -1$ in the ideal Veselago-Pendry lens (VPL) which cannot be realized physically, one has $k_z = -k_0 n$ (the inverse backward wave), where the RI $n = \sqrt{(-1)(-1)} = 1$. The mentioned exotic medium $\varepsilon = \mu = -1$ (or anti-vacuum) can not be created in form of metallic PC contrary to the statement in [49] (essentially it is mentioned already in [1]). Formally it corresponds to hypothetical diluted collisionless plasma of electric and magnetic charges (monopoles) at extremely low frequency. The rarity is essential in order to neglect the collision losses and proper plasma fields which lead to gyrotropy and spatial dispersion. As some approach to this unti-vacuum one can consider the high-frequency lossless and not created at present time magnetic semiconductors (when the frequency is less than plasma frequency and the gyromagnetic resonance frequency) can serve yet. But such media must be anisotropic and gyrotropic. The listed below demands are contradictory, that causes the difficulties in such media creation even for narrow frequency band. For the electrical (denoted by index e) and magnetic (index m) polarization current densities in hypothetic media $\varepsilon = \mu = -1$ we have $\mathbf{J}_P^e = -2i\omega\varepsilon_0\mathbf{E}$ and $\mathbf{J}_P^m = -2i\omega\mu_0\mathbf{H}$. These currents support the wave and are in antiphase with the fields. If we apply the Pointing theorem in complex form with polarization currents as incident ones in vacuum (that is equivalent to taking into account the media), one can get the own field energy density U_{EM} in the following form $U_{EM} = U_{EM}^e + U_{EM}^m = \varepsilon_0 |\mathbf{E}|^2 / 4 + \mu_0 |\mathbf{H}|^2 / 4$. And for stored (electric and magnetic) reactive powers in this medium one has $P_r^e = \mathbf{E}\mathbf{J}_P^{e*} / 2 = i\omega\varepsilon_0 |\mathbf{E}|^2$ and $P_r^m = \mathbf{J}_P^m \mathbf{H}^* / 2 = -i\omega\mu_0 |\mathbf{H}|^2$. Therefore $U_{EM}^e = U_{EM}^m$, and the reactive electric and magnetic powers are equal and counterphased. As corresponding to this the equal averaged over the period stored electric and magnetic energy densities are the form $\langle U_{MED}^e \rangle = \langle U_{MED}^m \rangle = 2\langle U_{EM}^e \rangle = 2\langle U_{EM}^m \rangle = \langle U_{EM} \rangle$ (as in such medium $\mathbf{H} = \sqrt{\varepsilon_0 / \mu_0}\mathbf{E}$). This energy is not transferred to matter, and the full energy density for field and matter is $U = 3\langle U_{EM} \rangle$. Here the brackets $\langle ... \rangle$ designate the time averaging. Correspondingly the energy transport velocity in three times less than the velocity of light: $v_e = c / 3$. The phase shift $\pi / 2$ testifies to oscillations similar to some resonator modes. If one uses the formula (10) in [49] which is connecting v_p with v_g in such ideal collisionless plasma under the condition $\varepsilon = \mu = -1$, he has for phase velocity $v_p = -c$, $v_p > 0$, and $v_g = |\mathbf{v}_g| = c / 3$, $\mathbf{v}_g = -\mathbf{v}_p / 3$ for group velocity. Accordingly he gets $n = 1$ and the stored reactive matter

energy in two time greater than the transferred by field electromagnetic energy. Here the division of energy on matter and field part is possible as there is no any interaction energy (the photon scattering is perfectly elastic). The wave movement causes the media polarization currents and they in one's turn support the wave. Just these antiphases lead to backward wave. But the energy and the majority of its carriers - photons are moving forward (from the source). It does not give the negative light pressure as the field momentum moves from the source and along the Pointing vector direction (in our case along z-axis). It must be noted that in such exotic medium and in general case of media there are always the backward and the all directional photons having the some phase shifts from the wave. The resulting collective effect describes by quasi-photons (polaritons), and the resulting energy and momentum movement goes into positive direction i.e. from the source, but the phase in case of NR runs backward as the result of interference. In this connection there is the obvious mistake in the papers [49–52]. True, it is mentioned in [52] that the pressure is positive for vacuum-LHM plane boundary and the negative pressure disappears in low frequency limit. There has been shown in the paper [53] that the Minkowski energy-momentum tensor form in the nondispersive media is relativistic covariant, that once again testifies to Minkowski energy-momentum tensor and photon momentum in media $\mathbf{p}^M = \mathbf{D} \times \mathbf{B}$ benefit. But the introduction of RI in $\mathbf{p}^M$ for anisotropic and bianisotropic dispersive media is incompetent, including the substantiation of negative pressure and mass transferring to source when one introduces the NRI $n < 0$ (see [54]). By the way, conclusions in [49,50] contradict work [53]. According to last, if ε and μ are the negative constants (from impossibility of it here we abstract), then the electromagnetic field momentum density in medium is $\mathbf{p} = \varepsilon\mu\mathbf{E} \times \mathbf{H} / c^2 = n^2 \mathbf{S} / c^2$. I.e. the pressure is positive even at the negative n. This density is quantized value and also consists of quasiphotons momentum [55]. In [50,51] it is told about "the formula $P = \hbar k$ connecting the photon momentum value with its wave vector" (designations and citations are taken from [50]). Further the conclusion follows: "It is obvious that in case of an opposite orientation of phase and group speed when the wave vector k is negative, the specified form gives negative value of an momentum of a photon, and, thereby, at absorption or reflexion of light in medium with a negative refraction index the light pressure should be replaced with a light attraction". Without concerning of slip about "a negative" vector, we will notice that, speaking about a negative direction of a vector, it is necessary to specify, concerning what. In ideal (infinite-periodic and lossless) PC all directions are equivalent, and forward (direct) and backward (return) eigenwaves are indiscernible [48]. In finite (quasi-periodic) PC (plate) there are radiating losses because of periodicity infringement. Such PC layer is the multiband filter with strong attenuation in bandgap zones and with zones of a relative transparency. Here waves are forced, and it is important, where there is a source: at the left or on the right. If it is inside of a plate it is important as concerning how the observation point is located. The Pointing vector $\mathbf{S}$ flow goes from a source, and the phase in LHM can move as from a source (a forward wave), and to it (a backward wave). If a source at the left, the photon (quasiphoton) momentum in medium has the form $\mathbf{z}_0 |n| k_0 \hbar = \mathbf{z}_0 |n| \omega \hbar / c$ [54,55] without dependence how the phase moves. Such approach is used in [1] for construction of a beam picture: there the direction of a stream of energy is defined by a direction of a beam falling from a source.

Here it is appropriate to consider the question: wherefrom the backward wave arises? Let the source with carrier frequency ω has started to operate (has arose) at the instant $t_0 = 0$. In the homogeneous medium at the big time t it creates only forward (direct and inverse) quasi-monochromatic waves of both directions. In the inhomogeneous (for example, in periodic) medium there are the reflections from their elements. The reflections come to source from both directions with tardiness, in which connection as the delay

greater, the farther elements are located. As the interference result of multiple reflections at the instant $t \to \infty$ it may be that the phase is moving to the source whereas the energy and momentum are always traveling from the source. Therefore the negative light pressure - that's impossible and misunderstanding.

The radiated in both directions source loses the mass (see [51]), but its momentum is zero. The mass of all closed source-field-matter system is conserved and the constant, and the lost mass is also distributed in the field (the opposite momentum phonons have the mass), and, possibly, in the medium (the losses lead to heating, and the mass of warmed-up medium is greater) [54]. The energy and momentum flows go from the source, i.e. on the right side – to the right, and on the left side – to the left.

Let us consider a problem about pressure of light in the LHM with $\varepsilon = \mu = -1$. In proposal that the constitutive (material) equations $\mathbf{D} = -\varepsilon_0 \mathbf{E}$, $\mathbf{B} = -\mu_0 \mathbf{H}$ are true for nonstationary Maxwell equations (i.e. for any frequency) then we get $\mathbf{p}^M = \mathbf{D} \times \mathbf{B} = \mathbf{E} \times \mathbf{H} / c^2$. So the pressure is such like in the vacuum and positive in accordance with the momentum direction (cf. with the reasoning in [51]). The monochromatic wave does not press on the boundary vacuum-anti-vacuum and does not transmit the momentum to such medium. Further we will show that such approach is incorrect even for monochromatic wave. Let's note that all quantities here are unambiguously defined (no any roots). But the wave pulse of train will produce the pressure, as that such medium possessed the properties inherent in it, the very large (strictly speaking, infinitely large) time is necessary for accumulation of energy of its internal (intrinsic) oscillations. For more detailed consideration let's introduce the model of rarefied plasma with electric and hypothetical magnetic charges [1]: $\varepsilon(\omega) = 1 - \omega_{pe}^2 / [\omega(\omega - j\omega_{ce})]$, $\mu(\omega) = 1 - \omega_{pm}^2 / [\omega(\omega - j\omega_{cm})]$. We regard that the harmonic plane wave propagates in this media with the electric field polarization along the axis x ($E_x = E$), and the magnetic field directed along the y-axis ($H_y = H$). As distinct from [1, 49] we have taken into account the collisions here. Further we consider $\omega >> \max(\omega_{ce}, \omega_{cm})$ and $\omega_{pe} = \omega_{pm} = \omega_p$, from which we have $\varepsilon(\omega) = 1 - \omega_p^2 / \omega^2 - j\sigma_e / (\varepsilon_0 \omega)$, $\mu(\omega) = 1 - \omega_p^2 / \omega^2 - j\sigma_m / (\mu_0 \omega)$. If $\omega \approx \omega_p / \sqrt{2}$, then $\varepsilon(\omega) \approx -1 - j\sigma_e / (\varepsilon_0 \omega_p)$, $\mu(\omega) = -1 - j\sigma_m / (\mu_0 \omega_p)$. Here $\sigma_e = \varepsilon_0 \omega_p^2 / \omega_{ce}$, $\sigma_m = \mu_0 \omega_p^2 / \omega_{cm}$. It may be seemed that this wave complies with Maxwell equations in the form $\partial_z H = \varepsilon_0 \partial_t E - \sigma_e E$, $\partial_z E = \mu_0 \partial_t H + \sigma_m H$. If we get the balance equation for momentum from these equations using the well-known way (see [54,55]), that we find $\partial_z U_0 + \partial_t g^M = -f_e^L - f_m^L$. Here the Lorentz forces acting on the charges are in the right part, and term in the left part $g^M = S / c^2$ is the momentum density, $S = EH$ is the z-component of Pointing vector. The balance equation has the standard form, but the energy density of wave $U_0 = -(\varepsilon_0 E^2 + \mu_0 H^2)/2$ is negative (cf. with the argumentations in [1]). This density (by the implication of balance equation) is the momentum flow density in z-direction, therefore it may seems, that the momentum is really carried back, and the wave pressure is negative. But this is not the case. The power balance in considered equation forms also leads to such negative energy density U_0. We have made the gross error in our considerations by introducing the constants into nonstationary equations. Here the strict and taking into account of frequency (time) dispersion consideration is necessary, though the wave is monochromatic. This was indicated also is [1,51]. Such analysis in quasi-mono-chromatic approach gives the positive energy (see [32]) and the positive pressure. Here one must use the integral relations ([25], formula 77.3) between the inductions and the fields,

where the integral operator kernels $\varepsilon(t)$ and $\mu(t)$ are obtained from the Fourier-transforms of $\varepsilon(\omega)$ and $\mu(\omega)$. Particularly,

$$\varepsilon(t) = \delta(t) + \frac{\omega_p^2 \chi(t)}{\omega_{ce} - \omega_L}\left[\exp(-\omega_L t) - \exp(-\omega_{ce} t)\right] .$$

Here $\chi(t)$ is the Heaviside function and the Landau damping is introduced here to remove the pole from zero point in the spectral permittivity function $\varepsilon(\omega)$. The plane wave may be presented here as $E = E_0 \cos(\omega t - \beta z)\exp(-\alpha z)$, and $H = H_0 \cos(\omega t - \beta z - \varphi)\exp(-\alpha z)$. If $\omega = \omega_{pe} = \omega_{pm}$ then we have $H_0 = \sqrt{\varepsilon_0 / \mu_0} E_0$, and when the collision frequencies tend to zero, than $\beta \to k_0$ and the phase shift φ and attenuation constant α also tend to zero. Correspondingly we get $\langle U \rangle = \langle U_0 \rangle = 3\langle U_{EM} \rangle$, $\langle D \rangle = \varepsilon_0\left(1 + \omega_p^2 / \omega^2\right)\langle E \rangle$, $\langle B \rangle = \mu_0\left(1 + \omega_p^2 / \omega^2\right)\langle H \rangle$, i.e. for the energy and momentum transfer velocities at the frequency $\omega_p / \sqrt{2}$ we have $v_e = v_m = c / 3$, and the phase velocity is equal to c.

As the Dirac monopoles until now are not discovered yet, and the linear collisionless plasma can't be created in principle, the LHM with real and negative $\varepsilon < 0$ and $\mu < 0$ must be regarded as hypothetical. Also they do not satisfy causality principle [25,27]. From the equation (6) under the similar proposals one may extract the DEs in which there is the hermitian conjugated tensor $\hat{n}^*$. The difficulties of NRI introduction is discussed in the paper [44], and there is the suggestion in the paper [56] to hold always $n > 0$ taking the corresponding signs in the solutions of DE, in the Snell law formulas, and in others formulas. The present paper also uses this approach with that difference, that, even for isotropic media, it is would be better not to use the term n quite. It is so as it isn't posses the required analytical properties, and in another cases it cannot be unambiguously introduced in general.

There are different metamaterial models in literature. One from them may be taken in form of [6] with the taking into account the excitation of excitons. Such model is convenient for natural crystals or for metamaterials with nanodimensional inclusions when the averaging over the physical infinitesimal volume does not work already, and their proper permittivities and permeabilities and surface impedances are incorrect for use. It is shown in [6] that in this case $\varepsilon(\omega)$ and especially $\mu(\omega)$ have restricted physical meaning. Thus, the model $n(\omega) < 0$ is the very crude model which does not fully correspond to NR physics. But it is pictorial and allows one to do any qualitative conclusions using the geometrical optic approximation that has determined its spreading. The next footstep – it is the model $\varepsilon(\omega) < 0$, $\mu(\omega) < 0$. It is more rational here to consider the complex value with $\varepsilon'(\omega) < 0$, $\mu'(\omega) < 0$ and $\varepsilon''(\omega) > 0$, $\mu''(\omega) > 0$. For the LHM having weak cross-polarization effects the next level model is the usage of complex tensor permittivity and permeability. And the general model is the bianisotropic PC [47]. There is the question arising here: somebody could create a material with NR and scalar terms ε и and μ having the simultaneously negative its real parts? It is obvious that such PC must be 3-D periodic with cubic sells and similar elements in its nodes having central and axis symmetry. The split-ring resonators in DNM have not such symmetry. Possible approach here is to use the embedded 3-D-P cubic cells with various elements (resonators) orientations. The usage of magnetic semiconductor 3-D-P PC lower of ferromagnetic resonance frequency for getting $\mu'(\omega) < 0$ [1] demands the external magnetic field and leads to gyrotropia. Moreover, the losses in ferrites are quite high. Another and more useful approach is the creation of biisotripic (chiral and nonreciprocal) AM. They are described by the material equations

$$\mathbf{D} = \varepsilon_0\varepsilon\mathbf{E} + c^{-1}(\chi - i\kappa)\mathbf{H}, \quad \mathbf{B} = \mu_0\mu\mathbf{H} + c^{-1}(\chi + i\kappa)\mathbf{E} \qquad (10)$$

with four scalar values: permittivity, permeability, chirality κ and nonreciprocity χ. Therefore one couldn't use only n and ρ here [57]. We get the chiral AM if $\chi = 0$ [58], and κ may be of both signs. For example, the chaotic implantation of ideally conductive microhelixes in transparent dielectric background may serve as chiral media [58]. The sign of κ depends from helix winding. As far back as in 1823 Fresnel has introduced for optically active media two (but not one) RIs: for right-polarized and left-polarized waves correspondingly n_R and n_L with specific rotation $\pi(n_R - n_L)/\lambda$ [58]. If the right-winding and left-winding helixes are chaotically located and equiprobable, that one can try to create the medium with $\kappa = 0$ and zero specific rotation. The problem here is to get the NR in such metamaterials. Here the RI is complex, and the real losses under the NR are quite high from behind the resonances. The losses are increasing with the increase of frequency and the decrease of dimensions. Let's note that it is not necessarily to have $\varepsilon'(\omega) < 0$ and $\mu'(\omega) < 0$ for NR [9]. It is only necessarily to have the obtuse angle between $\mathbf{v}_e$ and $\mathbf{v}_p$. So the NRI is the big misunderstanding.

Let us summarize the conclusions. There is no real scalar RI in the NR media. It corresponds only to isotropic lossless and nondispersive media models. The usage of such RI is the very simplified models will lead to some mistakes. Both terms $\hat{n}$ and $\hat{n}^*$ which in customary meaning may correspond to n are complex and tensor (for anisotropic case). In general bianisotropic case even two tensors $\hat{n}$ and $\hat{n}^*$ do not describe the LHM, and in addition one should use four complex tensors. For hypothetical case of negative terms $\varepsilon < 0$ and $\mu < 0$ we may introduce one real positive RI $n = \sqrt{\varepsilon\mu}$, taking the sign of k_z, corresponding to backward wave, as just k_z (but not n) is the result of DE solution. Then this RI has the meaning of retardation $n = |k_z|/k_0 = |\mathbf{v}_p|/c$. The Fermat principle in such hypothetic media is the same as in [59] with such difference that instead of negative n we use the negative light way distance as the phase moves back to energy. The Snell law is modified by change of sign [56]. The positive scalar retardation coefficient n may be introduced for wave in any media and any directions $\mathbf{v}_p$ and $\mathbf{v}_e$. If the customary optic lens in the operating frequency range is absolute transparent (lossless), that the phase and group velocities are equal: $\mathbf{v}_p = \mathbf{v}_g$ [31,32]. Therefore all beams come to the lens focus in phase with equal group time of retardation $\tau_g = \tau_p = 1/\int |\mathbf{v}_p| dl = \left[c\int n dl\right]^{-1}$. But in the case of ideal VPL and focusing of normally located point dipole source all rays come to the focus in zero phase, but with different group times of retardation. These times lie in the infinite interval $8d/c \le \tau_g < \infty$. The time delay comes to infinity for ray angle near the angle $\pi/2$ relatively of lens axis. This lens does not focus quasistationary and especially nonstationary source. Even more so it does not focus short pulse, that is particularly established in [59]. The normally located at the distance $l < d$ harmonic source must act infinitely long for focusing. In case of tangential located monochromatic point dipole the full focusing is absent as their fields is not azimuthally symmetric, and the dipole does not create the convergent to the focus point semispherical wave as it has been shown for normally located case [21]. Appositely, the only such simplest case of normally located dipole is considered in all papers concerning to VPL. Also let's note that for finite lens thickness d and finite dipole location the Ewald-Oseen extinction theorem [43] is not proved for VLP, and, apparently, can't be proved. So the dipole located at the distance $l < d$ to the "ideally matched" VPL creates the reflected quasi-spherical wave which

especially strong, than the distance l smaller (it is corresponded with the microstructure influence). It is need to remember that the quasi-periodic layer of finite thickness d has the radiation losses [48]. So, it is needs to solve the Maxwell equations for complicated microstructures. The rigorous wave picture of real object image must be given by the combination of 3-D vector spatial (volumetric) and/or surface spectral integral transforms from source distributions in its volume (or on its surface) over all spatial variables k_x, k_y, k_z in the regions $(-\infty, \infty)$. Here all modes are included: the propagated under all angles and the damped evanescent ones. Such integral transform gives the image, i.e. transfers the source value fields from the object point $\mathbf{r}'$ to the point $\mathbf{r}$ of its observation. And the kernel of this transform is the tensor Green's function of the layer. In view of this there is always some resolution limit.

It is not necessary to consider this paper as the criticism of well-known works and articles on problem of NR. The goal here is to accent on possibility to use the electromagnetic material equations which more exactly correspond to real physical processes into the media with NR. It allows one to predict their properties more precisely including the interpretation of experimental data.

REFERENCES

1. Veselago V.G. The electrodynamics of substances with simultaneously negative values of ε and μ. Sov. Phys. Usp. 1968. V. 10. P. 509–514. (The Russian publication: Uspekhi physicheskikh nauk. 1967. V. 92. P. 517-526.).
2. Silin R.A. Unusual refraction and reflection lows. Moscow: Fasis, 1999. 80 p.
3. Silin R.A., Chepurnykh I.P. On media with negative dispersion // Journal of Communications Technology and Electronics. 2001, V. 46. No. 10. P. 1121-1125.
4. Silin R.A. Derivation of refraction and reflection laws by the isofrequency method // Journal of Communications Technology and Electronics. 2002. V. 47. No. 2. P. 169-174.
5. Silin R.A. On media with unusual quasi-optical properties // Electronic scientific Journal "It's Investigated In Russia". 2002. P. 948-951. [http://zhurnal.ape.relarn.ru/articles/2002/086.pdf]. (In Russian).
6. Agranovich V.M., Gartstein Yu.N. Spatial dispersion and negative refraction of light // Phys. Usp. 2006. V. 49. P. 1029–1044.
7. Agranovich V.M., Ginzburg V.L. Crystallooptics which taking into account the spatial dispersion and exciton theory. Moscow, Nauka. 1965.
8. Shevchenko V.V. Forward and backward waves: three definitions and their interrelation and applicability // Phys. Usp. 2007. V. 50. P. 287–292.
9. Tretyakov S.A. Negative refraction: revisiting electromagnetics from microwaves to optics // EPFL Latsis Symposium. 2005. Lausanne. P. 30-35.
10. Lewin L. Advanced Theory of Waveguides. Iliffe and Sons, Ltd. London. England, 1951. 215 p.
11. Brown W.F. Dielectrics. In Handbuch der Physik XVII. Berlin, Springer-Verlag, 1956.
12. Brown J. Artificial dielectrics // Progress in dielectrics. 1960. V. 2. P. 195–225.
13. Pendry J. Negative refraction index makes perfect lens // Phys. Rev. Lett. 2000. V. 85. P. 3966-3969.
14. Hooft G.W. Comment on "Negative Refraction Makes a Perfect Lens," // Phys. Rev. Lett. 2001. V. 87. P. 249701-1.
15. Williams J.M. Some Problems with Negative Refraction // Phys. Rev. Lett. 2001. V. 87. P. 249703-1.

16. Garcia N., Nieto-Vesperinas M. Left-Handed Materials Do Not Make a Perfect Lens // Phys. Rev. Lett. 2002. V, 88. P. 207403-1.
17. Garcia N., Nieto-Vesperinas M. Erratum: Left-Handed Materials Do Not Make a Perfect Lens [Phys. Rev. Lett. 88, 207403 (2002)] // Phys. Rev. Lett. 2003. V. 90. P. 229903-1.
18. Nieto-Vesperinas M., Garcia N. Nieto-Vesperinas and Garcia Reply // Phys. Rev. Lett. 2003. V. 91. P. 099702-1.
19. Mittra R. A critical look at metamaterials for antenna-related applications // Journal of communications technology and electronics. 2007. V. 52. No. 9. P. 972-978.
20. Valanju P.M., Walser R.M., Valanju A.P. Wave refraction in negative-index media: always positive and very inhomogeneous // Phys. Rev. Lett. 2002. V. 88. P. 187401.
21. Shevchenko V.V. On superfocusing of a flat lens of negative material // Jounal Radiotekhniki. 2007. No. 6. [ttp://jrt.cplire.ru/jre/jun07/5/text.html]. (In Russian).
22. Bliokh K.Yu., Bliokh Yu.P, What are the left-handed media and what is interesting about them? // Phys. Usp. 2004. V. 47. P. 393–400.
23. Smith D.R., Padillia W.J., Vier D.C., Nemant-Nasser S.C., Schultz S. Composite medium with simultaneousely negative permeability and permittivity // Phys. Rev. Lett. 2000. V. 84. P. 4184-4187.
24. Veselago V.G. Left-handed Materials and Phenomena of Negative Refraction // Proceedings of Antenna Workshop on Innovative Periodic Antennas (Santiago de Compostela, Spain: ESA VPP-22). 2005. P. 11-18.
25. Landau, L.D., Lifshitz, E.M. Electrodynamics of continuous media. 2ed. Oxford, Pergamon Press, 1960. 474 p.
26. Silin R.A. Periodic waveguides. Moscow, Fasis., 2002. 436 p. (In Russian).
27. Stockman M.I. Criterion for Negative Refraction with Low Optical Losses from a Fundamental Principle of Causality // Phys Rev. Lett. 2007. V. 98. P. 177404-4.
28. Pimenov A., Loidl A., Pizhislupski P., Dabrowski B. Negative refraction in ferromagnetic-superconductor superlattice // Phys Rev. Lett. 2005. V. 95. P. 247009-4.
29. Bakhmanov A.L., Yampols'skii V.A., Fan J.A., Capasso F., Nori F. Layered superconductors as negative-refractive-index metamaterials // Phys. Rev. B. 2010. V. 81 P. 075101-6. [arXiv: 0907.3564v2].
30. Linden S., Decker M., Wegener M. Model System for a One-Dimensional Magnetic Photonic Crystal // Phys Rev. Lett. 2006. V. 97. P. 083902-4.
31. Davidovich M.V. On the Hartman paradox, electromagnetic wave tunneling, and supraluminal velocities (comment on "Tunneling of electromagnetic waves: paradoxes and prospects" by A B Shvartsburg)" // Phys. Usp. 2009. V. 52. P. 415-418.
32. Davidovich M.V. Electromagnetic Energy Density and Velocity in a Medium with Anomalous Positive Dispersion // Technical Physics Letters. 2006. V. 32. No. 11. P. 982-986.
33. Bensoussan A., Lions J.L. Homogenization in deterministic and stochastic problems // Stochastic Problems in Dynamics (B.L. Clarkson, ed.). Pitman, London, 1977. P. 106-115.
34. Papanikolaou J.C. Electromagnetic problems for composite materials in linear and nonlinear regimes // Nonlinear Electromagnetics (P.L.E. Uslenghi, ed.). Academic Press, New York-London-Toronto-Sydney -Sun Francisco, 1980. P. 253-262.
35. Sanchez-Palencia E. Non-homogeneous media and vibration theory. Berlin-Heidelberg-New York: Springer-Verlag. 1980. 398 p.
36. Bakhvalov N.S., Panasenko G.P. Averaging of the processes in periodic media. Moscow, Nauka, 1984. 352 p. (In Russian).

37. El Feddi M., Ren Z., Razek A. homogenization technique for Maxwell equations in periodic structures // IEEE Trans. 1997. V. MAG-33. P. 1382-1385.
38. Smith D.R., Schultz S., Markos P., Soukoulis C.M. Determination of effective permittivity and permeability of metamaterials from reflection and transmission coefficients // Phys. Rev. B. 2002. V. 65 . P. 195 1041–5.
39. Bardzokas D.I, Zobnin A.I. Mathematical modeling of physical processes in composite materials of periodic structures. Moscow, Editorial URSS, 2003. 377 p.
40. Silveirinha M.G., Fernandes C.A. Homogenization of metamaterial surfaces and slab: the crossed wire mesh canonical problem // IEEE Trans. 2005. V. AP-53. No. 1. P, 59-69.
41. Silveirinha M.G., Fernandes C.A. Homogenization of 3-D-Connected and Nonconnected Wire Metamaterials // IEEE Trans. 2005. V. MTT-53. P. 1418-1430.
42. Ouchetto O, Zouhdi S, Bossavit A, et al. Modeling of 3-D periodic multiphase composites by homogenization // IEEE Trans. 2006. V. MTT-54. No. 6. P. 2615 - 2619.
43. Simovski C.R. Application of the Fresnel formulas for reflection and transmission of electromagnetic waves beyond the quasi-static approximation // Journal of Communications Technology and Electronics. 2007. V. 52. No. 9. P. 953-971.
44. Vinogradov A.P., Dorofeenko A.V., Zouhdi S. On the problem of the effective parameters of metamaterials // Phys. Usp. 2008, V. 51. P. 485–492.
45. Davidovich M.V., Stephuk J.V. Homogenization of periodic artificial media // Modeling in Applied Electromagnetics and Electronics // Modeling in Applied Electromagnetics and Electronics (Ed. M.V. Davidovich). Saratov University Press. 2007. Issue 8. P. 67–75.
46. Davidovich M.V., Stephuk J.V. Homogenization of periodic metamaterials // Mathematical Methods in Electromagnetic Theory. Proceedings of 12-th International Conference (MMET'2008). Odessa, Ukraine. 2008. P. 527–529.
47. Graglia R.D., Uslenghi P.L.E., Zich R.E.. Dispersion Relation for Bianisotropic materials and its symmetry properties // IEEE Trans. 1991. V. AP- 39. P. 83-90.
48. Davidovich M.V. Photonic crystals: Green's functions, integro-differential equations, and simulation results // Radiophysics and Quantum Electronics, 2006. Vol. 49, No. 2. P. 134-146.
49. Veselago V.G. Electrodynamics of materials with negative index of refraction // Phys. Usp. 2003. V. 46. P. 764–768.
50. Veselago V.G. Carrying of energy, momentum and mass at propagation of an electromagnetic wave in the media with negative refraction // Electronic scientific Journal "It's Investigated In Russia". 2009. [http://zhurnal.ape.relarn.ru/articles/2009/028.pdf]. (In Russian).
51. Veselago V.G. Energy, linear momentum, and mass transfer by an electromagnetic wave in a negative-refraction medium // Phys. Usp. 2009. V. 52. P. 649–654.
52. Yannopapas V., Galiatsatos P.G. Electromagnetic forces in negative-refractive-index metamaterials: A first-principles study // Phys. Rev. A. 2008. V. P. 77 043819-4.
53. Veselago V.G., Shchavlev V.V. On the relativistic invariance of the Minkowski and Abraham energy-momentum tensors // Phys. Usp. 2010. V. 53. P. 317–318.
54. Davidovich M.V. On energy and momentum conservation laws for an electromagnetic field in a medium or at diffraction on a conducting plate // Phys. Usp. 2010. V. 53. P. 595–609.
55. Ginzburg V.L. The laws of conservation of energy and momentum in emission of electromagnetic waves (photons) in a medium and the energy-momentum tensor in macroscopic electrodynamics // Sov. Phys. Usp. 1973. V. 16. P. 434–439.

56. Pokrovsky A.L., Efros A.L. Sign of refractive index and group velocity in left-handed media // Solid State Commun. 2002. V. 125. P. 283-287.
57. Pasynin L.A. Passage of electromagnetic wave through a biisotropic transitive layer. // Radio Physics and Astronomy. 2005. V. 10. No. 3. P. 284-290. (In Russian)
58. Osipov O.V., Volobuev A.N. On the physical sense of material equations of a chiral medium // Tech. Phys. Lett. 2009. V. 35. No. 8. P.753-755.
59. Veselago V.G. Formulating Fermat's principle for light traveling in negative refraction materials // Phys. Usp. 2002. V. 45. P. 1097–1099.

COUPLED ELECTROMAGNETIC-BIOHEAT PROBLEM FOR MICROWAVE HYPERTHERMIA AND ABLATION THERAPY MODELING

V.V. Komarov, *Member IEEE*, I.I. Novruzov

Saratov State Technical University, Saratov, Russia
E-mail: *vyacheslav.komarov@gmail.com*

Abstract – Mathematical model based on a coupled system of differential equations of electromagnetic and thermal fields is formulated. In general case of temperature-dependent lossy media this model allows analyzing microwave ablation processes of tumor in human body. Such analysis is simplified in modeling coaxial interstitial applicators or microwave hyperthermia therapy. Dielectric and thermal properties of some biological tissues taken in the literature are reviewed.

1. Introduction

Electromagnetic (EM) therapy is one of the most rapidly developing medical technologies nowadays. Along with infrared, radiofrequency and laser radiation microwaves find wide practical application in such technologies. In particular microwave energy is successfully utilized for hyperthermia or ablation of tumor tissues. Microwave exposed tumor is heated up to 43÷45ºC (*hyperthermia*) or 60÷90ºC (*ablation*) by means of specially designed devices, like contact type waveguide applicators [1], coaxial slotted antennas [2], reentrant cavities [3], microstrip or spiral arrays [4,5] operating at ISM (*industrial, scientific, medicine*) frequencies 433 MHz, 915 MHz, 2.45 GHz.

Numerous mathematical models (MM) are employed for computer-aided design (CAD) of given microwave devices. Most of them are based on 3D numerical techniques: finite element method (FEM) or finite difference time-domain (FDTD) method. Further upgrade of microwave medical applicators requires more deep understanding of processes of EM waves interaction with biological tissues and development of new computer memory saving MM.

The generalized MM for the EM and thermal fields distribution in human body irradiated by microwaves is given by the system of coupled Maxwell's and Pennes's equations with corresponding boundary and initial conditions. And besides, these equations are formulated usually for temperature independent lossy media. Such formulation is valid mainly for hyperthermia processes. But during ablation therapy temperature of tumor is increased on 20÷40ºC leading to coagulative necrosis. That is the temperature dependent dielectric and thermal properties of human tissues must be taken into account in the coupled MM.

Then the EM source parameters are neglected very often in the first Maxwell's equation despite on the fact that microwave heating takes place in the near antenna zone [6]. But as it is known [7] the source modulation influences on the EM field pattern and that is why the source term must be also considered in the coupled MM.

Accurate modeling of microwave ablation and hyperthermia processes is impossible without correct and complete information about all parameters included in EM and bio-heat equations at least at ambient temperature. But in most cases these data are incomplete and the influence of temperature is not known.

Different assumptions can be successfully employed in order to increase efficiency of simulation and CAD of microwave medical applicators. Few of them are considered in present paper.

2. Governing equations

Consider propagation and dissipation of EM waves in lossy temperature dependent human tissue with complex dielectric permittivity $\dot{\varepsilon}(T) = \varepsilon'(T) - j\varepsilon''(T)$ and complex magnetic permeability $\dot{\mu} = 1$, where ε' is the dielectric permittivity; ε'' is the loss factor; T is the temperature. EM fields for this case both for applicator and body zone are defined from Maxwell's equations:

$$rotH = \sigma_e(T)E + \varepsilon_0\dot{\varepsilon}(T)\frac{\partial E}{\partial \tau} + J_s, \tag{1}$$

$$rotE = -\mu_0\frac{\partial H}{\partial \tau}, \tag{2}$$

$$div\varepsilon_0\dot{\varepsilon}(T)E = \rho + \rho_s, \tag{3}$$

$$div\mu_0 H = 0, \tag{4}$$

where E and H are the vectors of electric and magnetic field; τ is the time; σ_e is the electrical conductivity of biological media; J_s is the density of source current; ρ is the specific charge density; ρ_s is the source charge density; ε_0, μ_0 are the dielectric and magnetic constants respectively.

Equations (1) – (4) can be rewritten for complex amplitudes of EM field in order to exclude time as parameter:

$$rot\dot{H} = j\omega\dot{\varepsilon}(T)\varepsilon_0\dot{E} + \dot{J}_s, \tag{5}$$

$$rot\dot{E} = -j\omega\mu_0\dot{H}, \tag{6}$$

$$div\varepsilon_0\varepsilon'(T)\dot{E} = \dot{\rho}_s, \tag{7}$$

$$div\dot{H} = 0, \tag{8}$$

Let's transform equation (7) as the following:

$$div\varepsilon_0\varepsilon'(T)\dot{E} = \varepsilon'(T)div\dot{E} + [\dot{E}, grad\varepsilon'(T)] = \frac{\dot{\rho}_s}{\varepsilon_0}, \tag{9}$$

$$div\dot{E} + \left[\frac{\dot{E}}{\varepsilon'(T)}, grad\varepsilon'(T)\right] = \frac{\dot{\rho}_s}{\varepsilon_0}. \tag{10}$$

And now combining (5) and (6) we can derive inhomogeneous Helmholtz equation for temperature dependent media [8]:

$$\nabla^2\dot{E} + k_0^2\dot{\varepsilon}(T)\dot{E} + grad\left[\frac{\dot{E}}{\dot{\varepsilon}(T)}, grad\varepsilon'(T)\right] = j\omega\mu_0\dot{J}_s - \frac{1}{j\omega\varepsilon_0}grad\left(\frac{div\dot{J}_s}{\varepsilon'(T)}\right). \tag{11}$$

If parameters of the source are not taken into account we obtain homogeneous Helmholtz equation for temperature dependent media which is well known [9]:

$$\nabla^2 \dot{E} + k_0^2 \dot{\varepsilon}(T)\dot{E} + grad\left[\frac{\dot{E}}{\dot{\varepsilon}(T)}, grad\varepsilon'(T)\right] = 0. \qquad (12)$$

Solutions of both (11) and (12) must satisfy Neumann's and Dirichlet's boundary conditions at metal applicator walls and condition of continuity of tangential components ($\dot{E}_t, \dot{H}_t$) of EM field at dielectric interfaces. Attenuation of EM waves in human body can be described by so-called absorbing boundary conditions:

$$\nabla_t \dot{E}_t = -jk_0\dot{E}_t + 2jk_0\nabla_n^2\dot{E}_t, \qquad (13)$$

where $k_0^2 = \omega^2\varepsilon_0\mu_0$ is the free space wavenumber and ω is the angular frequency. And besides complete damping of EM field is achieved if biological tissue boundary is shifted at some distance (L) from the antenna output port:

$$L = 1.15129\alpha^{-1}. \qquad (14)$$

Here α is the attenuation coefficient determined as:

$$\alpha = 1.48 \cdot 10^{-8} f\sqrt{\varepsilon'(T)\left(\sqrt{1 + \left(\frac{\varepsilon''(T)}{\varepsilon'(T)}\right)^2} - 1\right)}. \qquad (15)$$

In most cases medical applicators can be represented as single port microwave network with EM source in the input port [10]:

$$\dot{E}^{(input)} = M\exp(-j\beta z)\{1 + |R|\}, \qquad (16)$$

where M are the eigenvectors of input port; β is the phase constant of EM wave in the input port; $|R|$ is the reflection coefficient; z is the coordinate.

Specific absorption rate (SAR) and power density in the interaction zone:

$$SAR = \frac{Q_v}{\rho_t}, \qquad (17)$$

$$Q_v = 0.5\omega\varepsilon_0\varepsilon''(T)\dot{E}^2, \qquad (18)$$

where ρ_t is the density of biotissue.

The thermal field distribution is defined by Pennes's bioheat equation [11]:

$$\rho_t C_t \frac{\partial T}{\partial \tau} = \lambda_t\nabla^2 T - \rho_t\rho_b C_b F(T - T_b) + Q_m + Q_v, \qquad (19)$$

where ρ_t, ρ_b are the densities of the tissue and the blood correspondently; C_t, C_b are the heat capacities of the tissue and the blood; λ_t is the thermal conductivity of the tissue; F is the blood flow rate; Q_m is the specific power density caused by biochemical processes inside human body; T_b is the blood temperature. In more generalized formulation thermal parameters of blood and tissue depend on temperature: $\rho_t(T)$, $\rho_b(T)$, $C_t(T)$, $C_b(T)$, $\lambda_t(T)$.

Metabolic heat source is estimated about $Q_m = 4200$ W/m^3 [12] while $Q_v = 10^5 \div 10^6$ W/m^3 that is $Q_v \gg Q_m$ in many real situations. Blood flow rate values vary in the range $4.2 \cdot 10^{-7} \leq F$, m^3/kg·s $\leq 1.67 \cdot 10^{-5}$ [13].

Equation (19) must be completed by the initial condition: $T_0 = 37$°C at $\tau = 0$ and the boundary conditions defining heat exchange between i and $i+1$ dielectric layers:

$$T_i = T_{i+1}; \quad \lambda_{t_i} \frac{\partial T_i}{\partial n} = \lambda_{t(i+1)} \frac{\partial T_{i+1}}{\partial n}, \tag{20}$$

where n is the unit condition

So, the processes of microwave hyperthermia and ablation of human tissues are described by the coupled EM-bioheat problem which is formulated either for temperature dependent or independent parameters of biological media. Analytical solution of this problem is too complicated and that is why different numerical techniques are utilized for simulation of EM and temperature patterns. Computational resources used in such simulations can be essentially reduced when medical applicator design assumes 2D approximation.

3. Axial-symmetrical modeling

Coaxial-dipole or monopole antennas are widely employed in microwave interstitial hyperthermia systems [2, 6, 13, 14]. EM fields in such applicators can be successfully calculated in cylindrical coordinate system (r, φ, z) with the help of axial-symmetrical 2D models. Neglecting the source term in (1) – (4) we can write [15]:

$$\frac{\partial E_r}{\partial \tau} = -(\varepsilon_0 \varepsilon'(T))^{-1} \left(\frac{\partial H_\varphi}{\partial z} + \sigma_e(T) E_r \right), \tag{21}$$

$$\frac{\partial E_z}{\partial \tau} = (\varepsilon_0 \varepsilon'(T))^{-1} \left[r^{-1} \frac{\partial}{\partial r}(r H_\varphi) - \sigma_e(T) E_z \right], \tag{22}$$

$$\frac{\partial H_\varphi}{\partial \tau} = \mu_0^{-1} \left(\frac{\partial E_z}{\partial r} - \frac{\partial E_r}{\partial z} \right), \tag{23}$$

where H_φ is the azimuthally component of H-field; E_r and E_z are the radial and longitudinal components of the E-field respectively.

Then the power density in lossy media is found by:

$$Q_v = 0.5 \omega \varepsilon_0 \varepsilon''(T)(E_r^2 + E_z^2). \tag{24}$$

Finally temperature pattern will be determined by 2D bio-heat equation:

$$\rho_t C_t \frac{\partial T}{\partial \tau} = \lambda_t \left[r^{-1} \frac{\partial}{\partial r} \left(r \frac{\partial T}{\partial r} \right) + \frac{\partial^2 T}{\partial z^2} \right] - \rho_t \rho_b C_b F(T - T_b) + Q_m + Q_v. \tag{25}$$

Equations (21)-(25) must be completed by corresponding boundary conditions in cylindrical coordinates.

4. Numerical algorithms

Duration of EM processes (*nanoseconds*) is much shorter than thermal ones (*seconds or minutes*) and in order to overcome this discrepancy so-called time-scaling

factor ($\xi = \tau_t/\tau_{em}$) is introduced in bio-heat equation in FDTD algorithms of the coupled problem solution [16]:

$$\xi \frac{\partial T}{\partial \tau} = \xi a_t \left[\nabla^2 T - \frac{V_s}{\lambda_t}(T - T_b) + \frac{Q_m}{\lambda_t} + \frac{Q_v}{\lambda_t} \right], \tag{26}$$

where $a_t = (\lambda_t/C_t\rho_t)$ is the thermal diffusivity; $V_s = \rho_t\rho_b C_b F$.

The discrete form of equations (21) - (25) according to FDTD computational scheme is represented in [15,16]. Another approach: adiabatic approximation is used in frequency domain computational techniques like FEM. According to this assumption physical parameters of lossy media are not changed during several periods of EM field oscillation. Such approach allows avoiding employing two time scales. Then equation (11) is transformed to the matrix form:

$$[A]\{X\} - \Lambda[B]\{X\} = \{\hat{J}\}, \tag{27}$$

where [A] and [B] are the sparse nonsymmetrical global matrixes; Λ is the wavenumber which is known if $J_s \neq 0$ or the eigenvalue if $J_s = 0$; {X} are the EM field functions; $\{\hat{J}\}$ is the vector of source current. Final matrixes [A] and [B] can be solved with GMRES and SPOOLES algorithms [10].

Generalized numerical algorithm of the coupled problem solution for temperature dependent media can be found in [8,16,17]. EM part of the coupled problem is solved first and then results of this solution (power density values) are substituted in bio-heat equation. The most time consuming is the first stage.

When the coupling between EM and bio-heat equation is weak, that is human tissue parameters are taken temperature independent, modeling of EM and thermal patterns is simplified.

5. Analytical approaches

Sometimes simulation time can be essentially reduced with the help of analytical approaches implemented in computational procedures of the coupled problem solution. For example, as it has been proved in [6] the steady-state $T(r)$ and transient $T(r,\tau')$ temperature are defined in local heating area as:

$$T(r) = \int^{r_0} \int_V^z \int^\vartheta G(r/r_0) \otimes SAR(r_0)d\vartheta dz dr_0 , \tag{28}$$

$$T(r,\tau') = \int^{\tau'} \left(\int_V G(r/r_0,\tau) \otimes SAR(r_0,\tau)d\vartheta dz dr_0 \right)d\tau , \tag{29}$$

where r is the radial coordinate, r_0 is the source location point, τ' is the time period, G is the Green's function which can be formulated in cylindrical or spherical coordinates.

One more important observation made in [6] for SAR distribution in the transverse plane for the coaxial interstitial antenna immersed into biological tissue shows that the power density pattern is approximated by exponential function:

$$SAR(r) = Q_0 \exp(-qz), \tag{30}$$

where Q_0 is the peak amplitude of power density, q is the response coefficient responsible for the SAR pattern. Then the tissue area near the radiating slot can be subdivided on thin layers inside which temperature is calculated using analytical expressions obtained in [18].

6. Dielectric and thermal properties of bio-tissues

As it has been mentioned above correct estimation of dielectric and thermal parameters of human tissues is one of the key moments of mathematical modeling of microwave therapy processes. In most cases this information is available in the literature only for human body temperature about 37ºC [19]. Essentially less information is available about $\varepsilon'(T)$-$j\varepsilon''(T)$.

Example of temperature dependent complex dielectric permittivity of human blood is given in Table 1.

Table 1

Dielectric properties of blood at 2.45 GHz [19]

T°C	ε'	ε''	σ, (Ohm·m)[-1]
15	59.9	19.9	2.71
25	57.5	17.1	2.33
35	56	15.9	2.166

Investigations of cancerous biological samples show [20] that both ε' and ε'' of tumor are higher than the normal tissue because of higher water content (Table 2).

Table 2

Dielectric properties of breast tissue at room temperature and 2983 MHz [20]

Sample	Tissue	ε'	σ, (Ohm·m)[-1]	Bound water, %
Patient 1 (edge 47)	Normal	20.43	3.12	43
	Tumor	32.31	3.52	62
Patient 2 (edge 49)	Normal	18.85	2.71	42
	Tumor	38.73	4.12	65
Patient 3 (edge 51)	Normal	24.98	3.25	45
	Tumor	40.1	4.31	65

Solution of the coupled EM-bioheat problem requires data at least about five main physical parameters of human tissue: ε', ε'', ρ_t, C_t, λ_t. (Table 3).

Table 3
Physical constants of some human tissues [13, 19]

Parameters	Blood	Muscle	Liver	Skin	Fat	Brain
Dielectric permittivity at 2.45 GHz	60	49.6	44.04	40.4	5.3	42.5
Loss factor at 2.45 GHz	15	18.8	13.14	11.23	0.734	11.09
Density, kg/m^3	1060	1020	1070	1100	916	1030
Heat capacity, J/(kg·K)	3960	3500	3590	3500	2300	3640
Thermal conductivity, W/(m·K)	0.61	0.6	0.488	0.5	0.22	0.53

Table 4
Dielectric properties of human tissues at 37°C [21]

Tissue	433 MHz		915 MHz	
	ε'	σ (Ohm·m)$^{-1}$	ε'	σ (Ohm·m)$^{-1}$
Blood	66	1.27	62	1.41
Bone	5.2	0.11	4.9	0.15
Brain	57	0.83	50	1.0
Fat	15	0.26	15	0.35
Kidney	60	1.22	55	1.41
Liver	47	0.89	46	1.06
Muscle	57	1.12	55.4	1.45
Skin	47	0.84	45	0.97
Eye	66	1.32	55	1.4

Operating frequency of some contact type waveguide applicators [1, 3, 4] is taken lower than conventional frequency 2.45 GHz in order to increase penetration depth of EM field in lossy media. Two main ISM frequencies used for these purposes are 433 and 915 MHz. Dielectric properties of some body tissues (Table 3) at these frequencies can be found in [21]

7. Conclusion

Represented coupled mathematical model describes processes of microwave heating of biological tissues in human body. This model can be employed for simulation of both temperature-dependent and independent lossy media interaction with EM waves during microwave hyperthermia or ablation therapy. Some numerical and analytical approaches to the coupled problem solution have been analyzed. Considered model is easily adapted to FDTD or FEM algorithms of EM and thermal patterns computation in the interaction zone.

REFERENCES

1. Maruoka S., Nikawa Y. Focusing applicator for microwave heating // Proceedings of the 1st Global Congress on Microwave Energy Applications. Otsu. Japan. 2008. P. 795-798.
2. Hurter W., Reinbold F., Lorenz W.J. A dipole antenna for interstitial microwave hyperthermia // IEEE Trans. 1991. V. MTT-39. No. 6. P. 1048-1054.
3. Ishihara Y., Kameyama Y., Minegishi Y., Wadamori N. Heating applicator based on reentrant cavity with optimized local heating characteristics // International Journal of Hyperthermia. 2008. V. 24. No. 8. P. 694-704.
4. Rossetto F., Stauffer P.R. Theoretical characterization of dual concentric conductor microwave applicators for hyperthermia at 433 MHz // International Journal of Hyperthermia. 2001. V. 17. No. 3. P. 258-270.
5. Johnson J.E., Neuman D.G., Maccarini P.F., Juang T., Stauffer P.R., Turner P. Evaluation of dual-arm Archimedean spiral array for microwave hyperthermia // International Journal of Hyperthermia. 2006. V. 22. No. 6. P. 475-490.
6. Hardie D., Sangster A.J., Cronin N.J. Coupled field analysis of heat flow in the near field of a microwave applicator for tumor ablation // Electromagnetic Biology and Medicine. 2006. Vol. 25. P. 29-43.

7. Hong J.S. Effect of a modulated source on a multimode cavity // IEEE Microwave and Guided Wave Letters. 1994. V. 4. No. 2. P. 43-44.

8. Komarov V.V. Investigation of microwave heating processes taking into account convection heat exchange: theory and experiment // Applied Physics. 2006. No. 4. P. 34-41. (In Russian).

9. Ayappa K.G., Davis H.T., Davis E.A., Gordon J. Analysis of microwave heating of materials with temperature dependent properties // AIChE Journal. 1991. V. 37. No. 3. P. 313-322.

10. Volakis J.L., Chatterjee A., Kempel L.C. Finite element method for electromagnetics. IEEE Press. 1998.

11. Pennes H.H. Analysis of tissue and arterial blodd temperature in the resting human forearm // Journal of Applied Physics. 1948. V. 1. P. 93-122.

12. Majchrzak E., Dziatkiewicz G., Paruch M. The modeling of heating a tissue sugjected to external electromagnetic field // Acta of Bioengineering and Biomechanics. 2008. V. 10. No. 2. P. 29-37.

13. Kikuchi S., Saito K., Takahashi M., Ito K. Control of heating pattern for interstitial microwave hyperthermia by a coaxial-dipole antenna – aiming at treatment of brain tumor // Electronics and Communications in Japan. 2007. V. 90. No. 12. P. 31-38.

14. Cavagnaro M., Amabile C., Bernardi P. et al. Design and realization of a new type of interstitial antenna for ablation therapies // Proceedings of the 39th European Microwave Conference. 2009. Rome. Italy. P. 878-881.

15. Jerby E., Aktushev O., Dikhtyar V. Theoretical analysis of the microwave drill near-localized heating effect // Journal of Applied Physics. 2005. V. 97. 034909. 1-7.

16. Torres F., Jecko B. Complete FDTD analysis of microwave heating processes in frequency-dependent and temperature-dependent media // IEEE Transactions on Microwave Theory and Techniques. 1997. V. 45. No. 1. P. 108-117.

17. Alpert Y., Jerby E. Coupled thermal-electromagnetic model for microwave heating of temperature-dependent dielectric media // IEEE Transactions on Plasma Science. 1999. V. 27. No. 2. P. 555-562.

18. Likov A.V. Heat transfer theory. Moscow: High School, 1967. (in Rissian).

19. Stuchly M.A. Dielectric properties of biological substances – tabulated / M.A. Stuchly, S.S. Stuchly // International Journal of Microwave Power and Electromagnetic Energy. 1980. Vo. 15. No.1. P. 19-26.

20. Bingu G., Abraham S.J., Lonappan A.et al. Detection of dielectric contrast of breast tissues using confocal microwave technique // Microwave and Optical Technology Letters. 2006. V. 48. No. 6. P. 1187-1190.

21. Pethig R. Dielectric properties of biological materials: biophysical and medical applications // IEEE Trans. Electrical Insulation. 1984. V. 19. No. 5. P. 453-474.

THE FOUR-POTENTIAL AND ELECTROMAGNETIC FIELD
FOR A CHARGE MOVING ARBITRARILY IN A CYLINDRICAL WAVEGUIDE

G.M. Gorbik, K. Ilyenko, T.Yu. Yatsenko

Institute for Radiophysics and Electronics of NAS of Ukraine
vul. Akad. Proskury, 12, Kharkiv, 61085, Ukraine
e-mail: kost@ire.kharkov.ua

Abstract – Using the method of Green functions we found the four-potential and electromagnetic field components for a pointlike charged macroparticle moving along an arbitrary path in a perfectly conducting circular cylindrical waveguide. Solutions are expressed analytically through the Green functions of the d'Alembert operator with Dirichlet and Neumann boundary conditions. It is shown that if the waveguide is excited only by a longitudinal current density component and/or non-zero charge density (transverse current components) the obtained solution reduces to the well-known expressions for *TM* (*TE*) circular cylindrical waveguide modes. If transverse and longitudinal current density components and non-zero charge density are present simultaneously in the waveguide, then the radial structure of the excited electromagnetic field coincides with that of the superposition of *TM* and *TE* circular cylindrical waveguide modes. The results thus obtained allow one an *ab initio* calculation of the forces acting on an arbitrarily moving relativistic charge from the self-induced charges and currents at the waveguide walls. They also provide a basis for solution of rigorous self-consistent problem on the non-stationary propagation of relativistic electron beams in perfectly conducting circular cylindrical drift tubes with the account for space-charge effects.

1. Introduction

Modeling of intense charged-particle beams is an important subject in beam physics and to the development of high-power microwave oscillators and amplifiers, which use them as the working media.

The first task that arises at studies of charged beam dynamics in external and intrinsic (self) electromagnetic fields in waveguide structures is the beam equilibrium configurations. For axially-symmetric charged beams moving along the circular cylindrical drift tube axis, this problem has a sufficiently simple solution. For certain cases the use of conformal transformations and taking into account of particular symmetry properties of a problem could substantially assist in finding solution for beams, which do not move along with the symmetry axis of a guiding structure or drift tube. However, such methods cannot be generalized for charged beams moving in complicated electromagnetic fields and not possessing any symmetry or periodicity. Therefore, development of efficient three-dimensional analytical, semi-analytical and/or numerical methods for finding electromagnetic fields induced by arbitrarily moving charges in waveguide structures becomes one of the principal objectives in vacuum electronics.

Second, physics of weakly-relativistic and relativistic high-power microwave sources (such as klystrons, gyrotrons, free electron lasers, etc.) requires essential knowledge of space-charge influence on frequencies, start current and any other oscillation conditions, which cannot be satisfactory achieved without calculation of electromagnetic fields created by a moving charge.

Third, the well-known restrictions of differential methods, *i.e.* particles in cells codes, as opposed to integral methods, *i.e.* methods involving Green functions (see, for example, [1]) when the relativistic dynamics of charged-particle beams is important, call for solution of completely three-dimensional problem on the vector-potential (and inclusion of relativistic corrections to the electric field and the magnetic field of the total space-charge field of charged-particle beam). In generic (i.e. not only necessarily circular) cylindrical geometries such solutions are obstructed by coupling of transversal components of the sought four-potential and electromagnetic fields [2]. Therefore, finding of efficient

methods to solve coupled scalar partial differential equations analytically, could greatly assist with modeling of various state-of-the-art microwave vacuum electron devices.

For these reasons, we calculate analytically the four-potential and electromagnetic field components induced by a pointlike charged macroparticle moving arbitrarily in an infinite perfectly conducting circular cylindrical waveguide. Our solution generalizes that of [3] to the non-stationary situation and, under particular conditions of paper [4], reduces to the results on the four-potential presented there. Given by equations (23), (24) and (27) for the four-potential and (47) and (51) for the electromagnetic fields together with Green functions expressions (36), (37) and (43), (44), results presented here provide the general solution to the problem under consideration.

2. Problem setup

Under the Lorentz gauge condition, Maxwell's equations for the scalar and vector-potentials $\varphi(\bar{x},t)$ and $\bar{A}(\bar{x},t)$ in the circular cylindrical coordinate system take the form:

$$\left[\frac{1}{r}\frac{\partial}{\partial r}\left(r\frac{\partial}{\partial r}\right)-\frac{1}{r^2}+\frac{1}{r^2}\frac{\partial^2}{\partial\theta^2}+\frac{\partial^2}{\partial z^2}-\frac{1}{c^2}\frac{\partial^2}{\partial t^2}\right]A_r-\frac{2}{r^2}\frac{\partial A_\theta}{\partial\theta}=-\frac{4\pi}{c}j_r,\tag{1}$$

$$\left[\frac{1}{r}\frac{\partial}{\partial r}\left(r\frac{\partial}{\partial r}\right)-\frac{1}{r^2}+\frac{1}{r^2}\frac{\partial^2}{\partial\theta^2}+\frac{\partial^2}{\partial z^2}-\frac{1}{c^2}\frac{\partial^2}{\partial t^2}\right]A_\theta+\frac{2}{r^2}\frac{\partial A_r}{\partial\theta}=-\frac{4\pi}{c}j_\theta,\tag{2}$$

$$\left[\frac{1}{r}\frac{\partial}{\partial r}\left(r\frac{\partial}{\partial r}\right)+\frac{1}{r^2}\frac{\partial^2}{\partial\theta^2}+\frac{\partial^2}{\partial z^2}-\frac{1}{c^2}\frac{\partial^2}{\partial t^2}\right]A_z=-\frac{4\pi}{c}j_z,\tag{3}$$

$$\left[\frac{1}{r}\frac{\partial}{\partial r}\left(r\frac{\partial}{\partial r}\right)+\frac{1}{r^2}\frac{\partial^2}{\partial\theta^2}+\frac{\partial^2}{\partial z^2}-\frac{1}{c^2}\frac{\partial^2}{\partial t^2}\right]\varphi=-4\pi\rho,\tag{4}$$

where $\bar{j}(\bar{x},t)$, $\rho(\bar{x},t)$ are the current and charge density; r, θ, z, t are the circular cylindrical coordinates and time; c is the speed of light in vacuum. It should be noted that equations (1) and (2) are coupled one to another, while equations (3) and (4) are independent.

Boundary conditions for the scalar potential φ and vector-potential components A_ϕ and A_z follow from those for electromagnetic fields on the perfectly conducting surface assuming that $\rho(\bar{x},t)$ and $\bar{j}(\bar{x},t)$ vanish at the waveguide boundary. In particular, $\bar{n}\times\bar{E}=0$ and $\bar{n}\cdot\bar{B}=0$ at $r=a$ (a is the waveguide radius) lead to the conditions

$$A_\theta\big|_{r=a}=A_z\big|_{r=a}=\varphi\big|_{r=a}=0\tag{5}$$

(*cf.*, [3]). Apparently, the easiest way to deduce the boundary condition for the remaining component of the vector-potential, A_r, is to consider the gauge condition

$$\frac{1}{r}\frac{\partial(rA_r)}{\partial r}+\frac{1}{r}\frac{\partial A_\theta}{\partial\theta}+\frac{\partial A_z}{\partial z}+\frac{1}{c}\frac{\partial\varphi}{\partial t}=0\tag{6}$$

and, restricting it to the boundary, derive

$$\frac{\partial}{\partial r}(rA_r)\bigg|_{r=a}=0\,;\tag{7}$$

although, this result can be also obtained directly from Maxwell's equations. It is naturally assumed here that the fulfillment of the boundary conditions is achieved through radial dependence of the components of four-vector potential.

Source terms on the right-hand sides of Maxwell's equations must satisfy the continuity equation

$$\frac{1}{r}\frac{\partial(rj_r)}{\partial r}+\frac{1}{r}\frac{\partial j_\theta}{\partial\theta}+\frac{\partial j_z}{\partial z}+\frac{\partial\rho}{\partial t}=0\tag{8}$$

irrespectively of the chosen gauge condition.

Coupling of equations (1) and (2) provides the major obstacle for finding general solutions for A_r and A_θ.

3. Coupled equations

To solve the system of coupled equations (1) and (2) we propose the following procedure. We apply to the both sides of equation (1) operator $r^{-1}\partial(r\cdot)/\partial r$ and $\partial/(r\partial\theta)$ to those of (2). Adding them up, we have

$$\left[\frac{1}{r}\frac{\partial}{\partial r}\left(r\frac{\partial}{\partial r}\right)+\frac{1}{r^2}\frac{\partial^2}{\partial\theta^2}+\frac{\partial^2}{\partial z^2}-\frac{1}{c^2}\frac{\partial^2}{\partial t^2}\right]\mathrm{div}_\perp\vec{A}=-\frac{4\pi}{cr}\left[\frac{\partial(rj_r)}{\partial r}+\frac{\partial j_\theta}{\partial\theta}\right]\equiv-\frac{4\pi}{c}\mathrm{div}_\perp\vec{j}\,,\tag{9}$$

where we denoted

$$\mathrm{div}_\perp\vec{V}=\frac{1}{r}\left[\frac{\partial}{\partial r}\left(rV_r\right)+\frac{\partial V_\theta}{\partial\theta}\right].\tag{10}$$

Accordingly to (5) and (7), unknown function (10) on the left hand side in (9) obeys the Dirichlet boundary condition

$$\mathrm{div}_\perp\vec{A}\,|_{r=a}=0\,.\tag{11}$$

Applying operator $\partial/(r\partial\theta)$ to both sides of (1), $r^{-1}\partial(r\cdot)/\partial r$ to those of (2) and subtracting the obtained equations, we find

$$\left[\frac{1}{r}\frac{\partial}{\partial r}\left(r\frac{\partial}{\partial r}\right)+\frac{1}{r^2}\frac{\partial^2}{\partial\theta^2}+\frac{\partial^2}{\partial z^2}-\frac{1}{c^2}\frac{\partial^2}{\partial t^2}\right]\mathrm{rot}_z\vec{A}=-\frac{4\pi}{cr}\left[\frac{\partial(rj_\theta)}{\partial r}-\frac{\partial j_r}{\partial\theta}\right]\equiv-\frac{4\pi}{c}\mathrm{rot}_z\vec{j}\,,\tag{12}$$

where

$$\mathrm{rot}_z\vec{V}=\frac{1}{r}\left[\frac{\partial}{\partial r}\left(rV_\theta\right)-\frac{\partial V_r}{\partial\theta}\right].\tag{13}$$

The unknown function $\mathrm{rot}_z\vec{A}\equiv B_z$ on the left hand side in (12) is subject to the Neumann boundary condition

$$\left.\frac{\partial(\mathrm{rot}_z\vec{A})}{\partial r}\right|_{r=a}\equiv\left.\frac{\partial B_z}{\partial r}\right|_{r=a}=0\,.\tag{14}$$

To prove this boundary condition, we assume that $j_\theta\,|_{r=a}=0$ as discussed earlier and apply the derivative $\partial/\partial r$ to the right hand side of (13) written for $\vec{A}$. We find

$$\frac{\partial}{\partial r}\left[\frac{1}{r}\frac{\partial(rA_\theta)}{\partial r}-\frac{1}{r}\frac{\partial A_r}{\partial\theta}\right]=\frac{1}{r}\frac{\partial}{\partial r}\left(r\frac{\partial A_\theta}{\partial r}\right)-\frac{A_\theta}{r^2}+\frac{2}{r^2}\frac{\partial A_r}{\partial\theta}-\frac{1}{r^3}\frac{\partial^2(rA_r)}{\partial\theta\partial r}\,,\tag{15}$$

where the last summand on the right hand side of the equation above vanishes at the boundary because of (7). The rest of the right hand side vanishes on comparison with the restriction to the boundary of equation (2) and the use of (5). Thus, equations (9) and (12) can be solved for $\mathrm{div}_\perp\vec{A}(\bar{x},t)$ and $\mathrm{rot}_z\vec{A}(\bar{x},t)$ via the method of Green functions.

To find solutions for A_r and A_θ we additionally propose the following *ansatz*: let us introduce a pair of new scalar functions $P(\bar{x},t)$ and $Q(\bar{x},t)$ obeying the relations

$$A_r=\frac{\partial P}{\partial r}-\frac{1}{r}\frac{\partial Q}{\partial\theta},\quad A_\theta=\frac{1}{r}\frac{\partial P}{\partial\theta}+\frac{\partial Q}{\partial r}\tag{16}$$

with corresponding boundary conditions

$$P\big|_{r=a}=0,\quad\left.\frac{\partial Q}{\partial r}\right|_{r=a}=0.\tag{17}$$

Substitution of definitions (16) to (10) and (13) leads to Poisson equations in transversal coordinates for $P(\bar{x},t)$ and $Q(\bar{x},t)$:

$$\Delta_\perp P\equiv\left[\frac{1}{r}\frac{\partial}{\partial r}\left(r\frac{\partial}{\partial r}\right)+\frac{1}{r^2}\frac{\partial^2}{\partial\theta^2}\right]P=\mathrm{div}_\perp\vec{A},\tag{18}$$

$$\Delta_\perp Q\equiv\left[\frac{1}{r}\frac{\partial}{\partial r}\left(r\frac{\partial}{\partial r}\right)+\frac{1}{r^2}\frac{\partial^2}{\partial\theta^2}\right]Q=\mathrm{rot}_z\vec{A}\,.\tag{19}$$

Here the right hand sides are regarded as known functions. It can be proved that (16) and (17) are compatible with boundary conditions (5) and (7) for A_θ and A_r. For A_θ the compatibility follows directly from definitions in (16) while the proof for A_r calls for a

more involved consideration. The boundary condition for the radial component of the vector-potential is given by expression (7) and to secure our assertion it is sufficient to prove that $r^{-1}\partial(r\partial P/\partial r)/\partial r\,|_{r=a}\propto P\,|_{r=a}$. First, one can check that such a relation holds for any function of the form $J_n(vr/a)$ by virtue of the Bessel equation [$r^{-1}\partial(r\partial F/\partial r)/\partial r\equiv\partial^2 F/\partial r^2+r^{-1}\partial F/\partial r=-(v^2/a^2-n^2/r^2)F$; v/a is a constant of appropriate dimensions]. Second, the assumption that $P(r,\theta,z,t)$ obeys the Bessel equation (or, more generally, that P is expandable in Fourier and Fourier-Bessel series with the eigenfunctions $J_n(v_{nq}r/a)\{\cos/\sin\}[n\theta]$ of the "transverse" Laplace operator $\Delta_\perp$ with appropriate v_{nq}) obviously does not restrict the generality of such a consideration. Following [5, Sec. 13.1] we are certain that separation of variables possible in circular cylindrical coordinates [$P(r,\theta,z,t)=P^1(r,\theta)P^2(z,t)$ at least] and looking for the solution for $P^1(r,\theta)$ exactly among eigenfunctions of $\Delta_\perp$.

Thus, equations (9), (12), (18) and (19) can be solved for P and Q by the method of Green functions to provide [via definitions (16)] the analytical solutions of coupled equations (1) and (2) for the transversal components, A_r and A_θ, of the vector-potential.

It should be also noted that in this approach the Lorentz gauge condition can be set aside while solving system of equations (1) – (4). The possibility of this omission lies not only in the fact that the system had been derived using it, but also because the gauge condition can be inferred from equations (1) – (4) using the continuity equation. The very existence of such an interrelation is *a priori* understandable because the four-potential components are connected by five differential conditions (1) – (4) and (6) one of which can be shown to be a corollary of the others, and it is at our disposal which four equations to take as a complete set. To demonstrate this, we observe that equations (3) and (4) lead to the following equalities:

$$\left[\frac{1}{r}\frac{\partial}{\partial r}\left(r\frac{\partial}{\partial r}\right)+\frac{1}{r^2}\frac{\partial^2}{\partial\theta^2}+\frac{\partial^2}{\partial z^2}-\frac{1}{c^2}\frac{\partial^2}{\partial t^2}\right]\frac{\partial A_z}{\partial z}=-\frac{4\pi}{c}\frac{\partial j_z}{\partial z}, \quad (20)$$

$$\left[\frac{1}{r}\frac{\partial}{\partial r}\left(r\frac{\partial}{\partial r}\right)+\frac{1}{r^2}\frac{\partial^2}{\partial\theta^2}+\frac{\partial^2}{\partial z^2}-\frac{1}{c^2}\frac{\partial^2}{\partial t^2}\right]\left(\frac{1}{c}\frac{\partial\varphi}{\partial t}\right)=-\frac{4\pi}{c}\frac{\partial\rho}{\partial t}. \quad (21)$$

Adding to equation (9) equations (20) and (21), we find

$$\left[\frac{1}{r}\frac{\partial}{\partial r}\left(r\frac{\partial}{\partial r}\right)+\frac{1}{r^2}\frac{\partial^2}{\partial\theta^2}+\frac{\partial^2}{\partial z^2}-\frac{1}{c^2}\frac{\partial^2}{\partial t^2}\right]\left[\frac{1}{r}\frac{\partial(rA_r)}{\partial r}+\frac{1}{r}\frac{\partial A_\theta}{\partial\theta}+\frac{\partial A_z}{\partial z}+\frac{1}{c}\frac{\partial\varphi}{\partial t}\right]=$$

$$=-\frac{4\pi}{c}\left[\frac{1}{r}\frac{\partial(rj_r)}{\partial r}+\frac{1}{r}\frac{\partial j_\theta}{\partial\theta}+\frac{\partial j_z}{\partial z}+\frac{\partial\rho}{\partial t}\right]. \quad (22)$$

The right hand side of this equation must vanish by virtue of continuity equation (8), whereas the boundary condition for the unknown function on the left hand side is that of Dirichlet. It then follows that the unknown function on the left hand side of equation (22) vanishes identically. This shows that Lorentz gauge condition (6) holds.

4. Representation of four-potential

So far, we have reduced the problem of finding solutions of system (1) – (4) to the construction of appropriate Green functions $G^{D,N}(\bar{x},t;\bar{x}',t')$ and $G_\perp^{D,N}(\bar{x}_\perp;\bar{x}'_\perp)$ of the d'Alembert and $\Delta_\perp$ operators with the Dirichlet and Neumann boundary conditions, respectively, in cylindrical coordinates. Formally, we write the solutions of equations (1) – (4) as

$$A_r(\vec{x},t) = -\frac{1}{4\pi} \int_{S'} \left[\frac{\partial G_\perp^D(\vec{x}_\perp;\vec{x}_\perp')}{\partial r} \mathrm{div}_\perp' \, \vec{A} - \frac{\partial G_\perp^N(\vec{x}_\perp;\vec{x}_\perp')}{r\partial\theta} \mathrm{rot}_z' \, \vec{A} \right] dS',$$

$$A_\theta(\vec{x},t) = -\frac{1}{4\pi} \int_{S'} \left[\frac{\partial G_\perp^D(\vec{x}_\perp;\vec{x}_\perp')}{r\partial\theta} \mathrm{div}_\perp' \, \vec{A} + \frac{\partial G_\perp^N(\vec{x}_\perp;\vec{x}_\perp')}{\partial r} \mathrm{rot}_z' \, \vec{A} \right] dS', \tag{23}$$

$$A_z(\vec{x},t) = \iint_{V''t''} G^D(\vec{x},t;\vec{x}'',t'') j_z(\vec{x}'',t'') dV''dt'',$$

$$\varphi(\vec{x},t) = c \iint_{V''t''} G^D(\vec{x},t;\vec{x}'',t'') \rho(\vec{x}'',t'') dV''dt'',$$

where

$$\mathrm{div}_\perp' \, \vec{A}(\vec{x}_\perp',z,t) = \iint_{V''t''} G^D(\vec{x}_\perp',z,t;\vec{x}'',t'') \mathrm{div}_\perp'' \, \vec{j}(\vec{x}'',t'') dV''dt'',$$

$$\mathrm{rot}_z' \, \vec{A}(\vec{x}_\perp',z,t) = \iint_{V''t''} G^N(\vec{x}_\perp',z,t;\vec{x}'',t'') \mathrm{rot}_z'' \, \vec{j}(\vec{x}'',t'') dV''dt'', \tag{24}$$

and primes over operators show that they employ primed coordinates [for the definitions of involved operators see (10) and (13)].

For a pointlike macroparticle of charge q

$$\vec{j}(\vec{x},t) = q(d\vec{\bar{x}}(t)/dt)\delta(\vec{x} - \vec{\bar{x}}(t)),$$
$$\rho(\vec{x},t) = q\delta(\vec{x} - \vec{\bar{x}}(t)), \tag{25}$$

where $\vec{\bar{x}}(t)$ is the position of the macroparticle at the moment of time t.

Representations (23) exhibit certain symmetry between expressions for A_r and A_θ. In these representations one can immediately see that if $j_r = j_\theta = 0$ then $A_r = A_\theta = 0$, i.e. the transversal current induces an analogue of the *TE*-eigenmode of a circular waveguide [in fact, the second equation in (24) shows that this analogy is quite deep one]. If $\rho = j_z = 0$ then $\varphi = A_z = 0$, i.e. the charge density and longitudinal current induce an analogue of the *TM*-eigenmode of a circular waveguide. It should be also noted that by virtue of continuity equation (8) $\mathrm{div}_\perp \vec{A}$ vanishes identically under such a condition.

5. Green functions

Having reduced the problem of finding solutions of system (1) – (4) to the construction of the appropriate Green functions, let us proceed to the task of their explicit finding. Since the cases of Dirichlet and Neumann boundary conditions turn out to be completely identical, we shall demonstrate the accomplishing of our task for the Green functions of the d'Alembert and $\Delta_\perp$ operators with the Dirichlet boundary condition.

In the first case, we look for the solution $G^D(\vec{x},t;\vec{x}'',t'')$ to the equation

$$\left[\frac{1}{r}\frac{\partial}{\partial r}\left(r\frac{\partial}{\partial r}\right) + \frac{1}{r^2}\frac{\partial^2}{\partial\theta^2} + \frac{\partial^2}{\partial z^2} - \frac{1}{c^2}\frac{\partial^2}{\partial t^2} \right] G^D = -\frac{4\pi}{c}\delta(\vec{x} - \vec{x}'')\delta(t - t''). \tag{26}$$

In the dimensionless coordinates $\iota = r/a$, $\zeta = z/a$ and $\tau = ct/a$, we write

$$\left[\frac{1}{\iota}\frac{\partial}{\partial\iota}\left(\iota\frac{\partial}{\partial\iota}\right) + \frac{1}{\iota^2}\frac{\partial^2}{\partial\theta^2} + \frac{\partial^2}{\partial\zeta^2} - \frac{\partial^2}{\partial\tau^2} \right] G^D = -\frac{4\pi}{a^2\iota}\delta(\iota - \iota'')\delta(\theta - \theta'')\delta(\zeta - \zeta'')\delta(\tau - \tau''). \tag{27}$$

First, we expand the Green function into the Fourier and Fourier-Bessel series with the use of eigenfunctions of the bounded part of d'Alembert operator, thus, separating the transversal functional dependence (*cf.* [6]):

$$G^D = \frac{1}{2}G_0^{D1} + \sum_{n=1}^{+\infty}(G_n^{D1}\cos[n\theta] + G_n^{D2}\sin[n\theta]) \quad \text{and} \quad \begin{Bmatrix} G_n^{D1} \\ G_n^{D2} \end{Bmatrix} = \sum_{q=1}^{+\infty}\begin{Bmatrix} G_{nq}^{D1} \\ G_{nq}^{D2} \end{Bmatrix} J_n(\nu_{nq}\iota), \tag{28}$$

where

$$\begin{Bmatrix} G^{D1}_n(r,z,t;\bar{x}'',t'') \\ G^{D2}_n(r,z,t;\bar{x}'',t'') \end{Bmatrix} = \frac{1}{\pi}\int_0^\pi G^D(\bar{x},t;\bar{x}'',t'')\begin{Bmatrix} \cos[n\theta] \\ \sin[n\theta] \end{Bmatrix}d\theta,$$

$$\begin{Bmatrix} G^{D1}_{nq}(z,t;\bar{x}'',t'') \\ G^{D2}_{nq}(z,t;\bar{x}'',t'') \end{Bmatrix} = \frac{2}{J^2_{n+1}(\nu_{nq})}\int_0^1 \iota J_n(\nu_{nq}\iota)\begin{Bmatrix} G^{D1}_n(r,z,t;\bar{x}'',t'') \\ G^{D2}_n(r,z,t;\bar{x}'',t'') \end{Bmatrix}d\iota,$$

(29)

and ν_{nq} are the roots to the equation $J_n(x)=0$. Substituting these series and using the orthogonality relations for the involved eigenfunctions, we rewrite equation (27) in the form

$$\left[\frac{\partial^2}{\partial\tau^2} - \frac{\partial^2}{\partial\zeta^2} + \nu^2_{nq}\right]\begin{Bmatrix} G^{D1}_{nq} \\ G^{D2}_{nq} \end{Bmatrix} = \frac{8}{a^2}\frac{J_n(\nu_{nq}\iota'')}{J^2_{n+1}(\nu_{nq})}\begin{Bmatrix} \cos[n\theta''] \\ \sin[n\theta''] \end{Bmatrix}\delta(\tau-\tau'')\delta(\zeta-\zeta'').$$

(30)

Second, we observe that equation (30) is the (1+1)-dimensional Klein-Gordon equation with the roots ν_{nq} playing the role of mass terms (cf. [7, p. 93]). Now, we use the integral Fourier transform (see, e.g., [8, p. 183])

$$\begin{Bmatrix} G^{D1}_{nq} \\ G^{D2}_{nq} \end{Bmatrix} = \int_{-\infty}^{+\infty}\int_{-\infty}^{+\infty}\begin{Bmatrix} g^{D1}_{nq} \\ g^{D2}_{nq} \end{Bmatrix}\exp[i\kappa_\zeta(\zeta-\zeta'')]\exp[-iw(\tau-\tau'')]d\kappa_\zeta dw$$

(31)

and the following representation for the delta-functions:

$$\delta(\zeta-\zeta'')\delta(\tau-\tau'') = \frac{1}{4\pi^2}\int_{-\infty}^{+\infty}\int_{-\infty}^{+\infty}\exp[i\kappa_\zeta(\zeta-\zeta'')]\exp[-iw(\tau-\tau'')]d\kappa_\zeta dw$$

(32)

($\kappa_\zeta \equiv k_z a$ and $w \equiv \omega a/c$). Then, equation (30) results in the solutions for the coefficients g^{D1}_{nq} and g^{D2}_{nq}:

$$\begin{Bmatrix} g^{D1}_{nq}(\kappa_\zeta,w;\iota'',\theta'',\zeta'',\tau'') \\ g^{D2}_{nq}(\kappa_\zeta,w;\iota'',\theta'',\zeta'',\tau'') \end{Bmatrix} = -\frac{2}{\pi^2 a^2(w^2-\kappa^2_\zeta-\nu^2_{nq})}\frac{J_n(\nu_{nq}\iota'')}{J^2_{n+1}(\nu_{nq})}\begin{Bmatrix} \cos[n\theta''] \\ \sin[n\theta''] \end{Bmatrix}.$$

(33)

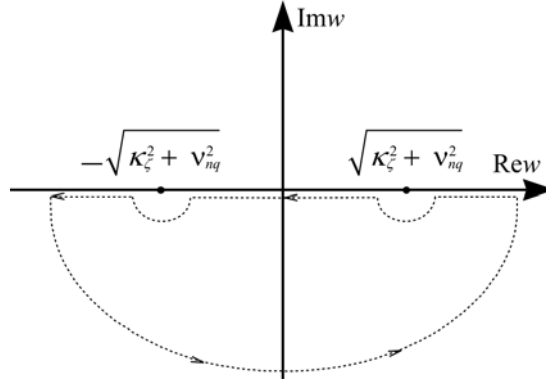It turns out that integral (31) can be solved explicitly with the use of (33). As a first step, we find

Fig. 1 Contour used for calculation of integral (34)

$$\int_{-\infty}^{+\infty}\frac{\exp[-iw(\tau-\tau'')]}{w^2-\kappa^2_\zeta-\nu^2_{nq}}dw = -\pi\frac{\sin[\sqrt{\kappa^2_\zeta+\nu^2_{nq}}(\tau-\tau'')]}{\sqrt{\kappa^2_\zeta+\nu^2_{nq}}},$$

(34)

which is obtained by contour integration (see Fig. 1). On the second step, we calculate

$$\int_{-\infty}^{+\infty}\exp[i\kappa_\zeta(\zeta-\zeta'')]\frac{\sin[\sqrt{\kappa^2_\zeta+\nu^2_{nq}}(\tau-\tau'')]}{\sqrt{\kappa^2_\zeta+\nu^2_{nq}}}d\kappa_\zeta = 2\int_0^{+\infty}\cos[\kappa_\zeta(\zeta-\zeta'')]\frac{\sin[\sqrt{\kappa^2_\zeta+\nu^2_{nq}}(\tau-\tau'')]}{\sqrt{\kappa^2_\zeta+\nu^2_{nq}}}d\kappa_\zeta =$$

$$= \pi J_0(\nu_{nq}\sqrt{(\tau-\tau'')^2-(\zeta-\zeta'')^2})\begin{Bmatrix} 1 \\ 0 \end{Bmatrix}\begin{Bmatrix} \tau-\tau''>|\zeta-\zeta''| \\ |\zeta-\zeta''|>\tau-\tau''>0 \end{Bmatrix} \equiv$$

(35)

$$\equiv \pi J_0(\nu_{nq}\sqrt{(\tau-\tau'')^2-(\zeta-\zeta'')^2})\vartheta[\tau-\tau''-|\zeta-\zeta''|],$$

33

where the penultimate equality is due to the known standard integral [9; Sec. 2.5.25, Eq. (9)]; $\vartheta[x]$ is the Heaviside step function. Finally, the Green function of the d'Alembert operator with the Dirichlet boundary condition takes the form:

$$G^D(\bar{x},t;\bar{x}'',t'') = \frac{2}{a^2}\left\{\frac{1}{2}\sum_{q=1}^{+\infty}\frac{J_0(\nu_{0q}r/a)J_0(\nu_{0q}r''/a)}{J_1^2(\nu_{0q})}J_0(\nu_{0q}\sqrt{c^2(t-t'')^2-(z-z'')^2}/a) + \right.$$

$$\left. \sum_{\substack{q=1\\n=1}}^{+\infty}\frac{J_n(\nu_{nq}r/a)J_n(\nu_{nq}r''/a)}{J_{n+1}^2(\nu_{nq})}\cos[n(\theta-\theta'')]J_0(\nu_{nq}\sqrt{c^2(t-t'')^2-(z-z'')^2}/a)\right\}\vartheta[(c(t-t'')-|z-z''|)/a].$$

(36)

An analogous calculation with the Neumann boundary condition $\partial G^N/\partial r\,|_{r=a}=0$ yields:

$$G^N(\bar{x},t;\bar{x}'',t'') = \frac{2}{a^2}\left\{\frac{1}{2}\sum_{q=1}^{+\infty}\frac{J_0(\nu'_{0q}r/a)J_0(\nu'_{0q}r''/a)}{J_0^2(\nu'_{0q})}J_0(\nu'_{0q}\sqrt{c^2(t-t'')^2-(z-z'')^2}/a) + \sum_{\substack{q=1\\n=1}}^{+\infty}\frac{\nu'^2_{nq}}{\nu'^2_{nq}-n^2}\times\right.$$

$$\left. \frac{J_n(\nu'_{nq}r/a)J_n(\nu'_{nq}r''/a)}{J_n^2(\nu'_{nq})}\cos[n(\theta-\theta'')]J_0(\nu'_{nq}\sqrt{c^2(t-t'')^2-(z-z'')^2}/a)\right\}\vartheta[(c(t-t'')-|z-z''|)/a],$$

(37)

where ν'_{nq} are the roots to the equation $dJ_n(x)/dx=0$.

In the second case, we look for the solution $G_\perp^D(\bar{x}_\perp;\bar{x}'_\perp)$ to the equation

$$\left[\frac{1}{r}\frac{\partial}{\partial r}\left(r\frac{\partial}{\partial r}\right)+\frac{1}{r^2}\frac{\partial^2}{\partial\theta^2}\right]G_\perp^D = -4\pi\delta(\bar{x}_\perp-\bar{x}'_\perp)$$

(38)

obeying the boundary condition $G_\perp^D(\bar{x}_\perp;\bar{x}'_\perp)|_{r=a}=0$. In the dimensionless coordinates $\iota=r/a$ and θ, we write

$$\left[\frac{1}{\iota}\frac{\partial}{\partial\iota}\left(\iota\frac{\partial}{\partial\iota}\right)+\frac{1}{\iota^2}\frac{\partial^2}{\partial\theta^2}\right]G_\perp^D = -\frac{4\pi}{\iota}\delta(\iota-\iota')\delta(\theta-\theta').$$

(39)

Note that Green function $G_\perp^D(\bar{x}_\perp;\bar{x}'_\perp)$ does not carry any dimensions. Again, let us expand the Green function into the Fourier and Fourier-Bessel series with the use of eigenfunctions of the bounded part of the d'Alembert operator:

$$G_\perp^D = \frac{1}{2}G_{\perp 0}^{D1} + \sum_{n=1}^{+\infty}(G_{\perp n}^{D1}\cos[n\theta]+G_{\perp n}^{D2}\sin[n\theta]) \quad\text{and}\quad \begin{Bmatrix}G_{\perp n}^{D1}\\G_{\perp n}^{D2}\end{Bmatrix} = \sum_{q=1}^{+\infty}\begin{Bmatrix}G_{\perp nq}^{D1}\\G_{\perp nq}^{D2}\end{Bmatrix}J_n(\nu_{nq}\iota),$$

(40)

where

$$\begin{Bmatrix}G_{\perp n}^{D1}(\iota;\bar{x}'_\perp)\\G_{\perp n}^{D2}(\iota;\bar{x}'_\perp)\end{Bmatrix} = \frac{1}{\pi}\int_0^\pi G_\perp^D(\bar{x}_\perp;\bar{x}'_\perp)\begin{Bmatrix}\cos[n\theta]\\\sin[n\theta]\end{Bmatrix}d\theta,$$

$$\begin{Bmatrix}G_{\perp nq}^{D1}(\bar{x}'_\perp)\\G_{\perp nq}^{D2}(\bar{x}'_\perp)\end{Bmatrix} = \frac{2}{J_{n+1}^2(\nu_{nq})}\int_0^1\iota J_n(\nu_{nq}\iota)\begin{Bmatrix}G_{\perp n}^{D1}(\iota;\iota',\theta')\\G_{\perp n}^{D2}(\iota;\iota',\theta')\end{Bmatrix}d\iota,$$

(41)

and ν_{nq} are the roots to the equation $J_n(x)=0$. Substituting these series and using the orthogonality relations for the involved eigenfunctions, we find from equation (39)

$$\begin{Bmatrix}G_{\perp nq}^{D1}\\G_{\perp nq}^{D2}\end{Bmatrix} = \frac{8J_n(\nu_{nq}\iota')}{\nu_{nq}^2 J_{n+1}^2(\nu_{nq})}\begin{Bmatrix}\cos[n\theta']\\\sin[n\theta']\end{Bmatrix}.$$

(42)

Finally, the Green function of the operator $\Delta_\perp$ with the Dirichlet boundary condition takes the form:

$$G_\perp^D(\bar{x}_\perp;\bar{x}'_\perp) = 8\left\{\frac{1}{2}\sum_{q=1}^{+\infty}\frac{J_0(\nu_{0q}r/a)J_0(\nu_{0q}r'/a)}{\nu_{0q}^2 J_1^2(\nu_{0q})}+\sum_{\substack{n=1\\q=1}}^{+\infty}\frac{J_n(\nu_{nq}r/a)J_n(\nu_{nq}r'/a)}{\nu_{nq}^2 J_{n+1}^2(\nu_{nq})}\cos[n(\theta-\theta')]\right\}.$$

(43)

An analogous calculation with the Neumann boundary condition $\partial G_\perp^N/\partial r\,|_{r=a}=0$ yields:

$$G_\perp^N(\bar{x}_\perp;\bar{x}'_\perp) = 8\left\{\frac{1}{2}\sum_{q=1}^{+\infty}\frac{J_0(\nu'_{0q}r/a)J_0(\nu'_{0q}r'/a)}{\nu'^2_{0q}J_0^2(\nu'_{0q})}+\sum_{\substack{n=1\\q=1}}^{+\infty}\frac{J_n(\nu'_{nq}r/a)J_n(\nu'_{nq}r'/a)}{(\nu'^2_{nq}-n^2)J_n^2(\nu'_{nq})}\cos[n(\theta-\theta')]\right\},$$

(44)

where ν'_{nq} are the roots to the equation $dJ_n(x)/dx=0$.

34

6. Expressions for electromagnetic fields

Having found expressions for the four-potential, we can obtain the corresponding electromagnetic fields by direct differentiation via formulas:

$$\vec{E} = -\vec{\nabla}\varphi - \frac{1}{c}\frac{\partial \vec{A}}{\partial t} \ , \quad \vec{B} = \operatorname{rot}\vec{A} \ . \tag{45}$$

In performing these calculations, it is important to keep in mind the commutation property of the d'Alembert operator with the derivatives

$$\frac{\partial}{\partial \theta} \ , \quad \frac{\partial}{\partial z} \quad \text{and} \quad \frac{\partial}{\partial t} \ . \tag{46}$$

This property allows one to shift the aforementioned derivatives from the Green functions to sources in the final formulas [cf. (20) and (21)].

It also should be mentioned that we have effectively found the z-component of the magnetic field [see (26)]. We, therefore, can write

$$E_z(\vec{x},t) = -\iint_{V''t''} G^D(\vec{x},t;\vec{x}'',t'')\left[c\frac{\partial\rho(\vec{x}'',t'')}{\partial z''} + \frac{\partial j_z(\vec{x}'',t'')}{c\partial t''} \right]dV''dt'',$$

$$B_z(\vec{x},t) = \iint_{V''t''} G^N(\vec{x},t;\vec{x}'',t'')\operatorname{rot}''_z \vec{j}(\vec{x}'',t'')dV''dt''. \tag{47}$$

Moreover, we shall also need other auxiliary relations involving Green functions. First, using the definition of Green function $G_\perp^D(\vec{x}_\perp;\vec{x}'_\perp)$, one can write the following identities

$$j_z(\vec{x}'',t'') = -\frac{1}{4\pi}\int_{S'} G_\perp^D(\vec{x}''_\perp;\vec{x}'_\perp)\Delta'_\perp j_z(\vec{x}'_\perp,z'',t'')dS',$$

$$\rho(\vec{x}'',t'') = -\frac{1}{4\pi}\int_{S'} G_\perp^D(\vec{x}''_\perp;\vec{x}'_\perp)\Delta'_\perp \rho(\vec{x}'_\perp,z'',t'')dS'. \tag{48}$$

Second, observing that obviously the d'Alembert and $\Delta_\perp$ operators commute with one another $(\Delta - c^{-2}\partial^2/\partial t^2)\Delta_\perp W(\vec{x}_\perp,z,t) = \Delta_\perp(\Delta - c^{-2}\partial^2/\partial t^2)W(\vec{x}_\perp,z,t) = (4\pi)^2 c^{-1}F(\vec{x}_\perp,z,t)$ and restricting ourselves to functions $W(\vec{x},t)$, which are eigenfunctions of $\Delta_\perp$ with the Dirichlet boundary condition, we may check the equality

$$W(\vec{x},t) = \int_{S'} G_\perp^D(\vec{x}_\perp;\vec{x}'_\perp)\left\{ \iint_{V''t''} G^D(\vec{x}'_\perp,z,t;\vec{x}'',t'')F(\vec{x}'',t'')dV''dt'' \right\}dS' =$$

$$= \iint_{V''t''} G^D(\vec{x},t;\vec{x}'',t'')\left\{ \int_{S'} G_\perp^D(\vec{x}''_\perp;\vec{x}'_\perp)F(\vec{x}'_\perp,z'',t'')dS' \right\}dV''dt''. \tag{49}$$

Results (48) and (49) (note the positions of arguments of F in both lines of the equality above) are extremely useful in transforming representations for $A_z(\vec{x},t)$ and $\varphi(\vec{x},t)$ in (23) to the form

$$A_z(\vec{x},t) = -\frac{1}{4\pi}\int_{S'} G_\perp^D(\vec{x}_\perp;\vec{x}'_\perp)\left\{ \iint_{V''t''} G^D(\vec{x}'_\perp,z,t;\vec{x}'',t'')\Delta''_\perp j_z(\vec{x}'',t'')dV''dt'' \right\}dS',$$

$$\varphi(\vec{x},t) = -\frac{c}{4\pi}\int_{S'} G_\perp^D(\vec{x}_\perp;\vec{x}'_\perp)\left\{ \iint_{V''t''} G^D(\vec{x}'_\perp,z,t;\vec{x}'',t'')\Delta''_\perp \rho(\vec{x}'',t'')dV''dt'' \right\}dS'. \tag{50}$$

Using (45), the first two relations in (23) and (50), we *finally* obtain

$$E_r(\vec{x},t) = \frac{1}{4\pi}\int_{S'}\left\{ \frac{\partial G_\perp^D(\vec{x}_\perp;\vec{x}'_\perp)}{\partial r}\iint_{V''t''} G^D(\vec{x}'_\perp,z,t;\vec{x}'',t'')\left[c\Delta''_\perp \rho(\vec{x}'',t'') + \frac{\partial}{c\partial t''}\operatorname{div}''_\perp \vec{j}(\vec{x}'',t'') \right]dV''dt'' - \right.$$

$$\left. \frac{\partial G_\perp^N(\vec{x}_\perp;\vec{x}'_\perp)}{r\partial\theta}\iint_{V''t''} G^N(\vec{x}'_\perp,z,t;\vec{x}'',t'')\frac{\partial}{c\partial t''}\operatorname{rot}''_z \vec{j}(\vec{x}'',t'')dV''dt'' \right\}dS',$$

$$E_\theta(\bar{x},t) = \frac{1}{4\pi}\int_{S'}\left\{\frac{\partial G_\perp^D(\bar{x}_\perp;\bar{x}_\perp')}{r\partial\theta}\iint_{V''t''}G^D(\bar{x}_\perp',z,t;\bar{x}'',t'')\left[c\Delta_\perp''\rho(\bar{x}'',t'') + \frac{\partial}{c\partial t''}\text{div}_\perp''\,\bar{j}(\bar{x}'',t'')\right]dV''dt'' + \right.$$

$$\left. \frac{\partial G_\perp^N(\bar{x}_\perp;\bar{x}_\perp')}{\partial r}\iint_{V''t''}G^N(\bar{x}_\perp',z,t;\bar{x}'',t'')\frac{\partial}{c\partial t''}\text{rot}_z''\,\bar{j}(\bar{x}'',t'')dV''dt''\right\}dS',$$

(51)

$$B_r(\bar{x},t) = -\frac{1}{4\pi}\int_{S'}\left\{\frac{\partial G_\perp^D(\bar{x}_\perp;\bar{x}_\perp')}{r\partial\theta}\iint_{V''t''}G^D(\bar{x}_\perp',z,t;\bar{x}'',t'')\left[\Delta_\perp''j_z(\bar{x}'',t'') - \frac{\partial}{\partial z''}\text{div}_\perp''\,\bar{j}(\bar{x}'',t'')\right]dV''dt'' - \right.$$

$$\left. \frac{\partial G_\perp^N(\bar{x}_\perp;\bar{x}_\perp')}{\partial r}\iint_{V''t''}G^N(\bar{x}_\perp',z,t;\bar{x}'',t'')\frac{\partial}{\partial z''}\text{rot}_z''\,\bar{j}(\bar{x}'',t'')dV''dt''\right\}dS',$$

$$B_\theta(\bar{x},t) = \frac{1}{4\pi}\int_{S'}\left\{\frac{\partial G_\perp^D(\bar{x}_\perp;\bar{x}_\perp')}{\partial r}\iint_{V''t''}G^D(\bar{x}_\perp',z,t;\bar{x}'',t'')\left[\Delta_\perp''j_z(\bar{x}'',t'') - \frac{\partial}{\partial z''}\text{div}_\perp''\,\bar{j}(\bar{x}'',t'')\right]dV''dt'' + \right.$$

$$\left. \frac{\partial G_\perp^N(\bar{x}_\perp;\bar{x}_\perp')}{r\partial\theta}\iint_{V''t''}G^N(\bar{x}_\perp',z,t;\bar{x}'',t'')\frac{\partial}{\partial z''}\text{rot}_z''\,\bar{j}(\bar{x}'',t'')dV''dt''\right\}dS'.$$

Expressions (47) and (51) can also be derived directly from Maxwell's equations for the electromagnetic fields [*cf.* (57), (62) & (65) and (66) & (69)].

7. Direct derivation of electromagnetic fields

Let us derive expressions for the components of electromagnetic field directly from Maxwell's equations using technique described in Section III. Maxwell's equations read:

$$\text{div}\,\bar{E} = 4\pi\rho, \qquad \text{div}\,\bar{B} = 0,$$

$$\text{rot}\,\bar{E} = -\frac{1}{c}\frac{\partial\bar{B}}{\partial t}, \quad \text{rot}\,\bar{B} = \frac{4\pi}{c}\bar{j} + \frac{1}{c}\frac{\partial\bar{E}}{\partial t}.$$

(52)

Using relations

$$\text{rot}\left(\frac{1}{c}\frac{\partial\bar{E}}{\partial t}\right) = -\frac{1}{c^2}\frac{\partial^2\bar{B}}{\partial t^2} \quad \text{and} \quad \text{rot}\left(\frac{1}{c}\frac{\partial\bar{B}}{\partial t}\right) = \frac{4\pi}{c^2}\frac{\partial\bar{j}}{\partial t} + \frac{1}{c^2}\frac{\partial^2\bar{E}}{\partial t^2}$$

(53)

obtained by differentiation of the second line in (52), we find

$$-\text{rotrot}\,\bar{E} - \frac{1}{c^2}\frac{\partial^2\bar{E}}{\partial t^2} = \frac{4\pi}{c^2}\frac{\partial\bar{j}}{\partial t} \quad \text{and} \quad -\text{rotrot}\,\bar{B} - \frac{1}{c^2}\frac{\partial^2\bar{B}}{\partial t^2} = -\frac{4\pi}{c}\text{rot}\,\bar{j}.$$

(54)

Taking into account the known relation $\Delta\bar{V} = \nabla\,\text{div}\,\bar{V} - \text{rotrot}\,\bar{V}$ and the first line in (52), one can rewrite (49) as

$$\Delta\bar{E} - \frac{1}{c^2}\frac{\partial^2\bar{E}}{\partial t^2} = \frac{4\pi}{c}\left(c\bar{\nabla}\rho + \frac{1}{c}\frac{\partial\bar{j}}{\partial t}\right) \quad \text{and} \quad \Delta\bar{B} - \frac{1}{c^2}\frac{\partial^2\bar{B}}{\partial t^2} = -\frac{4\pi}{c}\text{rot}\,\bar{j}.$$

(55)

Boundary conditions for the field components are

$$\frac{\partial(rE_r)}{\partial r}\bigg|_{r=a} = 0, \; E_\theta\big|_{r=a} = E_z\big|_{r=a} = B_r\big|_{r=a} = 0, \; \frac{\partial(rB_\theta)}{\partial r}\bigg|_{r=a} = \frac{\partial B_z}{\partial r}\bigg|_{r=a} = 0$$

(53)

and finiteness at $r = 0$.

For E_z and B_z, we obtain

$$\left[\frac{1}{r}\frac{\partial}{\partial r}\left(r\frac{\partial}{\partial r}\right) + \frac{1}{r^2}\frac{\partial^2}{\partial\theta^2} + \frac{\partial^2}{\partial z^2} - \frac{1}{c^2}\frac{\partial^2}{\partial t^2}\right]E_z = \frac{4\pi}{c}\left[\frac{c\partial\rho}{\partial z} + \frac{\partial j_z}{c\partial t}\right],$$

$$\left[\frac{1}{r}\frac{\partial}{\partial r}\left(r\frac{\partial}{\partial r}\right) + \frac{1}{r^2}\frac{\partial^2}{\partial\theta^2} + \frac{\partial^2}{\partial z^2} - \frac{1}{c^2}\frac{\partial^2}{\partial t^2}\right]B_z = -\frac{4\pi}{c}\text{rot}_z\,\bar{j}.$$

(56)

These equations can be solved by the method of Green functions. The solutions read

$$E_z(\bar{x},t) = -\iint_{V''t''}G^D(\bar{x},t;\bar{x}'',t'')\left[c\frac{\partial\rho(\bar{x}'',t'')}{\partial z''} + \frac{\partial j_z(\bar{x}'',t'')}{c\partial t''}\right]dV''dt'',$$

$$B_z(\bar{x},t) = \iint_{V''t''}G^N(\bar{x},t;\bar{x}'',t'')\text{rot}_z''\,\bar{j}(\bar{x}'',t'')dV''dt'',$$

(57)

36

where $G^D(\bar{x},t;\bar{x}'',t'')$ and $G^N(\bar{x},t;\bar{x}'',t'')$ are the Green functions of the d'Alembert operator with the Dirichlet and Neumann boundary conditions. These expressions obviously coincide with those obtained from the four-potential [*cf.* (47)].

As to the transversal components, we rewrite some of Maxwell's equations in the form

$$\text{div}_\perp \bar{E} = 4\pi\rho - \frac{\partial E_z}{\partial z}, \qquad \text{rot}_z \bar{E} = -\frac{1}{c}\frac{\partial B_z}{\partial t}; \qquad \text{div}_\perp \bar{B} = -\frac{\partial B_z}{\partial z}, \qquad \text{rot}_z \bar{B} = \frac{4\pi}{c}j_z + \frac{1}{c}\frac{\partial E_z}{\partial t}; \qquad (58)$$

the right hand sides in (58) can be regarded as known functions given by ρ, $\bar{j}$ and (57). Partial derivatives of E_z and B_z can be calculated using commutation relations with the d'Alembert operator. In particular, we have

$$\frac{\partial E_z}{\partial z} = -\iint_{V''t''} G^D(\bar{x},t;\bar{x}'',t'')\left[c\frac{\partial^2\rho(\bar{x}'',t'')}{\partial z''^2} + \frac{\partial^2 j_z(\bar{x}'',t'')}{c\partial z''\partial t''}\right]dV''dt'',$$

$$\frac{1}{c}\frac{\partial E_z}{\partial t} = \iint_{V''t''} G^D(\bar{x},t;\bar{x}'',t'')\left[\frac{\partial}{\partial z''}\text{div}''\,\bar{j}(\bar{x}'',t'') - \frac{\partial^2 j_z(\bar{x}'',t'')}{c^2\partial t''^2}\right]dV''dt'', \qquad (59)$$

$$\frac{1}{c}\frac{\partial B_z}{\partial t} = \iint_{V''t''} G^N(\bar{x},t;\bar{x}'',t'')\frac{\partial}{c\partial t''}\text{rot}''_z\,\bar{j}(\bar{x}'',t'')dV''dt'',$$

$$\frac{\partial B_z}{\partial z} = \iint_{V''t''} G^N(\bar{x},t;\bar{x}'',t'')\frac{\partial}{\partial z''}\text{rot}''_z\,\bar{j}(\bar{x}'',t'')dV''dt''.$$

Here in the second line continuity equation (8) has been used. Using relations, which follow from the definition of Green function (26), one can write the obvious identities:

$$4\pi\rho(\bar{x},t) = -c\iint_{V''t''} G^D(\bar{x},t;\bar{x}'',t'')\left[\Delta'' - \frac{1}{c^2}\frac{\partial^2}{\partial t''^2}\right]\rho(\bar{x}'',t'')dV''dt'',$$

$$\frac{4\pi}{c}j_z(\bar{x},t) = -\iint_{V''t''} G^D(\bar{x},t;\bar{x}'',t'')\left[\Delta'' - \frac{1}{c^2}\frac{\partial^2}{\partial t''^2}\right]j_z(\bar{x}'',t'')dV''dt''. \qquad (60)$$

For further convenience, we then calculate (using again the continuity equation)

$$4\pi\rho(\bar{x},t) - \frac{\partial E_z}{\partial z} = -c\iint_{V''t''} G^D(\bar{x},t;\bar{x}'',t'')\left[\Delta''_\perp\rho(\bar{x}'',t'') + \frac{1}{c^2}\frac{\partial}{\partial t''}\text{div}''_\perp\bar{j}(\bar{x}'',t'')\right]dV''dt'',$$

$$\frac{4\pi}{c}j_z(\bar{x},t) + \frac{1}{c}\frac{\partial E_z}{\partial t} = -\iint_{V''t''} G^D(\bar{x},t;\bar{x}'',t'')\left[\Delta''_\perp j_z(\bar{x}'',t'') - \frac{\partial}{\partial z''}\text{div}''_\perp\bar{j}(\bar{x}'',t'')\right]dV''dt''. \qquad (61)$$

Representations (61) not only provide a concise form of two right hand sides of (58) but also effectively dispose off singularities of the point-charge-type [delta-functions in $\rho(\bar{x},t)$ and $j_z(\bar{x},t)$]. Summarizing, the last two expressions of (59) and expressions (61) provide the right hand sides to equations (58). To continue with equations (58), we employ the following *ansatz*.

1. Electric field. Let us introduce a pair of scalar functions $P_E(\bar{x},t)$ and $Q_E(\bar{x},t)$ obeying the relations

$$E_r = \frac{\partial P_E}{\partial r} - \frac{1}{r}\frac{\partial Q_E}{\partial\theta} \quad \text{and} \quad E_\theta = \frac{1}{r}\frac{\partial P_E}{\partial\theta} + \frac{\partial Q_E}{\partial r} \qquad (62)$$

with boundary conditions

$$P_E|_{r=a} = 0 \quad \text{and} \quad \left.\frac{\partial Q_E}{\partial r}\right|_{r=a} = 0. \qquad (63)$$

Substitution of (62) to the first pair of equations of system (58) leads to Poisson equations in transversal coordinates

$$\left[\frac{1}{r}\frac{\partial}{\partial r}\left(r\frac{\partial}{\partial r}\right) + \frac{1}{r^2}\frac{\partial^2}{\partial\theta^2}\right]P_E = 4\pi\rho - \frac{\partial E_z}{\partial z},$$

$$\left[\frac{1}{r}\frac{\partial}{\partial r}\left(r\frac{\partial}{\partial r}\right) + \frac{1}{r^2}\frac{\partial^2}{\partial\theta^2}\right]Q_E = -\frac{1}{c}\frac{\partial B_z}{\partial t}. \qquad (64)$$

It can be verified that if radial parts of $P_E(\bar{x},t)$ and $Q_E(\bar{x},t)$ are given by Bessel functions then (62) and (63) are compatible with (53). The solutions to (64) with boundary conditions (63) read

$$P_E(\bar{x},t) = \frac{1}{4\pi} \int_{S'} G_\perp^D(\bar{x}_\perp; \bar{x}_\perp') \left\{ \iint_{V''t''} G^D(\bar{x}_\perp', z, t; \bar{x}'', t'') \left[c\Delta_\perp'' \rho(\bar{x}'', t'') + \frac{\partial}{c\partial t''} \operatorname{div}_\perp'' \vec{j}(\bar{x}'', t'') \right] dV'' dt'' \right\} dS',$$

$$Q_E(\bar{x},t) = \frac{1}{4\pi} \int_{S'} G_\perp^N(\bar{x}_\perp; \bar{x}_\perp') \left\{ \iint_{V''t''} G^N(\bar{x}_\perp', z, t; \bar{x}'', t'') \frac{\partial}{c\partial t''} \operatorname{rot}_z'' \vec{j}(\bar{x}'', t'') dV'' dt'' \right\} dS'. \tag{65}$$

The transversal components of electric field are then obtained via formulas (62).

2. Magnetic induction. Again, we introduce a pair of scalar functions $P_B(\bar{x},t)$ and $Q_B(\bar{x},t)$ obeying the relations

$$B_r = -\frac{1}{r}\frac{\partial P_B}{\partial \theta} + \frac{\partial Q_B}{\partial r} \quad \text{and} \quad B_\theta = \frac{\partial P_B}{\partial r} + \frac{1}{r}\frac{\partial Q_B}{\partial \theta} \tag{66}$$

(note the order of auxiliary scalar functions) with boundary conditions

$$P_B|_{r=a} = 0 \quad \text{and} \quad \left.\frac{\partial Q_B}{\partial r}\right|_{r=a} = 0. \tag{67}$$

Substitution of (66) to the second pair of equations of system (58) leads to Poisson equations in transversal coordinates

$$\left[\frac{1}{r}\frac{\partial}{\partial r}\left(r\frac{\partial}{\partial r}\right) + \frac{1}{r^2}\frac{\partial^2}{\partial \theta^2} \right] P_B = \frac{4\pi}{c} j_z + \frac{1}{c}\frac{\partial E_z}{\partial t},$$

$$\left[\frac{1}{r}\frac{\partial}{\partial r}\left(r\frac{\partial}{\partial r}\right) + \frac{1}{r^2}\frac{\partial^2}{\partial \theta^2} \right] Q_B = -\frac{\partial B_z}{\partial z}. \tag{68}$$

It can be again checked that if radial parts of $P_B(\bar{x},t)$ and $Q_B(\bar{x},t)$ are given by Bessel functions then (66) and (67) are compatible with (53). The solutions to (68) with boundary conditions (67) read

$$P_B(\bar{x},t) = \frac{1}{4\pi} \int_{S'} G_\perp^D(\bar{x}_\perp; \bar{x}_\perp') \left\{ \iint_{V''t''} G^D(\bar{x}_\perp', z, t; \bar{x}'', t'') \left[\Delta_\perp'' j_z(\bar{x}'', t'') - \frac{\partial}{\partial z''} \operatorname{div}_\perp'' \vec{j}(\bar{x}'', t'') \right] dV'' dt'' \right\} dS',$$

$$Q_B(\bar{x},t) = \frac{1}{4\pi} \int_{S'} G_\perp^N(\bar{x}_\perp; \bar{x}_\perp') \left\{ \iint_{V''t''} G^N(\bar{x}_\perp', z, t; \bar{x}'', t'') \frac{\partial}{\partial z''} \operatorname{rot}_z'' \vec{j}(\bar{x}'', t'') dV'' dt'' \right\} dS'. \tag{69}$$

The transversal components of magnetic induction are then obtained via formulas (66).

Thus obtained electromagnetic field obviously coincides with that one found in the preceding Section.

<div align="center">REFERENCES</div>

1. Giannessi L. Simulation codes for high brightness beam free-electron laser experiments // Phys. Rev. ST Accel. Beams. 2003. V. 6. No. 11. P. 114802.
2. Hess M., Park C.S., Bolton D. Green's function based space-charge field solver for electron source simulations // Phys. Rev. ST Accel. Beams. 2007. V. 10. No. 5, P, 0542201.
3. Kisunko G.V. To the theory of waveguide excitation // Zh. Tekhn. Fiz. (Sov. J. Tech. Phys.) . 1946, V. 16. No. 5. P. 565-576. (In Russian).
4. Hartemann F.V., Le Sage G.P., McDermott D.B., Luhmann N.C. Coherent synchrotron radiation in acylindrical waveguide with a helical wiggler // Phys. Plasmas. 1994. V. 1. No. 5. P. 1306-1317.
5. Feshbach H., Morse P.M. Methods of Theoretical Physics, New York, McGraw Hill, 1953.
6. Ilyenko K.V. , Gorbik G.M. , Yatsenko T.Yu. On the calculation of the force acting upon a moving charge in a cylindrical drift tube // Telecommun. Radio Eng. 2005. V. 67. No. 10. P. 871-882.
7. Duffy D.G. Green's functions with applications, Boca Raton, Chapman & Hall/CRC, 2001.

8. Jackson J. Classical Electrodynamics, New York, Wiley, 1962.
9. Prudnikov A.P., Brychkov Yu.A., Marichev O.I. Integraly i ryady. Elementarnye funktsii, (vol. 1), Moscow, Fizmatlit, 2003. 435 p. (In Russian) / Eng. transl.: Integrals and series, New York, Gordon and Breach.

WAVE EQUATIONS FOR THE DESCRIPTION OF THE POCKELS EFFECT BY THE EXAMPLE OF CRYSTALS OF BARIUM TITANATE AND STRONTIUM-BARIUM NIOBATE

M.V. Pavlova, *Member IEEE,* Yu.A. Zyuryukin

Saratov State Technical University, Saratov, Russia
E-mail: *pavlova@sstu.ru*

Abstract - The structured mathematical description and algorithm of theoretical research of effect Поккельса in crystals of barium titanate and strontium-barium niobate on the basis of wave equations is offered. The appropriate conclusions about the optimal use of the Pockels effect for process control of the optical modulation devices on the given crystals are performed.

Introduction

For the selection of optimum modes of modulation of light on the concrete crystal it is necessary to carry out research of electro-optical properties of this crystal. Traditionally, at studying of propagation of electromagnetic waves in anisotropic mediums, including the presence of an external electric field, the method of an ellipsoid of refractive exponents (or an optical indicatrix) is used [1-11]. The given method, though is a consequence of the electromagnetic theory of light, however it is not always convenient and evident for quantitative assessment of the effect in anisotropic mediums, in particular in electro-optical crystals.

The purpose of the present work is the theoretical description of the Pockels effect in electro-optical crystals (barium titanate $BaTiO_3$, strontium-barium niobate $Sr_{0,75}Ba_{0,25}Nb_2O_6$), realized on the basis of the electromagnetic theory. Problem statement about the Pockels effect [12] in the form of Maxwell equations has allowed us to transfer directly to wave equations and to find their solutions, i.e. to gain the expressions determining phase velocities and polarization of the optical plane waves, propagating in the given crystals in any direction for various cases of influence of external static electric field.

The appropriate conclusions about the optimal use of the Pockels effect for process control of the optical modulation device based on the given crystals are performed on the basis of the carried out research and the analysis of the gained results.

1. Problem statement about the Pockels effect in crystals of barium titanate and strontium-barium niobate

Using general statement of the problem about the Pockels effect in the form of Maxwell equations presented earlier in work [12] we made following operations:

1. the expressions defining the additives to components of the impermeability tensor, caused by the linear electro-optical effect, are gained in a general view;

2. the expressions for components of the electric intensity vector of the optical plane wave propagating in considered electro-optical crystals are obtained;

3. the Maxwell equations which have been written down concerning required components of the electric inductance vector and the magnetic intensity vector of the optical plane wave, taking into account the Pockels effect for the considered crystals, are obtained.

Now we will be turned to system of the homogeneous Maxwell equations, which completely describe an electromagnetic field of optical wave propagating in a crystal. Substituting in them expressions for the components of the electric intensity of the wave propagating in crystal BaTiO_3 or $\text{Sr}_{0,75}\text{Ba}_{0,25}\text{Nb}_2\text{O}_6$ taking into account the Pockels effect, we obtain following equations:

$$\frac{\partial H_z}{\partial y} - \frac{\partial H_y}{\partial z} = \frac{\partial D_x}{\partial t}, \qquad \frac{\partial H_x}{\partial z} - \frac{\partial H_z}{\partial x} = \frac{\partial D_y}{\partial t}, \qquad \frac{\partial H_y}{\partial x} - \frac{\partial H_x}{\partial y} = \frac{\partial D_z}{\partial t}; \qquad (1)$$

$$\left\langle r_{51}E_x^{\text{cr}}\right\rangle\frac{\partial D_x}{\partial y} + \left\langle r_{51}E_y^{\text{cr}}\right\rangle\frac{\partial D_y}{\partial y} + \left\langle \eta_{zz}^{\circ} + r_{33}E_z^{\text{cr}}\right\rangle\frac{\partial D_z}{\partial y} - \left\langle \eta_{yy}^{\circ} + r_{13}E_z^{\text{cr}}\right\rangle\frac{\partial D_y}{\partial z} - \left\langle r_{51}E_y^{\text{cr}}\right\rangle\frac{\partial D_z}{\partial z} = -\mu\mu_0\varepsilon_0\frac{\partial H_x}{\partial t},$$

$$\left\langle \eta_{xx}^{\circ} + r_{13}E_z^{\text{cr}}\right\rangle\frac{\partial D_x}{\partial z} + \left\langle r_{51}E_x^{\text{cr}}\right\rangle\frac{\partial D_z}{\partial z} - \left\langle r_{51}E_x^{\text{cr}}\right\rangle\frac{\partial D_x}{\partial x} - \left\langle r_{51}E_y^{\text{cr}}\right\rangle\frac{\partial D_y}{\partial x} - \left\langle \eta_{zz}^{\circ} + r_{33}E_z^{\text{cr}}\right\rangle\frac{\partial D_z}{\partial x} = -\mu\mu_0\varepsilon_0\frac{\partial H_y}{\partial t},$$

$$\left\langle \eta_{yy}^{\circ} + r_{13}E_z^{\text{cr}}\right\rangle\frac{\partial D_y}{\partial x} + \left\langle r_{51}E_y^{\text{cr}}\right\rangle\frac{\partial D_z}{\partial x} - \left\langle \eta_{xx}^{\circ} + r_{13}E_z^{\text{cr}}\right\rangle\frac{\partial D_x}{\partial y} - \left\langle r_{51}E_x^{\text{cr}}\right\rangle\frac{\partial D_z}{\partial y} = -\mu\mu_0\varepsilon_0\frac{\partial H_z}{\partial t}. \qquad (2)$$

These Maxwell equations are written concerning required the components of the electric inductance D_x, D_y, D_z and magnetic intensity H_x, H_y, H_z of the optical plane wave, taking into account the Pockels effect, for crystals of BaTiO_3 and $\text{Sr}_{0,75}\text{Ba}_{0,25}\text{Nb}_2\text{O}_6$. Then we will obtain wave equations, having excluded H_x, H_y, H_z by substitution (2) in (1), and we will find their solutions for the optical plane wave propagating in considered crystals taking into account the Pockels effect. The obtained results are represented below.

2. The wave equations for research of the Pockels effect
in crystals of barium titanate and strontium-barium niobate

Let's define influence of external electric field $\vec{E}^{\text{cr}}$ on propagation of the beam of light in crystals of barium titanate and strontium-barium niobate. Depending on a direction of intensity of the applied enclosed electric field its influence on propagating of the beam of light will be different.

1.1) Let the electric field is applied along the optical axis z, and the beam of light is propagating along the axis x (or y), i.e.

$$\begin{cases} E_z^{\text{cr}} \neq 0, \\ \dfrac{\partial}{\partial x} \neq 0 \ \ \text{or} \ \ \dfrac{\partial}{\partial y} \neq 0. \end{cases}$$

In this case from Maxwell equations (1)-(2) two combined equations follow:

$$\frac{\partial^2 D_z}{\partial x^2} - \left(\frac{\mu\mu_0\varepsilon_0}{\eta_{zz}^0 + r_{33}E_z^{\text{cr}}}\right)\frac{\partial^2 D_z}{\partial t^2} = 0, \qquad (3)$$

$$\frac{\partial^2 D_y}{\partial x^2} - \left(\frac{\mu\mu_0\varepsilon_0}{\eta_{yy}^0 + r_{13}E_z^{\text{cr}}}\right)\frac{\partial^2 D_y}{\partial t^2} = 0, \qquad (4)$$

where $v_z^2 = \dfrac{\eta_{zz}^0 + r_{33}E_z^{\text{ст}}}{\mu\mu_0\varepsilon_0} = c^2\left(\dfrac{1}{n_e^2} + r_{33}E_z^{\text{ст}}\right)$ – phase velocity of the extraordinary wave

polarized along the axis z, under the influence of the static electric field $E_z^{\text{ст}}$,

$v_y^2 = \dfrac{\eta_{yy}^0 + r_{13}E_z^{\text{ст}}}{\mu\mu_0\varepsilon_0} = c^2\left(\dfrac{1}{n_o^2} + r_{13}E_z^{\text{ст}}\right)$ – phase velocity of the ordinary wave polarized along

the axis y, under the influence of the static electric field $E_z^{\text{ст}}$. Here we take into account,

that $\eta_{xx}^{\text{o}} = \eta_{yy}^{\text{o}} = \dfrac{1}{\varepsilon_\perp} = \dfrac{1}{n_o^2}$, $\eta_{zz}^{\text{o}} = \dfrac{1}{\varepsilon_\parallel} = \dfrac{1}{n_e^2}$, $\mu \approx 1$.

Such configuration (in the conditions of the transverse Pockels effect) can be used for making of the modulation device of laser beam with the low control voltage.

1.2) Let the electric field is applied along the optical axis z, and the beam of light is propagating also along the axis z, i.e.

$$\begin{cases} E_z^{\text{ст}} \neq 0, \\ \dfrac{\partial}{\partial z} \neq 0. \end{cases}$$

In this case Maxwell equations (1)-(2) will be transformed into the following wave equations:

$$\frac{\partial^2 D_x}{\partial z^2} - \left(\frac{\mu\mu_0\varepsilon_0}{\eta_{xx}^0 + r_{13}E_z^{\text{ст}}}\right)\frac{\partial^2 D_x}{\partial t^2} = 0, \tag{5}$$

$$\frac{\partial^2 D_y}{\partial z^2} - \left(\frac{\mu\mu_0\varepsilon_0}{\eta_{yy}^0 + r_{13}E_z^{\text{ст}}}\right)\frac{\partial^2 D_y}{\partial t^2} = 0. \tag{6}$$

From here follows that at propagating of light wave along the optical axis z the double refraction will not be observed also as in case of absence of the Pockels effect. For waves of initial polarization along the axis x or y, or any polarization in the plane (xy) phase velocity will be defined by following expression:

$$v_x^2 = v_y^2 = \frac{\eta_{xx}^0 + r_{13}E_z^{\text{ст}}}{\mu\mu_0\varepsilon_0} = c^2\left(\frac{1}{n_o^2} + r_{13}E_z^{\text{ст}}\right), \tag{7}$$

where $\eta_{xx}^0 = \eta_{yy}^0$.

Thus, if the modulating electric field is applied along the axis z, then beam of light propagating along the axis z, will have the same phase incursion irrespective of its polarization. Such modulation device can modulate the phase of the nonpolarized laser beam.

2.1) Let the electric field is applied along the axis x, and the beam of light is propagating also along the optical axis z, i.e. $E_x^{\text{ст}} \neq 0$, $\dfrac{\partial}{\partial z} \neq 0$. In this case Maxwell equations will be transformed into the following equations:

$$\frac{\partial^2 D_y}{\partial z^2} - \frac{\mu\mu_0\varepsilon_0}{\eta_{yy}^0}\frac{\partial^2 D_y}{\partial t^2} = 0, \tag{8}$$

$$\frac{\partial^2 D_x}{\partial z^2} - \frac{\mu\mu_0\varepsilon_0}{\eta_{xx}^0}\frac{\partial^2 D_x}{\partial t^2} = 0. \tag{9}$$

2.2) Let the electric field is applied along the axis x, and the beam of light is propagating also along the axis x, i.e. $E_x^{cr} \neq 0$, $\dfrac{\partial}{\partial x} \neq 0$. Then Maxwell equations will be transformed into the following equations:

$$\frac{\partial^2 D_y}{\partial x^2} - \frac{\mu\mu_0\varepsilon_0}{\eta_{yy}^0} \frac{\partial^2 D_y}{\partial t^2} = 0 \,,$$

(10)

$$\frac{\partial^2 D_z}{\partial x^2} - \frac{\mu\mu_0\varepsilon_0}{\eta_{zz}^0} \frac{\partial^2 D_z}{\partial t^2} = 0 \,.$$

(11)

2.3) Let the electric field is applied along the axis x, and the beam of light is propagating also along the axis y, i.e. $E_x^{cr} \neq 0$, $\dfrac{\partial}{\partial y} \neq 0$. Equations (1)-(2) will be transformed into the following equations:

$$\frac{\partial^2 D_z}{\partial y^2} - \frac{1}{\left(v_z^0\right)^2} \frac{\partial^2 D_z}{\partial t^2} = -\frac{r_{51}E_x^{cr}}{\eta_{zz}^0}\frac{\partial^2 D_x}{\partial y^2} \,,$$

(12)

$$\frac{\partial^2 D_x}{\partial y^2} - \frac{1}{\left(v_x^0\right)^2} \frac{\partial^2 D_x}{\partial t^2} = -\frac{r_{51}E_x^{cr}}{\eta_{xx}^0}\frac{\partial^2 D_z}{\partial y^2} \,,$$

(13)

where $\left(v_x^0\right)^2 = \dfrac{1}{\mu\mu_0\varepsilon_0\varepsilon_\perp} = \dfrac{c^2}{n_o^2}$, $\left(v_z^0\right)^2 = \dfrac{1}{\mu\mu_0\varepsilon_0\varepsilon_\parallel} = \dfrac{c^2}{n_e^2}$ – phase velocities of the waves polarized along the axis x or z accordingly, in case of absence of the Pockels effect. These equations are not independent from each other, therefore we use Euler's substitution and we obtain following set of the algebraic equations:

$$\frac{\varepsilon_\parallel r_{51}E_x^{cr}}{v^2}\ D_x^0 - \left(\frac{1}{\left(v_z^0\right)^2} - \frac{1}{v^2}\right)D_z^0 = 0 \,,$$

(14)

$$\left(\frac{1}{\left(v_x^0\right)^2} - \frac{1}{v^2}\right)D_x^0 - \frac{\varepsilon_\perp r_{51}E_x^{cr}}{v^2}\ D_z^0 = 0 \,,$$

(15)

Equating the determinant of the considered combined equations to zero, we obtain the quadratic concerning the quadrate of required velocity $\left(v^2\right)$:

$$\left(v^2\right)^2 - \left(\left(v_x^0\right)^2 + \left(v_z^0\right)^2\right)v^2 + \left(v_x^0\right)^2\left(v_z^0\right)^2\left(1 - \varepsilon_\perp\varepsilon_\parallel(r_{51}E_x^{cr})^2\right) = 0 \,,$$

the corresponding solutions are defined as expression:

$$v_{1,2}^2 = \frac{\left(v_x^0\right)^2 + \left(v_z^0\right)^2}{2} \pm \frac{\left(v_x^0\right)^2 - \left(v_z^0\right)^2}{2}\sqrt{1 + \frac{4\left(v_x^0\right)^2\left(v_z^0\right)^2}{\left(\left(v_x^0\right)^2 - \left(v_z^0\right)^2\right)^2}\ \varepsilon_\perp\varepsilon_\parallel\left(r_{51}E_x^{cr}\right)^2} \,.$$

(16)

Let's introduce the following designation:

$$\Delta^2 = \frac{2\left(v_x^0\right)^2\left(v_z^0\right)^2}{\left(\left(v_x^0\right)^2 - \left(v_z^0\right)^2\right)^2}\ \varepsilon_\perp\varepsilon_\parallel\left(r_{51}E_x^{cr}\right)^2 = 2\left(\frac{n_o^2 n_e^2 r_{51}E_x^{cr}}{n_e^2 - n_o^2}\right)^2 \,,$$

(17)

Then the expression (16) defining required velocity, will assume the final form:

$$v_{1,2}^2 = \frac{\left(v_x^0\right)^2 + \left(v_z^0\right)^2}{2} \pm \frac{\left(v_x^0\right)^2 - \left(v_z^0\right)^2}{2}\sqrt{1+2\Delta^2}\,.\tag{18}$$

From corresponding calculation [13] follows that $2\Delta^2 \ll 1$, then it is possible to consider that $\sqrt{1+2\Delta^2} \approx 1+\Delta^2$, and in this case we obtain expressions for phase velocities in the form:

$$v_1^2 = c^2\left(\frac{1}{n_o^2} + \frac{n_e^2\left(r_{51}E_x^{\text{cт}}\right)^2}{\left(\dfrac{n_o}{n_e}\right)^2 - 1}\right),\tag{19}$$

$$v_2^2 = c^2\left(\frac{1}{n_e^2} + \frac{n_o^2\left(r_{51}E_x^{\text{cт}}\right)^2}{\left(\dfrac{n_e}{n_o}\right)^2 - 1}\right).\tag{20}$$

The polarization directions x' and z' of the light waves propagating in the crystal along the axis y under the influence of external electric field $E_x^{\text{cт}}$ with velocities v_1 and v_2 accordingly, are obtained from the equations (14), (15), taking into account solutions (19), (20), as following expression:

$$tg\gamma = \frac{D_z^0}{D_x^0} = \frac{\varepsilon_\parallel r_{51}E_x^{\text{cт}}}{v_1^2\left(\dfrac{1}{\left(v_z^0\right)^2} - \dfrac{1}{v_1^2}\right)} = \frac{\varepsilon_\parallel r_{51}E_x^{\text{cт}}}{\dfrac{v_1^2}{\left(v_z^0\right)^2} - 1} = \frac{r_{51}E_x^{\text{cт}}}{\dfrac{1}{n_o^2} - \dfrac{1}{n_e^2} + \dfrac{n_e^2\left(r_{51}E_x^{\text{cт}}\right)^2}{\left(\dfrac{n_o}{n_e}\right)^2 - 1}}\,,\tag{21}$$

where γ - the corner defining induced polarization directions x' and z', relative to crystal-physics directions x and z. The calculations show that, value γ is very small, even for moderately strong electric fields and consequently is physically inessential demonstration of electro-optical effect in the considered crystal.

3.1) Let the electric field is applied along the axis y, and the beam of light is propagating along the optical axis z, i.e. $E_y^{\text{cт}} \neq 0$, $\dfrac{\partial}{\partial z} \neq 0$. In this case Maxwell equations will be transformed into the following equations:

$$\frac{\partial^2 D_y}{\partial z^2} - \frac{\mu\mu_0\varepsilon_0}{\eta_{yy}^0}\frac{\partial^2 D_y}{\partial t^2} = 0\,,\tag{22}$$

$$\frac{\partial^2 D_x}{\partial z^2} - \frac{\mu\mu_0\varepsilon_0}{\eta_{xx}^0}\frac{\partial^2 D_x}{\partial t^2} = 0\,.\tag{23}$$

3.2) Let the electric field is applied along the axis y, and the beam of light is propagating along the axis y, i.e. $E_y^{\text{cт}} \neq 0$, $\dfrac{\partial}{\partial y} \neq 0$. Then we have the following equations:

$$\frac{\partial^2 D_x}{\partial y^2} - \frac{\mu\mu_0\varepsilon_0}{\eta_{xx}^0}\frac{\partial^2 D_x}{\partial t^2} = 0\,,\tag{24}$$

$$\frac{\partial^2 D_z}{\partial y^2} - \frac{\mu\mu_0\varepsilon_0}{\eta_{zz}^0}\frac{\partial^2 D_z}{\partial t^2} = 0. \tag{25}$$

3.3) Let the electric field is applied along the axis y, and the beam of light is propagating along the axis x, i.e. $E_y^{\text{ст}} \neq 0$, $\dfrac{\partial}{\partial x} \neq 0$. In this case Maxwell equations will be transformed into the following equations:

$$\frac{\partial^2 D_z}{\partial x^2} - \frac{1}{\left(v_z^0\right)^2}\frac{\partial^2 D_z}{\partial t^2} = -\frac{r_{51}E_y^{\text{ст}}}{\eta_{zz}^0}\frac{\partial^2 D_y}{\partial x^2}, \tag{26}$$

$$\frac{\partial^2 D_y}{\partial x^2} - \frac{1}{\left(v_y^0\right)^2}\frac{\partial^2 D_y}{\partial t^2} = -\frac{r_{51}E_y^{\text{ст}}}{\eta_{xx}^0}\frac{\partial^2 D_z}{\partial x^2}, \tag{27}$$

where $\left(v_y^0\right)^2 = \dfrac{1}{\mu\mu_0\varepsilon_0\varepsilon_\perp} = \dfrac{c^2}{n_o^2}$, $\left(v_z^0\right)^2 = \dfrac{1}{\mu\mu_0\varepsilon_0\varepsilon_\parallel} = \dfrac{c^2}{n_e^2}$.

3. The analysis of wave equations

On the basis of results of the analysis of the obtained wave equations for crystals of barium titanate $BaTiO_3$ and strontium-barium niobate $Sr_{0,75}Ba_{0,25}Nb_2O_6$ following generalizations are made.

1) If for the considered crystals the modulating electric field is applied along the optical axis z (E_z),then the beam of light propagating along the axis z, will have the same phase incursion irrespective of its polarization, according to the obtained expressions:

$$n_x = n_y = n_o - n_o^3 r_{13}\frac{E_z^{\text{ст}}}{2}, \qquad \Delta\varphi_x = \Delta\varphi_y = n_o^3 r_{13}\frac{E_z^{\text{ст}}}{2}kl, \tag{28}$$

where at light wave length $\lambda = 0,633$ (μm) value of electro-optical coefficient $r_{13} = 8\cdot10^{-12}$ (m/V) – for $BaTiO_3$; $r_{13} = 67\cdot10^{-12}$ (m/V) – for $Sr_{0,75}Ba_{0,25}Nb_2O_6$ [13].

Therefore, such modulation device (on the longitudinal Pockels effect) can modulate the phase of the nonpolarized laser beam.

2) If for the considered crystals the modulating electric field is applied along the axis z (E_z),and the beam of light polarized along the axis z, is propagating along the axis x or y, or in any direction in the plane xy, then as result of double refraction the extraordinary wave will appear. This wave will have the maximum induced phase incursion which is proportional to length of crystal, according to expressions:

$$n_z = n_e - n_e^3 r_{33}\frac{E_z^{\text{ст}}}{2}, \qquad \Delta\varphi_z = n_e^3 r_{33}\frac{E_z^{\text{ст}}}{2}kl, \tag{29}$$

where at light wave length $\lambda = 0,633$ (μm) value of electro-optical coefficient $r_{33} = 28\cdot10^{-12}$ (m/V) – for $BaTiO_3$; $r_{33} = 1640\cdot10^{-12}$ (m/V) – for $Sr_{0,75}Ba_{0,25}Nb_2O_6$ [13].

Hence, such configuration (in the conditions of the transverse Pockels effect) can be used for making of the modulation device of laser beam with the low control voltage. Obviously, the most perspective is the linear electro-optical crystal with structure of tetragonal barium titanate – strontium-barium niobate $Sr_{0,75}Ba_{0,25}Nb_2O_6$, possessing the highest measured value of coefficient r_{33}.

3) In crystals of barium titanate $BaTiO_3$ and strontium-barium niobate $Sr_{0,75}Ba_{0,25}Nb_2O_6$ in case of the electric field is applied along the axis x or y, the linear electro-optical effect at any direction of propagation of the beam of light is actually insignificant small.

Thus, for providing with phase modulation, the maximum change of the refractive index for the given linear polarization is necessary. This is optimal reached in the conditions of realization of the transverse Pockels effect (the electric field is applied along the optical axis) for the crystal of strontium-barium niobate $Sr_{0,75}Ba_{0,25}Nb_2O_6$.

Conclusions

Thus, in the present work by the example of crystals of barium titanate and strontium-barium, the structured mathematical description and also algorithm of research of the Pockels effect in arbitrary electro-optical crystal for various cases of propagating of the plane light waves are composed. Using the method of transformation of coordinates, it is possible to obtain the expressions defining phase velocities of light waves, propagating in electro-optical crystals in any direction. This is not represented in the present work.

As result of analysis of wave equations corresponding conclusions about the optimal use of the linear electro-optical effect for control of operation of light modulators are drawn.

REFERENCES

1. Vereshchagin I.K., Kosyachenko L.A., Kokin S.M. Introduction in optoelectronics. Moscow: Vysshaya shkola, 1991.
2. Vasilevskiy A.M., Kropotkin M.A., Tikhonov V.V. Optical electronics. Moscow: Energoatomizdat, 1990.
3. Yariv A., Yukh P. Optical waves in crystals. Moscow: Mir, 1987.
4. Mustel Ye.P., Parygin V.N. Methods of modulation and light scanning. Moscow: Nauka, 1970.
5. Bayborodin Yu.V., Garazha S.A. Electro-optical effect in crystals. Moscow: Mashinostroyeniye, 1967.
6. Zheludev I.S. The electrooptical phenomena in crystals // Successes of physical sciences. 1969. V. 88. Issue.2. P.253-286.
7. Sonin A.S., Vasilevskaya A.S. Electro-optical crystals. Moscow: Atomizdat, 1971.
8. Kuzminov Yu.S. Electrooptical and non-linear-optical crystal of lithium niobate. Moscow: Nauka, 1987.
9. Berezhnoy A.A. Electrooptical modulators and shutters // Optical magazine. 1999. No. 7. P. 3-19.
10. Berezhnoy A.A. Anisotropy of electrooptical interaction in crystals of LiNbO3 // Optics and spectroscopy. 2002. V. 92. No. 3. P. 503-509.
11. Nyunkhem R.E. Properties of materials. Anisotropy, symmetry, structure. RKhD. 2007.
12. Zyuryukin Yu.A., Pavlova M.V. The formulation of a problem about the Pockels electro-optical effect in form of the Maxwell equations for some crystals: lithium niobate, barium titanate, strontium-barium niobate // Modeling in Applied Electrodynamics and Electronics. 2009, No. 9, Saratov University Press. P. 26-31.
13. Grigoryev I.S., Meylikhov Ye.Z. Physical quantities. The reference book. Moscow: Energoatomizdat, 1991.

DISPERSION IN OPEN HELIX

M.V. Davidovich[1], *Senior Member IEEE*, N.A. Bushuev[2], J.V.Stephuk[1]

[1]Saratov State University, 410012, Saratov, Russia,
E-mail: *DavidovichMV@info.sgu.ru*
[2]State industrial enterprise "Almaz", Saratov, 410033, Saratov, Russia,
E-mail: *almaz@overta.ru*
:

Abstract – The dispersion equation for open periodic helix with thin wire has been obtained and the dispersion dependences have been investigated numerically using the periodic Green's function and the integral equation approach.

Introduction

Since 1943 as R. Kompfner for the first time has used the helix in the slow wave system, many attempts have been undertaken for approximate and accurate descriptions of periodic helix dispersion. Among approximate approaches, for example, one can mention the helix-conductive (anisotropic-conductive) cylinder model [1-4]. Its disadvantages reveals when the wavelength is compared with the helix period, as the model does not obviously consider the periodicity of helix winding (correspondingly the periodicity of fields) and the finiteness of wire radius (the mode matching technique is applied on the infinite thin cylindrical surface) [1,4]. The rigorous models even for most simple open helix case still have not realized that corresponds with sufficiently complicated conductor configurations. As the exception, on must point to the papers in which the thin wire conductor approximation for helix has been used (see. [5], Chapter 6 in the monograph [4], and the references there). The same approach has been used in the papers [6-8] for modeling of thin finite length helix in the cylindrical screens. Such approximation (the surface current replacement by the linear wire axis one) for thin helix is highly precise and allows one to bring the problem to one-dimensional integral equation. At the same time we neglects the transverse current on the wire and the longitudinal current change depending on transverse conductor coordinates, that is completely defensible claim. In present paper this approach was used with the application of different (more convenient in our opinion) analysis as in [4,5]. It is based on the periodical Green's function (GF). The methods of more precise taking into account of conductor configuration also have been considered. Though the modern electromagnetic simulation program complexes (such as HFSS, for example) allow one to modeling also the helix [9], the construction of particularized mathematical models for helix structures simulation is still relevant [10.11].

1. The approximate helix dispersion equation

The equations for central helix curve for one winding period in parametric form are

$$\rho = \rho_0 \ , \qquad \varphi = \Omega t \ , \qquad z = ht \ , \quad s = tL, \quad L = \sqrt{\Omega^2 \rho_0^2 + h^2} \ , \qquad 0 \le t \le 1 \ . \quad (1)$$

Here $\Omega = 2\pi$ is the full azimuth angle, h is the helix period (step), ρ_0 is the winding radius, L is the arc length per period, t is the non-dimensional variable. Let us go from surface current density to axis wire current $I(s)$, which is the function of arc length s of helix curve. We count off it from begin of helix period ($t = 0$) along the wire axis. For the current components we have

$$I_\varphi(s) = \Omega \rho_0 I(s)/L \quad , \qquad I_z(s) = hI(s)/L \quad , \tag{4}$$

where the full curve linear current is

$$I(s) = \sqrt{I_\varphi^2(s) + I_z^2(s)} . \tag{5}$$

The helix current density at that describes by the relations

$$J_\varphi(\rho,\varphi,z) = I_\varphi(s)\delta(\rho - \rho_0)\delta(z - ht) \quad , \tag{6}$$

$$J_z(\rho,\varphi,z) = I_z(s)\delta(\rho - \rho_0)\delta(\varphi - \Omega t)/\rho_0 . \tag{7}$$

Here we use the scalar one-dimensional periodic GF form in the cylindrical coordinate system from the paper [12]:

$$\widetilde{G}(\rho,\varphi,z \mid \rho',\varphi',z') = \frac{1}{4ih}\sum_{m=-\infty}^{\infty}\sum_{n=-\infty}^{\infty}\exp(-in(\varphi-\varphi') - i(k_z + 2m\pi/h)(z-z'))\Phi_{mn}(\rho,\rho') . \tag{8}$$

Here the time dependence $\exp(i\omega t)$ is omitted and the following functions are introduced:

$$\Phi_{mn}(\rho,\rho') = \begin{cases} J_n(\kappa_m\rho)H_n^{(2)}(\kappa_m\rho'), \rho < \rho' \\ H_n^{(2)}(\kappa_m\rho)J_n(\kappa_m\rho'), \rho > \rho' \end{cases}, \tag{9}$$

in which the $\kappa_m = -i\sqrt{(k_z + 2m\pi/h)^2 - k_0^2}$ is transverse component. The GF (8) satisfies the inhomogeneous Helmholtz equation [12]

$$(\nabla^2 + k_0^2)\widetilde{G}(\rho,\varphi,z \mid \rho',\varphi',z') = -\frac{\Omega\exp(-ik_z(z-z'))}{h\rho'}\delta(\rho-\rho')\widetilde{\delta}(\varphi-\varphi')\widetilde{\delta}(\Omega(z-z')/h). \tag{10}$$

Here the tilde denotes the periodic Dirac delta-functions with the period Ω, which are defined by the second relation from the formulas (2.23) in [13]. This follows from the fact that GF (8) is obtained from satisfying (10) initial periodic GF by residue integration method. This fact also may be proved directly. Just, at $\rho \neq \rho'$ GF (8) satisfies homogeneous Helmholtz equation (10). The functions (9) are continuous at $\rho \neq \rho'$, but they have the step of derivatives. Under the second differentiation on ρ from this step and owing to well-known relation for cylindrical functions

$$H_n^{(2)'}(\rho\kappa_m)J_n(\rho\kappa_m) - J_n'(\rho\kappa_m)H_n^{(2)}(\rho\kappa_m) = H_{n-1}^{(2)}(\rho\kappa_m)J_n(\rho\kappa_m) - J_{n-1}(\rho\kappa_m)H_n^{(2)}(\rho\kappa_m) = \frac{2}{\pi i\rho\kappa_m}$$

we have additionly the delta-function $\delta(\rho-\rho')/\rho'$ which is proportional to the step. After the reduction on this delta-function in (10) and on the factor $\exp(-ik_z(z-z'))$ one get the identity

$$\frac{1}{2\pi h}\sum_{n=-\infty}^{\infty}\exp(-in(\varphi-\varphi'))\sum_{n=-\infty}^{\infty}\exp(-i2m\pi(z-z')/h) = \widetilde{\delta}(\varphi-\varphi')\widetilde{\delta}(z-z'),$$

in which the second delta-function has the period h.

Let us further consider only the slow waves. For these $k_0^2 < |k_z|^2$, at that there are the solutions $\pm|k_z|$ where $|k_z| \leq \pi/h$. By virtue of periodicity on k_z these solutions may be continued on all values $|k_z| > \pi/h$. Therefore, always $(k_z + 2m\pi/h)^2 > k_0^2$ and $\kappa_m = -i\chi_m$, $\chi_m > 0$ are fulfilled for slow wave. Correspondingly if $k_0^2 > k_z^2$ (fast wave) the value κ_m may be both real and imaginary (under big $|m|$). In the first case we have the radiation (leakage) for lower number spatial harmonics owing to Hankel functions $H_n^{(2)}$ asymptotic behavior. Whereas for slow wave ($k_z^2 > k_0^2$) the radial damping always takes place, as the Hankel function argument is imaginary and $H_n^{(2)}(-i|\kappa_m|\rho) = (2/\pi)(-i)^{-(n+1)}K_n(\chi_m\rho)$. Similarly for Bessel functions one has $J_n(-i|\kappa_m|\rho) = (-i)^n I_n(\chi_m\rho)$.

In the loss case the attenuation in the energy leakage form is always present, but for slow wave it is low. The electric vector-potential according to relations (6), (7) has the components

$$A_\varphi(\rho,\varphi,z\,|) = \frac{\Omega^2\rho_0^2}{4ihL}\int_0^1 I(t)\sum_{m=-\infty}^{\infty}\sum_{n=-\infty}^{\infty}\exp(-in(\varphi-\Omega t)-i(k_z+2m\pi/h)(z-ht))\Phi_{mn}(\rho,\rho_0)dt \ .$$

(11)

$$A_z(\rho,\varphi,z\,|) = \frac{h}{4iL}\int_0^1 I(t)\sum_{m=-\infty}^{\infty}\sum_{n=-\infty}^{\infty}\exp(-in(\varphi-\Omega t)-i(k_z+2m\pi/h)(z-ht))\Phi_{mn}(\rho,\rho_0)dt \ . \quad (12)$$

The usage of periodically located source GF (periodic GF) straight away leads to expanded in spatial harmonics vector-potential and the fields. The resulting integral equation (IE) may be solved only on the one period. We need further only two electrical field components:

$$E_\varphi = \frac{Z_0}{ik_0}\left\{k_0^2 A_\phi + \frac{1}{\rho}\frac{\partial}{\partial\varphi}\left[\frac{1}{\rho}\frac{\partial A_\phi}{\partial\varphi}+\frac{\partial A_z}{\partial z}\right]\right\} \ , \quad E_z = \frac{Z_0}{ik_0}\left\{k_0^2 A_z + \frac{\partial}{\partial z}\left[\frac{1}{\rho}\frac{\partial A_\phi}{\partial\varphi}+\frac{\partial A_z}{\partial z}\right]\right\}. \quad (13)$$

Here $Z_0 = \sqrt{\mu_0/\varepsilon_0}$ is the vacuum wave impedance. Let us take two helix curves like (1) with the winding radiuses $\rho = \rho_0 \pm r$. Here r is the wire radius, and we consider $r << \rho_0$. Obviously, these curves lie on the helix conductor surface. Both unit tangential vectors $\vec{l}^{\pm}$ to these curves have the components $(0,\Omega(\rho_0 \pm r)/L^{\pm},h/L^{\pm})$. Here $L^{\pm} = \sqrt{\Omega^2(\rho_0 \pm r)^2 + h^2}$ are the lengths per period for corresponding helix curves. If we consider the electric field on these curves, we must demand the boundary conditions $E_\tau^{\pm}(t) = E_\varphi^{\pm}(t)l_\varphi^{\pm} + E_z^{\pm}(t)l_z^{\pm} = 0$ for tangential electric field. Accordingly on the helix surface we have

$$E_\varphi^{\pm}(t) = \frac{Z_0}{ik_0}\left\{k_0^2 A_\phi + \frac{1}{\rho_0 \pm r}\left[\frac{1}{\rho_0 \pm r}\frac{\partial^2 A_\phi}{\partial\varphi^2}+\frac{\partial^2 A_z}{\partial\varphi\partial z}\right]\right\} =$$

$$= \frac{-Z_0}{4k_0 L}\int_0^1 I(t')\sum_{m=-\infty}^{\infty}\sum_{n=-\infty}^{\infty}\exp(-i[(n+m)\Omega+k_z h](t-t'))\xi_{mn}^{\pm}\Phi_{mn}(\rho_{\pm},\rho_0)dt',$$

$$E_z^{\pm}(t) = \frac{Z_0}{jk_0}\left\{k_0^2 A_z + \left[\frac{1}{\rho_0 \pm r}\frac{\partial^2 A_\phi}{\partial\varphi\partial z}+\frac{\partial^2 A_z}{\partial z^2}\right]\right\} =$$

$$= \frac{-Z_0}{4k_0 L}\int_0^1 I(t')\sum_{m=-\infty}^{\infty}\sum_{n=-\infty}^{\infty}\exp(-i[(n+m)\Omega+k_z h](t-t'))\eta_{mn}^{\pm}\Phi_{mn}(\rho_{\pm},\rho_0)dt'.$$

Here $\rho = \rho_{\pm} = \rho_0 \pm r$, $\varphi = \Omega t$, $z = ht$ and the designated values are introduced as:

$$\xi_{mn}^{\pm} = \left[\frac{\Omega^2\rho_0^2}{h}\left(k_0^2-\frac{n^2}{\rho_{\pm}^2}\right)-\frac{nh}{\rho_{\pm}}\left(k_z+\frac{2m\pi}{h}\right)\right], \quad (14)$$

$$\eta_{mn}^{\pm} = \left[h\left(k_0^2-\left(k_z+\frac{2m\pi}{h}\right)^2\right)-\frac{n\Omega^2\rho_0^2}{h\rho_{\pm}}\left(k_z+\frac{2m\pi}{h}\right)\right]. \quad (15)$$

Now the tangential electric field takes the form:

$$E_\tau^{\pm}(t) = \frac{-Z_0}{4k_0 LL^{\pm}}\int_0^1 I(t')\sum_{m=-\infty}^{\infty}\sum_{n=-\infty}^{\infty}[\Omega\rho_{\pm}\xi_{mn}^{\pm}+h\eta_{mn}^{\pm}]\Phi_{mn}(\rho_{\pm},\rho_0)\exp(-i[(n+m)\Omega+k_z h](t-t'))dt' \ . \quad (16)$$

The boundary conditions $E_\tau^{\pm}(t) = 0$, $0 \le t \le 1$ are, as a matter of fact, the IE for the unknown current. Since $r << \rho_0$, the boundary conditions may be applied on any helix curve

belonging to the surface. Of course, there are infinitely many such curves and one can draw its beginning at any point on the wire circle cross section of radius r. Then the averaging over such conditions can be fulfilled [12]. For the lossless helix it is convenient to take the boundary conditions as arithmetical mean (omitting the factor 1/2):

$$E_\tau^+(t) + E_\tau^-(t) = 0 \; . \tag{17}$$

Imposing the slow wave condition one has

$$E_\tau^+(t) = \frac{Z_0}{2\pi i k_0 L L^+} \sum_{m=-\infty}^{\infty} \sum_{n=-\infty}^{\infty} \left[\Omega \rho_+ \xi_{mn}^+ + h \eta_{mn}^+\right] I_n(\chi_m \rho_+) K_n(\chi_m \rho_0) \int_0^1 I(t') \exp(-i[(n+m)\Omega + k_z h](t-t')) dt'$$

,

$$E_\tau^-(t) = \frac{Z_0}{2\pi i k_0 L L^-} \sum_{m=-\infty}^{\infty} \sum_{n=-\infty}^{\infty} \left[\Omega \rho_- \xi_{mn}^- + h \eta_{mn}^-\right] I_n(\chi_m \rho_0) K_n(\chi_m \rho_-) \int_0^1 I(t') \exp(-i[(n+m)\Omega + k_z h](t-t')) dt'$$

.

Let us proceed from IE (17) to quadratic functional

$$\Lambda(k_0, k_z, I) = \int_0^1 I(t)\left[E_\tau^+(t) + E_\tau^-(t)\right] dt \; . \tag{18}$$

Setting the approximate wire axis current distribution $I(t)$, we get the dispersion equation (DE) $\Lambda(k_0, k_z, I) = 0$. Fore example, it is well known, that the current distribution in form of traveling wave with the speed of light along the helix curve is the sufficiently good approximation in the frequency wide band [5]: $I(s) = A\exp(-ik_0 s) = A\exp(-iLk_0 t)$. But the question of current approximation chouse is highly not simple. Such investigation will be performed further. At first we take the real current $I(t) = A\cos(Lk_0 t)$ for functional (18). It is convenient to put $A = 1$. For complex current amplitudes one can use, as a matter of fact, the weight functions both $I^*(t)$ and $I(t)$ in generally. In the first case the real functional part is zero. Putting the imaginary part to zero, we have the DE

$$\Lambda(k_0, k_z) = \Lambda^+(k_0, k_z) + \Lambda^-(k_0, k_z) = 0, \tag{19}$$

where

$$\Lambda^\pm(k_0, k_z) = \frac{Z_0}{2\pi i k_0 L L^\pm} \sum_{m=-\infty}^{\infty} \sum_{n=-\infty}^{\infty} \left[\Omega \rho_\pm \xi_{mn}^\pm + h \eta_{mn}^\pm\right] \begin{Bmatrix} I_n(\chi_m \rho_+) K_n(\chi_m \rho_0) \\ I_n(\chi_m \rho_0) K_n(\chi_m \rho_-) \end{Bmatrix} I_{mn}(k_0, k_z), \tag{20}$$

$$I_{mn}(k_0, k_z) = \int_0^1\int_0^1 \cos((\alpha_{mn} - \beta)(t-t')) dt' dt = 2\frac{1-\cos(k_z h - k_0 L)}{[(n+m)\Omega + k_z h - k_0 L]^2}, \tag{21}$$

$$\alpha_{mn} = (n+m)\Omega + k_z h, \quad \beta = k_0 L \; . \tag{22}$$

Further the DE will have the form (19), (20) with different relations like (21). The form (21) does not satisfy the symmetry condition $\Lambda^\pm(k_0, -k_z) = \Lambda^\pm(k_0, k_z)$. This incorrectness corresponds with the fact that we initially set the positive direction for current wave propagation. In this approach all complex power is zero. If the weight function is $I(t) = \exp(-iLk_0 t)$ then we get the complex value of (18). Taking zero real part, we find

$$I_{mn}(k_0, k_z) = \frac{\sin(\alpha_{mn} + \beta) - \sin(\alpha_{mn} - \beta) - \sin(2\beta)}{\alpha_{mn}^2 - \beta^2} \; . \tag{23}$$

If we use the function $I(t) = \cos(Lk_0 t)$ as weight, then

$$I_{mn}(k_0, k_z) = \frac{1 - \cos(\alpha_{mn} + \beta)}{2(\alpha_{mn} + \beta)^2} + \frac{1 - \cos(\alpha_{mn} - \beta)}{2(\alpha_{mn} - \beta)^2} +$$
$$+ \frac{1 + \cos(2\beta) - \cos(\alpha_{mn} + \beta) - \cos(\alpha_{mn} - \beta)}{2(\alpha_{mn}^2 - \beta^2)}. \tag{24}$$

The approximation $I(t) = \cos(Lk_0 t)$ and nonconjugated weight function both determine the forward and backward waves. But the cosine describes the standing current wave that does not correspond to current distribution in helix. The expression (23) turns into zero at $\beta = 0$ (with respect to $k\Omega$). In case $\alpha_{mn} = \pm\beta$, that $I_{mn}(k_0, k_z) = \mp\sin^2(\alpha_{mn})/\alpha_{mn}$. The expression (21) at $\alpha_{mn} = \beta$ turns into unit. Let $k_z h = \pm k\Omega$, $k = 0,1,2,...$ и $k_0 = 0$. At the same time (23) turns into zero, i.e. indicated values are the points (initial and terminal) of dispersion branches. Let $k_z h = \pm k_0 L + k\Omega$, $k = 0,\pm1,\pm2,...$ Then the value $k = 0$ corresponds to geometric retardation $N_g = L/h$. Substituting this value into (19), (20), we get the equation for resonant frequencies determination. If one uses (21), that under $k_z h = k_0 L$ the nonzero and equal to unit terms in the series are keeping for $n = -m$, that gives

$$\Lambda^{\pm}(k_0, k_0 L/h) = \frac{Z_0}{\pi i k_0 L L^{\pm}} \sum_{n=-\infty}^{\infty} \left[\Omega\rho_{\pm}\xi_{n(-n)}^{\pm} + h\eta_{n(-n)}^{\pm}\right] \left\{ \begin{matrix} I_n(\chi_n\rho_+)K_n(\chi_n\rho_0) \\ I_n(\chi_n\rho_0)K_n(\chi_n\rho_-) \end{matrix} \right\}. \tag{25}$$

Let $k_z = \pm k_0 + k\Omega/h$. Evidently (23) now is always zero if $k_0 = 0$, i.e. the limit retardation for main branch is $N = k_z/k_0 = 1$. If we take only azimuthally symmetric term in (19) ($n = 0$), then, using (21) and $k_z = k_0 L$, we essentially have $m = 0$. Then

$$\Lambda^{\pm}(k_0, k_z) \approx \frac{Z_0 k_0^2 \Omega^2 \rho_0^2}{\pi i k_0 L L^{\pm}} \left[\frac{\Omega\rho_{\pm}}{h} - 1\right] \left\{ \begin{matrix} I_0(\chi_0\rho_+)K_0(\chi_0\rho_0) \\ I_0(\chi_0\rho_0)K_0(\chi_0\rho_-) \end{matrix} \right\}.$$

Functional (19) turns into zero for any frequency, but only if $N_g \approx \sqrt{2}$, that says about highly approximate character of azimuthally symmetric model (21) and taken approach for current.

Let us investigate the possibility of geomantic retardation achievement for relation (23). It is equal to zero always, if only $n \neq -m$, or $(n+m)\Omega + 2k_0 L \neq 0$. Let $(n+m)\Omega + 2k_0 L \neq 0$. The equality $n = -m$ corresponds to the case $\alpha_{mn} = \beta$ (with the accurate within $\kappa\pi$), i.e. $I_{(-n)n} = -\sin^2(k_0 L)/(k_0 L)$. Consequently, we have the equation (25), which is distinct by multiplier $I_{(-n)n}$ having the additional roots $k_0 = k\pi/L$. Such roots are realized under the condition $(n+m)\Omega + 2k_0 L = 0$. It is clear that the values $k_0 L = \pi$ at any integer k determine the zeros of relation (23). For the first dispersion branch the value $k_z = \pi/h$ corresponds to $k_0 = \pi/L$. This point is the beginning of bandgap, at that the corresponding group velocity equal to zero and the retardation achieves the value N_g. The correlation (24) has need of numerical investigation.

Thus, the taken approach of helix current wave moving with the speed of light along wire for quadratic functional gives the correct extreme results. Namely, for small k_0 and k_z the waves are moving with the phase velocity c in both directions along z-axis, the dispersion branches are even and periodic on k_z with the inverse lattice period $2\pi/h$, and for $k_0 = k\pi/L$ there are the extremums of dispersion branches in the points $k_z = (2l-1)\pi/h$, $l = 1,2,...$ For the first branch the maximal retardation is equal to geometric one. The extreme points of dispersion branches do not depend on value r.

2. The constructions of rigorous models

The used current representations give approximate results (within the framework of applied approach $r << \rho_0$) and need in several explanations, though as (23), so (24) give the correct results for $k_z h = k\pi$ ($k = 0,\pm 1,..$). To solve the DE (18) correctly, it is need to expand the current $I(t)$ into series using some basis functions

$$I(t) = \sum_{k=1}^{K} I_k u_k(t) \tag{26}$$

and taking the extremum of quadratic form (18). For real functions u_k one has for the integrals

$$I_{mn}^{kk'} = I_{mn}^{k'k*} = \int_0^1 \exp(-i\alpha_{mn}t)u_k(t)dt \int_0^1 \exp(i\alpha_{mn}t')u_{k'}(t')dt', \tag{27}$$

i.e. gets the hermitian matrix elements and correspondingly the real DE roots. For such bases one can use, fore example, the trigonometric of finite element (FE) function, in particulars, the simplest piecewise constant FEs [5]. For complex functions in (26) one must use the conjugate weight functions (the another wave is to take the real part of functional). If we take $I(t) = \exp(-ik_z ht)$, then we get $I_{mn} = \delta_{m(-n)}$ and the functional (25) in which we have the k_0 and k_z as the unknown parameters of seeking. But the numerical investigation of such DE does not lead to correct results. Let therefore consider he possible current representations.

By virtue of G. Floquet's theorem one can approximately (by truncation of series) write the complex current as

$$\dot{I}(t) = \sum_{k=-K}^{K} I_k \exp(-i(k_z h + k\Omega)t) = \exp(-ik_z ht)I(t). \tag{28}$$

Here the periodic complex function has the form

$$I(t) = I_c(t) - iI_s(t) = \sum_{k=0}^{K} \left[\frac{I_k + I_{-k}}{1 + \delta_{k0}} \cos(k\Omega t) - i(I_k - I_{-k})\sin(k\Omega t) \right].$$

The conjugated to (28) weight function leads to independent on k_z integrals $I_{mn}^{kk'}$ and not well numerical results. If one gives the weight function in the same form (28), then the good result will be obtained by putting the real part of functionals to zero. The reason of these misunderstandings consists in as follows. The used in the IE and in the functional GF is the source function of phasing and periodically located sources. Therefore the factors $\exp(-i(k_z ht + m\psi))$ are already are contained in the GF and we must not include they into the current. Here for zero sell $m = 0$, and the term $\psi = k_z h$ is the phase shift per sell. The current (28) must be used with the customary nonperiodic GF: $G(\vec{r} - \vec{r}') = (4\pi|\vec{r} - \vec{r}'|)^{-1} \exp(-jk_0|\vec{r} - \vec{r}'|)$ (its representations in cylindrical system are in [13]). Therefore for real current (26) with taking into account the relation (28) we must use the expansion

$$I(t) = \sum_{k=0}^{K} \frac{2I_k}{1 + \delta_{k0}} \cos(k\Omega t). \tag{29}$$

Such periodic current has not any jumps at $t = 0$ and $t = 1$, as distinction from function $\cos(k_z ht)$. The sufficiently simple approximation (29) with $K = 1$ has the form $I(t) = I_0/2 + I_1 \cos(\Omega t)$. It is convenient to put $I_0 = 2$. The DE is derived from the quadratic form extremum as zero of determinant:

$$\Lambda_0(k_0, k_z) = \Lambda_{00}(k_0, k_z)\Lambda_{11}(k_0, k_z) - |\Lambda_{01}(k_0, k_z)|^2 = 0. \tag{30}$$

All terms in the left part of (30) have the form of (19), (20), in with instead of (21) one must replace the matrix elements (27):

$$I_{mn}^{(0,0)} = \int_0^1\int_0^1 \cos\big([(n+m)\Omega + k_z h](t - t')\big)dt'dt, \tag{31}$$

$$I_{mn}^{(0,1)} = I_{mn}^{(1,0)*} = \int_0^1\int_0^1 \exp\big(-i[(n+m)\Omega + k_z h](t - t')\big)\cos(k_z h t')\cos(\Omega t')dt'dt, \tag{32}$$

$$I_{mn}^{(1,1)} = \int_0^1\int_0^1 \cos(\Omega t)\sin\big([(n+m)\Omega + k_z h](t - t')\big)\cos(\Omega t')dt'dt. \tag{33}$$

The integral (31) leads from (21), if we put $\beta = 0$. The remanding integrals are also simply calculated and therefore not presented. In general case the rigorous K order model leads to the necessity to find the roots of K order determinant. The losses and the impedance boundary conditions on helix demand to use the complex current expansion and correspondingly the seeking of complex roots k_z for complex determinant. In this case the direct and backward lower and upper (corresponded to frequency) dispersion branches are closed in the bandgap where now the wave propagation is possible with large attenuation [12].

3. The simulation results

We search the DE (19) roots by the besection method on k_0 with usage of relations (21), (23) and (24). The simulation results for relation (23) with $r_0/h = 1.7$ ($N_g = 10.7766$) are presented in the fig. 1 and 2. Fig. 1 demonstrates the normalized wavenumber and inverse retardation versus the phase shift per sell (helix) period, and fig, 2 – the frequency dependence of retardation. The bold lines 1 correspond to $r/h > 0.1$. There is no any dependence from wire radius for lower r values. The used approach has not applied for $r/h > 0.1$. The series in (19) is fast convergent by virtue of well-known relation for large arguments [14]:

$$I_n(\chi_m\rho_0)K_n(\chi_m\rho_0) \approx \left\{1 - \frac{1}{2}\frac{\mu-1}{(2\chi_m\rho_0)^2} + \frac{1}{2}\frac{3}{4}\frac{(\mu-1)(\mu-9)}{(2\chi_m\rho_0)^4} - \frac{1}{2}\frac{3}{4}\frac{5}{8}\frac{(\mu-1)(\mu-9)(\mu-25)}{(2\chi_m\rho_0)^6} + \ldots\right\}.$$

Here $\mu = 4n^2$ is fixed. But the separately calculation of the second kind cylindrical functions in (20) at large arguments and indexes leads to ill-conditioned algorithms. In the presented results we have used the 7 azimuth and 101 index m terms in the series. One can get practically the same accuracy by restriction of 21-31 m-terms. Also we have investigated the cases of usage 5, 9, 11 and 13 of azimuth members. Even so the results differ only insignificantly. The modified Bessel functions are obtained by calculation if integrals with the accuracy of 6-7 significant digits in their integral expressions [14]. The numerical exploration of formula (24) shows that it is not very good as the dispersion in this case is strongly nonlinear with the anomalous zone that not corresponds to helix.
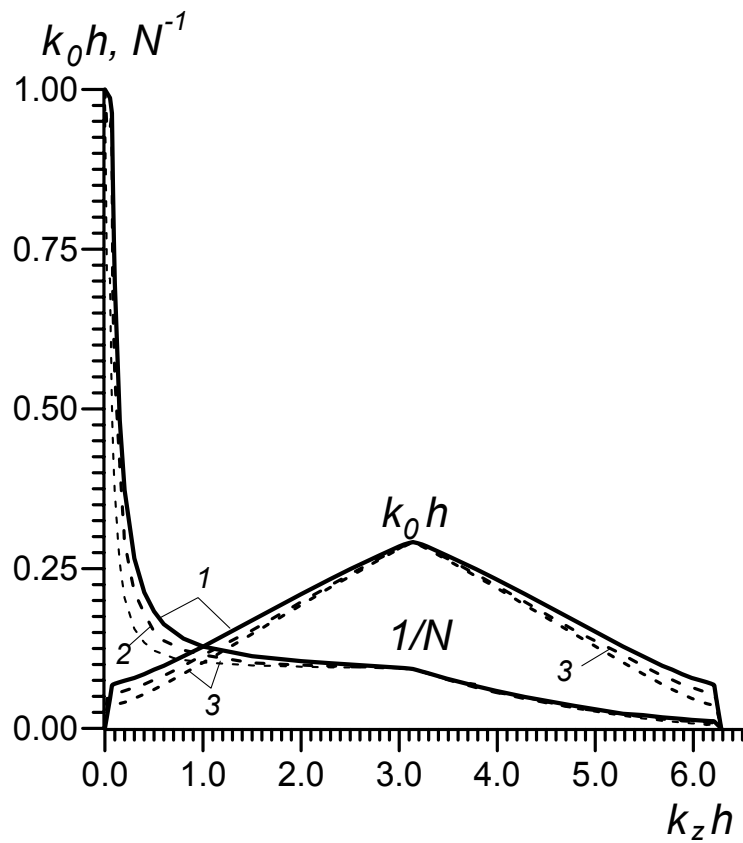
Fig. 1. Normalized dispersion and inverse retardation for helix with $\rho_0/h = 1.7$, $r/h = 0.001$ versus phase shift per cell $\psi = k_z h$. The line 1, 2, 3 correspond to $r/h = 0.001$, 0.05 and 0.1
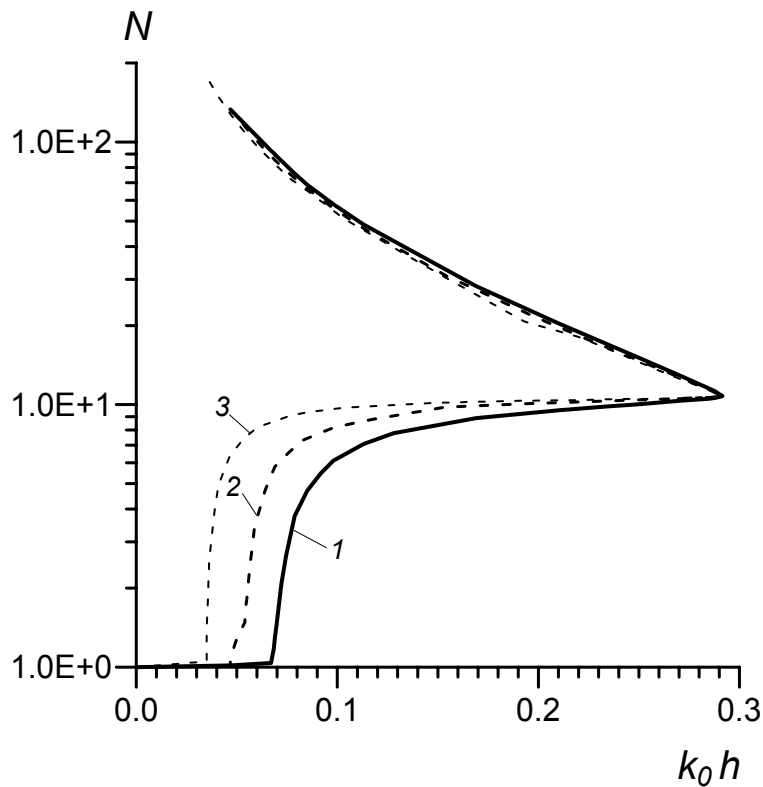

Fig. 2. The retardation frequency dependence for the case of fig. 1

The DE $\Lambda_{00}(k_0, k_z) = 0$, which is corresponded to the case $I_1 = 0$ in (30), is also has been investigated numerically. The simulation gives the understated retardation coefficient N values. That says that zero-order approximation of constant along helix current also is not good.

Conclusions

The cylindrical coordinate system periodic GF form efficiency has been shown for simulation of infinite periodic helix slow wave system dispersion. The results also may be used for fast wave leakage analysis in long helix antennas. This method leads to solving one-dimensional IE for wire axis current. It allows one to simulate the conductors with arbitrary cross-sections and multiple-start winding helixes. Here the several helix current curves arise instead one helix current and correspondingly the several coupled linear (one-dimensional) IEs. In particular, it is convenient to analyze the ribbon helixes by setting several multiple-thread helix currents, uniformly located on ribbon helix surface. In any respect such approach is equivalent to the auxiliary sources method. The only essential approximation here is the absence of transverse currents on helix conductors.

In this paper the approximate closed relations for helix DE are obtained. Their examination by numerical simulation shows that the relations (23) in (19) and (20) sufficiently well describes the helix dispersion. Evidently, appropriately to use the continuous real finite elements for current expansion and to construct the high order algorithms. One of possible low-order and convenient complex current approximations may be taken in the form $I(t) = I_0 \exp(-ik_0 Lt) + I_1 \exp(-ik_z ht)$, which also leads to closed explicit DE.

REFERENCES

1. Weinstein L.A. Electromagnetic waves. Moscow, Radio i Svyaz, 1988. 440 p. (in Russian)
2. Bushuev N.A., Altshuler E.Y., Brovko A.V., Rozhnev A.G. Finite element method for the analysis of helix slow wave systems with complex configuration of dielectric rods and thin metallic supports // Elektromagnitnye volny i elektronnye sistemy. 2001. V. 6. No. 2-3. P. 48-53. (In Russian).
3. Brovko A.V., Rozhnev A.G., Manenkov A.B. Advanced Numerical Methods For Open Electromagnetic Structures // Modeling in Applied Electromagnetics and Electronics. Saratov University Press. 2006. Issue 7. P. 44-48.
4. Silin R.A. Slow wave systems. Moscow.: Soviet Radio, 1969. 632 p. (In Russian).
5. Kolobaeva T.E., Penzyakov V.V., Phinkelstein Yu.H. Slow wave system analysis by inyegral equation method // Electronnaya Tekhnika. Ser. Microwave electronics. Issue. 10 (334) 1981. P. 31-35. (In Russian).
6. Davidovich M.V., Shilin I.V. Excitation of cylindrical structures by helix and axis currents // International Conference on Actual Problems of Electron Devices Engineering (APEDE 2004). Saratov, SSTU, 2004. P. 226–230.
7. Davidovich, M.V., Shilin, I.V. Integral equation for excitation of cylindrical resonator by helix and axial currents // International Conference on Actual Problems of Electron Devices Engineering (APEDE 2004). Saratov, SSTU, 2004. P. 240–244.
8. Davidovich M.V., Shilin I.V. Excitation of cylindrical waveguide and resonator by helix and axis currents // Proc. SPIE. 2005. V. 5776. P. 37-42.
9. Alaria M.K., Sinha A.K., Srivastava V. Analysis of helix slow-wave structure for space TWT using Ansoft HFSS // IEEE International Vacuum Electronics Conference. 2006. P. 147-148.

10. Azov G.A., Khritkin S.A. Simulation of the helical slow-wave structure of a high-power traveling-wave tube // Journal of Communications Technology and Electronics . 2010. V. 55. No. 3. P. 343-346.
11. Balakirev V.A., Markov P.I., Sotnikov G.V. Helix slow wave structures for MILO // Electromagnetic phenomena. 2001. V. 2. No. 7 . P. 302-323 (In Russian).
12. Davidovich M.V. Photonic crystals: Green's functions, integro-differential equations, and simulation results // Radiophysics and Quantum Electronics, 2006. V. 49. No. 2. P. 134-146.
13. Markov G.T., Chaplin A.F. Excitation of electromagnetic waves. Moscow, Radio i Svyaz, 1983. 296 p. (In Russian).

CYLINDRICAL REENTRANT CAVITY RESONATOR: COMBINED MODELING AND DESIGN EQUATIONS

A.A. Dovgan', V.V. Komarov, *Member IEEE*

Saratov State Technical University, 410054, Russia
E-mail: *vyacheslav.komarov@gmail.com*

Abstarct - Given paper is focused on analytical and numerical modeling of cylindrical reentrant cavity resonator. Analytical model taken in the literature is based on the equivalent network method. It can be used only for approximate calculation of resonant wavelengths of such devices. Results of calculations can be improved if analytical model is completed with additional closed form expression obtained in present study using finite element method. Proposed simplified analytical approach can be a useful tool in computer-aided design of various microwave components on reentrant cavity resonator.

1. Introduction

Cylindrical reentrant cavity resonators (RCR) are used nowadays in klystron and solid state generators, dielectrometers, medicine applicators, particle accelerators, microwave filters, telecommunication antennas and etc. Electrodynamic properties of such resonators are defined mainly by sizes of capacitance gap formed by one or two metal posts in cylindrical cavity. And besides double post resonator (Fig.1) can be considered as combination of two single post cavities with XY symmetry plane. Geometrical model of RCR is completely described by aspect ratio ($a \times b$) and sizes of capacitance gap ($d \times t$), but number of freedom degrees can be reduced from four to three using normalized parameters: b/a, t/a, d/b.
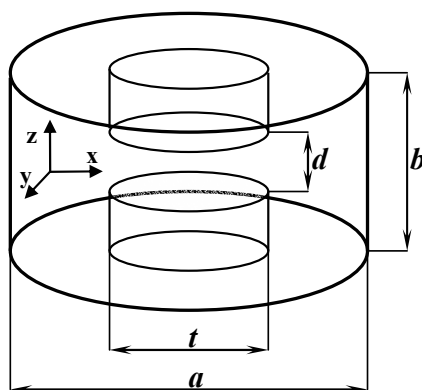

Fig.1. Cylindrical reentrant cavity

Such properties of RCR as quasi-uniform distribution of dominant mode electric field in capacitance gap and smaller aspect ratio sizes in comparison with convenient cylindrical resonators at fixed frequency can be successfully utilized for design of laboratory scaled microwave heating chambers, intended for investigations of processes of electromagnetic (EM) waves interaction with different substances, for example, in microwave chemistry [1], microwave biology and etc. Low impedance makes RCR easily compatible with coaxial lines which play role of feeders. That is RCR with one input port and respectively one

excitation element (coaxial probe or loop) is usually analyzed in the literature [2-4]. Significantly rarely RCR with two input ports is designed for special purposes [5].

Despite on a wide practical application analytical theory of RCR is absent up to now and it is usually simulated numerically employing finite element method (FEM) [2], finite difference time domain method [6], mode matching method [7], method of moments and finite integration method [8]. All these algorithms require serious computational resources and corresponding software.

If capacitance gap height (d) of RCR is small enough simple analytical expressions based on equivalent network method [9] or theoretical function [10] can be derived. Given simplified approaches are quite useful in engineering practice but good accuracy of these methods is achieved only for the dominant mode and limited range of cavity dimensions variation.

The main objective of this study was to improve equivalent network method using the results of 3D numerical simulations.

2. Simplified analytical model

It is known that the electric field of the lowest mode in reentrant cavity is mainly concentrated in the central part of the cavity (capacitance gap) and the magnetic field is distributed in peripheral region closer to the side cavity walls. According to equivalent network method we can introduce quasi-static approximation and analyze both fields separately neglecting penetration of the E-field in peripheral region and the H-field in capacitance gap. Then resonant wavelength will be determined as:

$$\lambda = 2\pi c \sqrt{L_e C_e} , \qquad (1)$$

where c is the velocity of light; L_e is the equivalent inductance; C_e is the equivalent capacity. Using approach proposed in [9] and cavity sizes labeling (Fig.1) two main parameters of equivalent circuit can be expressed as:

$$L_e = \frac{\mu' \mu_0 b}{2\pi} \ln \frac{a}{t} , \qquad (2)$$

$$C_e = \frac{\varepsilon' \varepsilon_0 \pi t^2}{4d} + 2\pi \varepsilon' \varepsilon_0 t \ln \frac{b}{d} , \qquad (3)$$

where ε_0, μ_0 are the dielectric and magnetic constants respectively; ε' is the dielectric permittivity; μ' is the magnetic permeability of media inside cavity.

Substituting (2) and (3) in (1) and assuming that for air $\varepsilon' = \mu' = 1$ normalized resonant wavelength of the reentrant cavity [9]:

$$\frac{\lambda}{a} = \frac{\pi t}{2a} \sqrt{ \frac{2(b/a)}{(d/a)} \left[1 + 4 \frac{(d/a)}{(t/a)} \ln \left(\frac{(b/a)}{(d/a)} \right) \right] \ln \left(\frac{a}{t} \right) } . \qquad (4)$$

As it was mentioned in [9] multiple testing of equation (4) derived for any aspect ratio b/a has shown that accuracy of λ calculation is nearby $10 \le \Delta\% \le 20$ when $0.2 \le t/a \le 0.5$; $0.1 \le d/b \le 0.5$.

When $b/a = const$ formula (4) describes a function of two variables $\lambda = f(t/a, d/b)$ geometrical interpretation of which is a surface. And now it is necessary to find intervals of both geometrical parameters variation ensuring minimal computational error.

58

3. FEM model and design equation

3D finite element model of the reentrant cavity (Fig.1) has been built using commercial software COMSOL V.3.5 (www.comsol.com). Symmetrical half of geometrical model shown in Fig.1 with magnetic wall boundary conditions at the symmetry XZ-plane was analyzed. Mesh model included about $120{,}000 \div 160{,}000$ tetrahedral edge elements. Variable density mesh was employed with denser mesh in capacitance gap region taking into account peculiarities of electric field distribution for dominant mode. Introduction of electric wall boundary condition at XY symmetry plane easily transforms double post RCR model in single post model with half reduced sizes along Z axis: $b_1 = 0.5b$ and $d_1 = 0.5d$.

EM field in the cavity under study is described by Helmholtz equation which can be expressed in matrix form as [6]:

$$[A]\{X\} = \Lambda[B]\{X\}, \tag{5}$$

where $[A]$ and $[B]$ are the sparse symmetrical matrixes; Λ are the eigenvalues; $\{X\}$ are the eigenvectors of electromagnetic field.

General Minimal Residue (GMRES) algorithm was utilized for matrix equation (5) solution. Numerical model was tested both for single post and double post RCR using experimental data obtained in [6, 11]. Comparison of numerical and experimental approaches is given in Table I.

Table 1
RCR resonance wavelengths

Single post RCR: $a = 30$ mm, $b_1 = 10$ mm, $t = 20$ mm, $d_1 = 1.5$ mm.		Double post RCR: $a = 1900$ mm, $b = 1450$ mm, $t = 600$ mm, $d = 450$ mm.	
Measured [11]	Simulated	Measured [6]	Simulated
$\lambda/a = 2.87$	$\lambda/a = 2.95$	$\lambda/a = 2.09$	$\lambda/a = 2.1$

Described numerical model was implemented for the calculation of the lowest mode resonant wavelengths (λ) of the double post RCR (Fig.1) as a function of two geometrical parameters t/a and d/b when $0.2 \leq b/a \leq 1$. Two examples of such functions for $0.1 \leq t/a \leq 0.8$ and $0.1 \leq d/b \leq 0.9$ are represented in Fig.2.
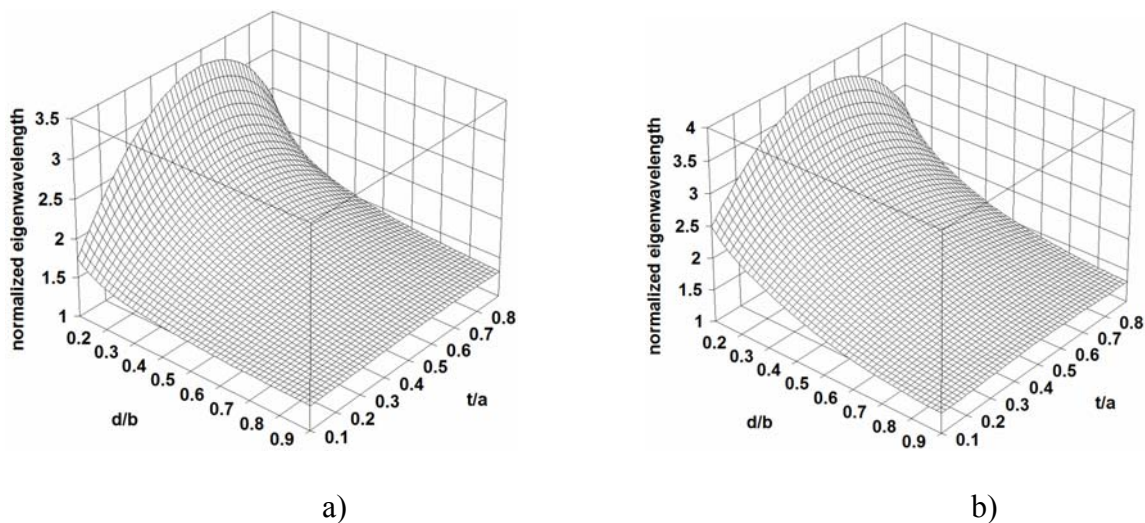

a)   b)

Fig.2. Dominant mode resonant wavelengths in reentrant resonator with b/a = 0.2 (a); 0.8 (b)

Intersection of each of these surfaces with function $\lambda/a = f(t/a, d/b)$ obtained analytically by means of (4) has demonstrated that the maximum accuracy of analytical modeling is achieved for $0.2 \leq b/a \leq 1$ and $0.1 \leq t/a \leq 0.8$ only when capacitance gap height is described by approximate function:

$$\frac{d}{a} = u_1 + u_2 \ln\left(\frac{b}{a}\right) + u_3\left(\frac{t}{a}\right) + u_4\left(\ln\left(\frac{b}{a}\right)\right)^2 + u_5\left(\frac{t}{a}\right)^2 + u_6\left(\frac{t}{a}\right)\ln\left(\frac{b}{a}\right) + u_7\left(\ln\left(\frac{b}{a}\right)\right)^3 +$$
$$+ u_8\left(\frac{t}{a}\right)^3 + u_9\left(\frac{t}{a}\right)^2 \ln\left(\frac{b}{a}\right) + u_{10}\left(\frac{t}{a}\right)\left(\ln\left(\frac{b}{a}\right)\right)^2 \tag{6}$$

where $u_1 \div u_{10}$ coefficients values are given in Table 2. Equation (6) has been derived with the help of surface fitting procedures and Table Curve 3D V.4 software (www.sigmaplot.com). Determination coefficient for expression (6): $R^2 = 0.9988$.

Table 2
Empirical coefficients for equation (6)

u_1	u_2	u_3	u_4	u_5
0.528129	0.85474	1.45029	0.436696	-1.44782
u_6	u_7	u_8	u_9	u_{10}
0.578403	0.073195	-0.056704	-0.6079025	-0.01729

In order to check equations (4) and (6) five RCR (Fig.1) designs with different arbitrary taken sizes were simulated employing FEM model described above. Results of comparison of numerical and analytical data are shown in Table 3.

Table3
Testing results of analytical model

RCR design	b/a	t/a	d/a	λ/a, anal.	λ/a, FEM
1	0.25	0.78	0.072	1.9444	1.9383
2	0.37	0.63	0.230	1.5705	1.5546
3	0.58	0.51	0.459	1.4184	1.4284
4	0.72	0.37	0.584	1.3866	1.4051
5	0.93	0.24	0.725	1.4443	1.4141

Represented analytical model which includes equations (4) and (6) can be used for calculation in first approximation the eigenwavelengths of the dominant mode in RCR with $0.2 \leq b/a \leq 1$ and $0.1 \leq t/a \leq 0.8$. And besides two steps approach is necessary here:
1) determination of capacitance gap height values according to (6);
2) normalized wavelengths calculation by means of (4).
Main advantage of this model is it simplicity and main drawback is the limited range of capacitance gap height variations defined by condition (6) where basic equation (4) demonstrates best accuracy.

4. Conclusion

Analytical expression determining restrictions on known equivalent network model and allowing approximate calculating resonance wavelengths of RCR has been derived and tested.

REFERENCES

1. Kalhori S., Elander N., Svennebrink J. and Stone-Elander S., A reentrant cavity for microwave-enhanced chemistry // Int. J. Microwave Power and EM Energy. 2003 V. 38. No. 2. P.125-135.
2. Kelly M.B. and Sangster A.J., Cylindrical re-entrant cavity resonator design using finite element simulation // Microwave and Optical Technology Letters. 1998. V. 18. No. 2. P. 112-117.
3. Barroso J.J., Castro P.J., Aguiar O.D. and Carneiro L.A. Reentrant cavities as electromechanical transducers // Review of Scientific Instruments. 2004, V. 75. No. 4. P. 1000-1005.
4. Ishihara Y., Kameyama Y., Minegishi Y.and Wadamori N. Heating applicator based on reentrant cavity with optimized local heating characteristics // Int. J. Hyperthermia. 2008, V. 24. P. 694-704.
5. Hadjistamov B.N., Levcheva V.P. and Dankov P.I., Dielectric substrate characterization with re-entrant resonator // Mediterranean Microwave Symposium, Budapest, Hungary, May 2007. P. 183-186.
6. Kanai Y., Tsukamoto T., Miyakawa M., and Kashiwa T., Resonant frequency analysis of reentrant cavity applicator − comparison of finite element and finite difference time domain methods // IEEE Trans. 2000. V. Magnetics-36. No.4. P. 1750-1753.
7. Jaworski M., On the resonant frequency of a reentrant cylindrical cavity // IEEE Trans. 1978. V. MTT-26. P. 256-260.
8. Carter R. G., Feng J., and Becker U., Calculation of the properties of reentrant cylindrical cavity resonators // IEEE Trans. 2007. V. MTT-55. P. 2531-2538.
9. Grigoriev A.D., Electrodynamics and Microwave Engineering, Lan' Publishing, Sankt-Peterburg, 2007. (In Russian).
10. Barroso J.J., Castro P.J., Neto J.P., and Aguiar O.D., Analysis and simulation of reentrant cylindrical cavities // Int. J. Infrared and Millimeter Waves. 2005. V. 26. P. 1071-1083.
11. Pandit H., et al, High T_c superconductor re-entrant cavity filter structures // Physica C, 2005. V. 425. P. 44–51.

THE N-TH ORDER SIMPLEX-SUM DESIGN OF NUMERICAL OR PHYSICAL EXPERIMENT DEVELOPMENT FOR SIMULATION OF SLOW-WAVE STRUCTURES ELECTRODYNAMICS CHARACTERISTICS

A. N. Savin, *Member IEE,* D.M. Doronin, I. A. Nakrap

Saratov State University, Saratov, 410012, Russia
Ee-mail: *SavinAN@sgu.info.ru*

Abstract — The results of optimal Simplex-Sum Design of experiment development for the numerical or physical modeling are presented. Using developed method, design of experiments, that possess the properties of symmetry, orthogonality, rotatability, D-optimality and contains a small number of experiments, has been constructed. The third-order design of experiment was calculated for the Slow-Wave Structures (SWS) with coupled cavity chain electrodynamics characteristics modeling. The wide range of factors variation allows using this design for devices of different functionality.

1. Introduction

The development of high-power microwave devices supposes mathematic modeling of waveguide systems (WS) and processes of electron beams interaction with electromagnetic fields of the WS, computation of characteristics of individual parts using models as well as an optimization of the whole device in order to achieve the required output parameters [1].

At the modern stage of computer modeling techniques the development of simulation of electrodynamics characteristics (EDC) of WS can be done quite accurately by the field methods based on Maxwell's equations for boundary conditions presented. Due to it's an awkward task to do the optimization of WS with loss and deterministic inhomogeneous, taking into account. Also, at the process of moving in the short-wave range it's difficult to account the manufacture inaccuracies and quality of the surface of WS, that has a significant influence on their parameters.

One of the ways of solving these problems is to use a polynomial regression models of EDC or parameters of equivalent circuit (for WS), constructed according to the numerical or physical designing experiments data and to take into account the implications of the above factors [2].

In this case a mathematical model can be represented by the following expression [3]:

$$\eta = f(x_1, x_2, \dots x_k), \tag{1}$$

where x_k - independent variable (factor) – for example, the sizes of the WS,

η - simulated electrodynamics parameter of the WS,

$f(x_1, x_2, \dots x_k)$ - polynomial of required order.

The problem of the adequate regression equation (1) construction using experimental data (i.e. solving of the task of coefficients determining in regression equation) is possible only under certain stringent requirements: design of the experiment should be symmetric, orthogonal, should ensure minimum error of the regression coefficients dispersion (D-optimal), etc. [4]

The theory of design of experiments [4-8] offers different ways of optimal design searching by various criteria. Often, the complete factory experiment, in which all possible combinations of factor levels implemented, is used. Also its fractional replicates are widely used. But high complexity and unsuitability of this method is conditioned on a necessary

number of experiments increasing with the number of factors taken into account addition. Therefore, all efforts of the design theory of experiments aimed at improving its efficiency by reducing the number of experiments with the model adequacy saving. In [9] the methods for constructing second-order Design, that available to reduce the number of experiments and improve the dispersion characteristics of the experimental data, are presented. The experiment was done on the base of second-order Simplex-Sum Design. The error of dispersion characteristics calculation by this model does not exceed 3% and the coupling resistance - 10%. Further reduction of the error of models could be achieved by using data from experiments that were done using designs of higher orders.

2. The Design of experiments on the base of a regular simplex

The principle of many single-factor experiments replacing by one multiple-factor [4] suggests using the experimental data, which belong to different single-factor dependence in single-factor experiments, for cross-averaging. For that purpose the allocation of experiments in the factors space must be performed in a special way, called the optimal design of experiment. One of the optimal design properties is that it does not only reduce the number of experiments, but also provides less dispersion of averaged results variance than in separate single-factor experiments.

Rotatable composite designs [5] are often used in the practice of the experiments designing and besides points of the first-order design contain extra "star" and central points. In [6] rotatable D-optimal designs on k-dimensional hyper sphere were suggested for a polynomial regression.

In [7] correct simplex was proposed to use as a design of experiments, which is defined as the set of $k+1$ equidistant points in a k-dimensional space. In one-dimensional space it is a line segment. For two factors the simplex is an equilateral triangle, for three - a tetrahedron (Fig. 1), etc. This design allows to approximate the required characteristics with the help of a first order polynomial.
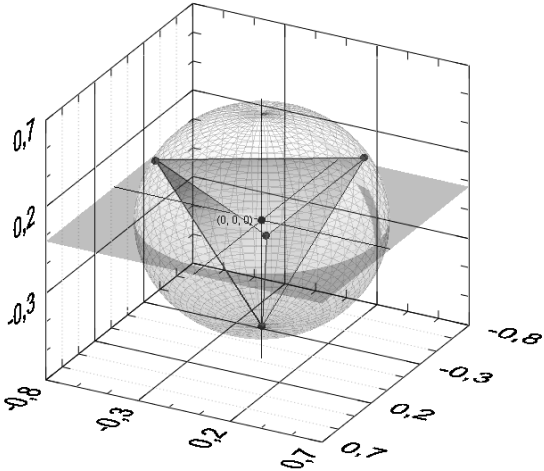

Fig. 1. The first-order simplex-design in the three dimensional factor space geometric interpretation
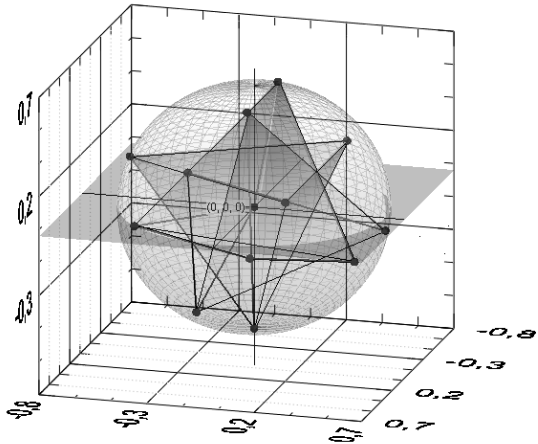
Fig. 2. The third-order simplex-sum design of experiments geometric interpretation in the three-dimensional factor space

The matrix of a simplex in the k-dimensional space can be expressed by the follow equation:

$$X = \begin{bmatrix} x_{11} & x_{12} & \cdot & x_{1(k-1)} & x_{1k} \\ x_{21} & x_{22} & \cdot & x_{2(k-1)} & x_{2k} \\ \cdot & \cdot & \cdot & \cdot & \cdot \\ x_{(m-1)1} & x_{(m-1)2} & \cdot & x_{(m-1)(k-1)} & x_{(m-1)k} \\ x_{m1} & x_{m2} & \cdot & x_{m(k-1)} & x_{mk} \end{bmatrix} = \begin{bmatrix} \vec{x}_1 \\ \vec{x}_2 \\ \cdot \\ \vec{x}_{m-1} \\ \vec{x}_m \end{bmatrix} = \begin{bmatrix} q_1 & q_2 & \cdot & q_{k-1} & q_k \\ -Q_1 & q_2 & \cdot & q_{k-1} & q_k \\ \cdot & \cdot & \cdot & \cdot & \cdot \\ 0 & 0 & \cdot & -Q_{k-1} & q_k \\ 0 & 0 & \cdot & 0 & -Q_k \end{bmatrix},$$

(2)

where $Q_j = \sqrt{\dfrac{j}{2(j+1)}}$ and $q_j = \sqrt{\dfrac{1}{2j(j+1)}}$ – radiuses of the round and inscribed in the j-dimensional simplex spheres ($j = 1,...,k$), respectively.

The matrix X is the design of the $m = k+1$ initial experimental series. The rows of the matrix (k-dimensional vector $\vec{x}_i$, $i = 1,...,m$) are the coordinates of vertices of the regular simplex in k-dimensional factor space. The columns presents the varied factors. This design allows to approximate the required characteristics using a first-order polynomial.

The matrix X of Simplex-Design of experiment has properties of symmetry, normalization, orthogonality, rotatability and D-optimality

In [8] it was proposed to use a regular simplex (2) as a basis for development of composite designs for the second-order polynomial. In addition, these designs can satisfy the requirements of symmetry, normalization and orthogonality, and also possess the properties of rotatability and D-optimality.

3. The Design of experiment for SWS with coupled-cavities-chains

In this work the third-order Simplex-Sum Design of experiment for the physical modeling of coupled-cavities-chain type SWS with bean-shaped slits bond (Fig. 3) (which has eight independent dimensions) EDCs was constructed on the base of developed methodology.
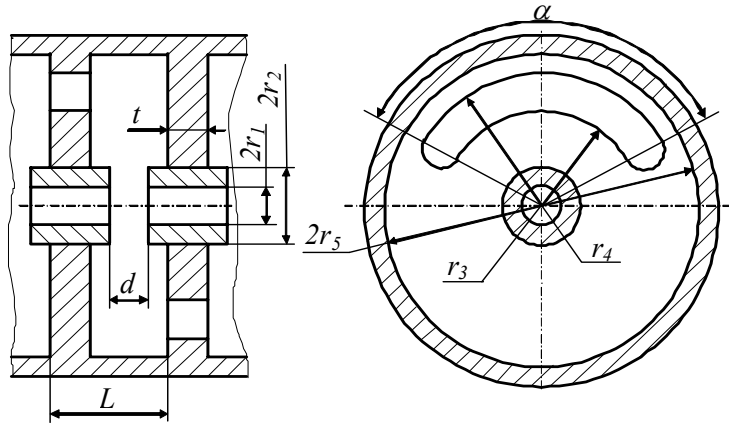

Fig. 3. Longitudinal and transverse sections of an SWS of coupled-cavities-chain type with bean-shaped coupling slots rotated through 180^0 slot: (L) period, (d) gap, (t) diaphragm thickness, ($r1,r2$) inner and outer radius of the drift tube, ($r3,r4$) inner and outer radius of the coupling slot, ($r5$) radius of the cavity, and (α) flare angle of the coupling slot

Regression equation of the response surface is represented as:

$$\eta = \beta_0 + \sum_{i=1}^{8} \beta_i x_i + \sum_{i \leq l}^{8} \beta_{il} x_i x_l + \sum_{i \leq l \leq k}^{8} \beta_{ilk} x_i x_l x_k , \qquad (3)$$

where x_k - independent variable factor; β_i - coefficient of regression.

Sufficiently wide range of factors, that needs to simulate the SWS of different functionality, was chosen (Table 1, 2).

Table 1.
Range of factors variation used in the Design of experiment

	t/L	$2r_5/L$	$r_4/2r_5$	r_3/r_4	α/π	r_2/r_5	r_1/r_2	d/L
min	0,1533	2,5800	0,4270	0,4670	23,5550	0,2082	0,5537	0,2133
max	0,2867	3,5867	0,4830	0,6368	37,8790	0,3047	0,7226	0,4000

Table 2.
The normalized third-order Simplex-Sum Design for SWS

№	t/L	$2r_5/L$	$r_4/2r_5$	r_3/r_4	α/π	r_2/r_5	r_1/r_2	d/L
1	0,2867	3,3667	0,4654	0,5787	0,58333	0,2693	0,6618	0,3467
2	0,1533	3,3667	0,4654	0,5787	0,58333	0,2693	0,6618	0,3467
3	0,2200	2,5800	0,4651	0,5778	0,58333	0,2687	0,6635	0,3467
4	0,2200	3,1067	0,4270	0,5829	0,58333	0,2682	0,6640	0,3467
5	0,2200	3,1067	0,4549	0,4670	0,58333	0,2682	0,6640	0,3467
6	0,2200	3,1067	0,4549	0,5566	0,41111	0,2682	0,6640	0,3467
7	0,2200	3,1067	0,4549	0,5566	0,55556	0,2082	0,6598	0,3467
8	0,2200	3,1067	0,4549	0,5566	0,55556	0,2597	0,5537	0,3467
9	0,2200	3,1067	0,4549	0,5566	0,55556	0,2597	0,6529	0,2133
10	0,2200	3,1067	0,4549	0,5566	0,55556	0,2597	0,6529	0,3333
11	0,2533	3,1333	0,4830	0,5595	0,51111	0,2638	0,6371	0,3333
12	0,1867	3,5867	0,4498	0,5620	0,51111	0,2639	0,6268	0,3333
13	0,1600	2,7067	0,4557	0,5622	0,51111	0,2636	0,6262	0,3333
14	0,2800	2,9733	0,4372	0,5590	0,51111	0,2623	0,6325	0,3333
15	0,2200	3,1067	0,4549	0,6179	0,66111	0,2597	0,6364	0,3333
16	0,2200	3,1067	0,4549	0,4764	0,62222	0,2597	0,6364	0,3333
17	0,2200	3,1067	0,4549	0,5566	0,55556	0,2940	0,7226	0,3333
18	0,2200	3,1067	0,4549	0,5566	0,55556	0,2146	0,7000	0,3333
19	0,2200	3,1067	0,4549	0,5566	0,55556	0,2597	0,6529	0,4000
20	0,1867	3,1333	0,4830	0,5286	0,57056	0,2511	0,6525	0,3133
21	0,2533	3,5867	0,4498	0,5289	0,57056	0,2547	0,6423	0,3133
22	0,1600	2,9733	0,4372	0,5282	0,57056	0,2489	0,6577	0,3133
23	0,2800	2,7067	0,4557	0,5297	0,57056	0,2512	0,6471	0,3133
24	0,2200	3,1067	0,4549	0,5849	0,41111	0,2489	0,6552	0,3133
25	0,2200	3,1067	0,4549	0,6368	0,62222	0,2489	0,6552	0,3133
26	0,2200	3,1067	0,4549	0,5566	0,55556	0,2790	0,5615	0,3133
27	0,2200	3,1067	0,4549	0,5566	0,55556	0,3047	0,6972	0,3133
28	0,2200	3,1067	0,4549	0,5566	0,55556	0,2597	0,6529	0,3800

As evident from the table 2 the Design contains 28 experiments that allows to construct a third-order polynomial model.

The design of experiment in natural sizes, rounded taking into account technological tolerances for manufacturing, is presented in table 3.

Table 3.
The third-order Simplex-Design of experiment for the SWS of coupled-cavities-chain type simulation

№	L, mm	t, mm	$2r_5, mm$	r_4, mm	r_3, mm	$\alpha, degree$	$2r_2, mm$	$2r_1, mm$	d, mm
1	15.0	4,3	50,5	23,5	13,6	105,0	13,6	9,0	5,2
2	15.0	2,3	50,5	23,5	13,6	105,0	13,6	9,0	5,2
3	15.0	3,3	38,7	18,0	10,4	105,0	10,4	6,9	5,2
4	15.0	3,3	46,6	19,9	11,6	105,0	12,5	8,3	5,2
5	15.0	3,3	46,6	21,2	9,9	105,0	12,5	8,3	5,2
6	15.0	3,3	46,6	21,2	11,8	74,0	12,5	8,3	5,2
7	15.0	3,3	46,6	21,2	11,8	100,0	9,7	6,4	5,2
8	15.0	3,3	46,6	21,2	11,8	100,0	12,1	6,7	5,2
9	15.0	3,3	46,6	21,2	11,8	100,0	12,1	7,9	3,2
10	15.0	3,3	46,6	21,2	11,8	100,0	12,1	7,9	5,0
11	15.0	3,8	47,0	22,7	12,7	92,0	12,4	7,9	5,0
12	15.0	2,8	53,8	24,2	13,6	92,0	14,2	8,9	5,0
13	15.0	2,4	40,6	18,5	10,4	92,0	10,7	6,7	5,0
14	15.0	4,2	44,6	19,5	10,9	92,0	11,7	7,4	5,0
15	15.0	3,3	46,6	21,2	13,1	119,0	12,1	7,7	5,0
16	15.0	3,3	46,6	21,2	10,1	112,0	12,1	7,7	5,0
17	15.0	3,3	46,6	21,2	11,8	100,0	13,7	9,9	5,0
18	15.0	3,3	46,6	21,2	11,8	100,0	10,0	7,0	5,0
19	15.0	3,3	46,6	21,2	11,8	100,0	12,1	7,9	6,0
20	15.0	2,8	47,0	22,7	12,0	102,7	11,8	7,7	4,7
21	15.0	3,8	53,8	24,2	12,8	102,7	13,7	8,8	4,7
22	15.0	2,4	44,6	19,5	10,3	102,7	11,1	7,3	4,7
23	15.0	4,2	40,6	18,5	9,8	102,7	10,2	6,6	4,7
24	15.0	3,3	46,6	21,2	12,4	74,0	11,6	7,6	4,7
25	15.0	3,3	46,6	21,2	13,5	112,0	11,6	7,6	4,7
26	15.0	3,3	46,6	21,2	11,8	100,0	13,0	7,3	4,7
27	15.0	3,3	46,6	21,2	11,8	100,0	14,2	9,9	4,7
28	15.0	3,3	46,6	21,2	11,8	100,0	12,1	7,9	5,7

Rounding leads to optimal properties modification, therefore its assessment was realized (results are presented in the table 4).

Table 4.
Comparison of design properties before and after rounding

Properties of Design		Design constructing with machine precision	Design taking into account of machine's capabilities
Symmetry	$\sum\limits_{i=1}^{n} x_{ij}$	$10^{-16} \div 10^{-17}$	0
Orthogonality	$\sum\limits_{i=1}^{n} x_{ij} x_{il}$	$10^{-17} \div 10^{-18}$	$10^{-15} \div 10^{-3}$
Rotatability	$X_i^T M^{-1} X_i$	0.2963 ± 10^{-4}	0.2963 ± 10^{-3}
D-optimality	$\det\left(X^T X\right)^{-1}$	0.0391	0.0393

Thus as it is shown in table. 4 properties of the experimental Design, taking into account technological tolerances, are close to optimum, i.e. it can be used for SWS EDCs modeling.

4. Results

As a result of this work the method of *n*-th order Simplex-Sum Designs constructing for numerical or physical experiments on modeling EDCs of the SWS of coupled-cavities-chain type using polynomials of higher order was developed. The algorithm of method is implemented in the graphical programming environment *LabVIEW 8.5*.

The third order simplex-design for the SWS of coupled-cavities-chain type with bean-shaped coupling slots rotated through 180° connection for the wide range of factors variation was constructed.

The properties assessment of experimental design was done with taking into account technological tolerances for manufacturing measurements. Its suitability was demonstrated. Developed design is proposed to be used in SWS EDCs modeling.

REFERENCES

1. Batura, M.P., Kuraev, A.A., Sinitsyn, A.K. Modeling and optimization of high-power microwave devices. Minsk. 2006.
2. Nalimov, V. V. The theory of experiment. M: Science, 1971.
3. Golikova, T. I., Panchenko, L. A. Systematics of designs to evaluate the second-order polynomial models // Optimal experiments designing. Moscow University Press, 1975. V. 48. P, 106 – 149.
4. Adler, Yu.P., Markova, E.V., Granovsky Y.V. Designing an experiment in the search for optimal conditions. M.: Nauka, 1976.
5. Box, G.E.P., Behnken, D.W. (1960) Simplex-sum designs: a class of second order rotatable designs derivable from those of first order. Ann. Math. Statistics. V. 31. No. 4. P. 838.
6. Kiefer J. Optimum experimental designs. Journal of the Royal Statistical Society. Ser, 21 No. 2. P. 272.
7. Kiefer J. Optimum designs in regression problems, II. // Annals of Mathematical Statistics. 1961. V. 32. No. 1 P. 298.
8. Gorsky, V.G., Brodsky, V.Z. Simplex method of the extreme experiments designing // Factory laboratory. 1965. V. 31. No. 7. P. 831-836.
9. Savin, A.N. Research of the vacuum electronics and magnetic microwave devices EDCs on the base of regression models. SSU Press, 2003.

POWER MULTIBEAM MONOTRON GENERATOR WITH DISTRIBUTED INTERACTION CAVITY

N.A. Akafyeva

Saratov State Technical University, Saratov, 410054, Russia
E-mail: *akafieva_na@mail.ru*

Abstract - The main goal of this publication is computational modeling of operating conditions and determination of optimal parameters for four-gap resonator with cophased oscillation mode that provides maximum value of electronic efficiency for multibeam monotron. A monotron generator that has multibeam structure and common four-gap resonator be able to provide high efficiency and output power, small overall dimensions and weight.

1. Introduction

Nowadays the development of high power microwave devices with a small mass and simple structure is getting great attention due to their possible application as a high power RF generators for different technological process (drying, defrosting, vulcanization, pasteurization, caking, destruction of materials, baking), where required power of continuous operation is up hundreds kilowatts. In addition they can be applied as a power generator in the charged particle accelerators. One kind of like devices is monotron - a high-power floating-drift generator with single cavity. Monotron may be utilized as high power microwave device for industrial and technological applications.

The traditional monotron generator with homogenous RF field in cavity's gap has low efficiency (2-5%) [1].

In relevant publications that devoted monotron generators with single one-gap cavity and heterogeneous RF field we can reveal if the RF field has the optimal distribution function in interaction area the efficiency is around 20% [2]. This value is actually if multibeam or circular stream used. More value of monotron generators efficiency (up to 50%) can be obtained if a two-gap cavity with different magnitude of electrical field in gaps is utilized [3]. The results of calculations are shown that like value of efficiency can be reached in the output gap cavity only at high magnitude of RF voltage. But this condition restricts a maximum output power such devices because of strong dependence of energy relations to signal level.

Thereby the research of availability of a three-gap and a four-gap cavity with 2π-mode, π-mode for applying in monotron generator with high efficiency is appropriately.

2. Mathematical simulation

The conditions of high efficiency are good grouping of beam, that is characterized by high magnitude of circulating current, effective magnitude RF field intensity in initial interaction area must be considerably less than field intensity in extraction of energy area (RF field must be increasing in direction of beam movement), low initial velocity spread and space charge in the beam.

Hereby, the main tasks of research are:
- Investigation of process interaction in different cavities types (three- and four-gaps);
- Investigations of electrons interaction features with RF field at different field distribution function along interaction area;
- Influence of space charge at the efficiency.

As a result of this stage of research a mathematical simulation of electrodynamic system has been made. The object of research was a four-gap resonant system operating in

2π-mode. Method of investigation - mathematical simulation of a physical process in electrodynamic system with «AZIMUTH» code [4].

Thereby the optimal construction of a four-gap cavity was found that has following parameters: resonance frequency 2450 GHz, characteristic impedance 83 Ohm, unloaded Q-factor- 3500, operation mode E_{040}.

Following functions field distribution in a discrete gap cavity that was synthesized in code «AZIMUTH» shown at figures 1-3.
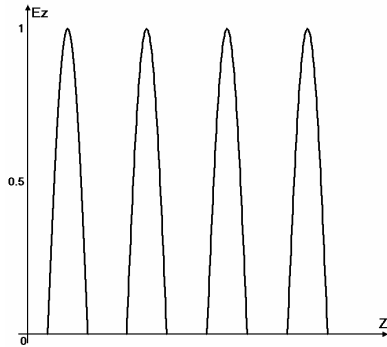

Fig. 1. Homogenous field distribution: $U_1/U_4=U_2/U_4=U_3/U_4=1.0$
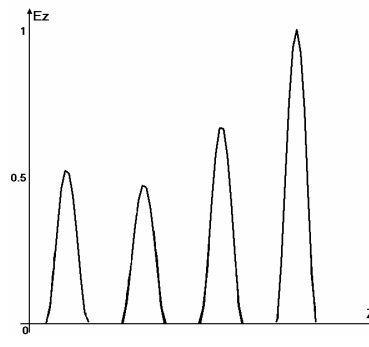
Fig. 2. Heterogeneous field distribution: $U_1/U_4=0.52$, $U_2/U_4=0.47$, $U_3/U_4=0.68$
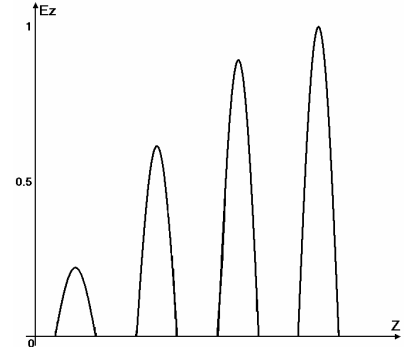
Fig. 3. Optimal field distribution: $U_1/U_4=0.22$, $U_2/U_4=0.6$, $U_3/U_4= 0.89$

For various values ξ ($\xi=\tilde{U}/U_0$, where $\tilde{U}$- relative amplitude of RF voltage in cavity; U_0-accelerating voltage) the dependences of a first harmonic normalized amplitude of convection current and a electron efficiency (η_e) against accelerating voltage was found using «DISKLY» code (fig.4,5) [5]. These curves correspond to field distributions (fig.1-3).
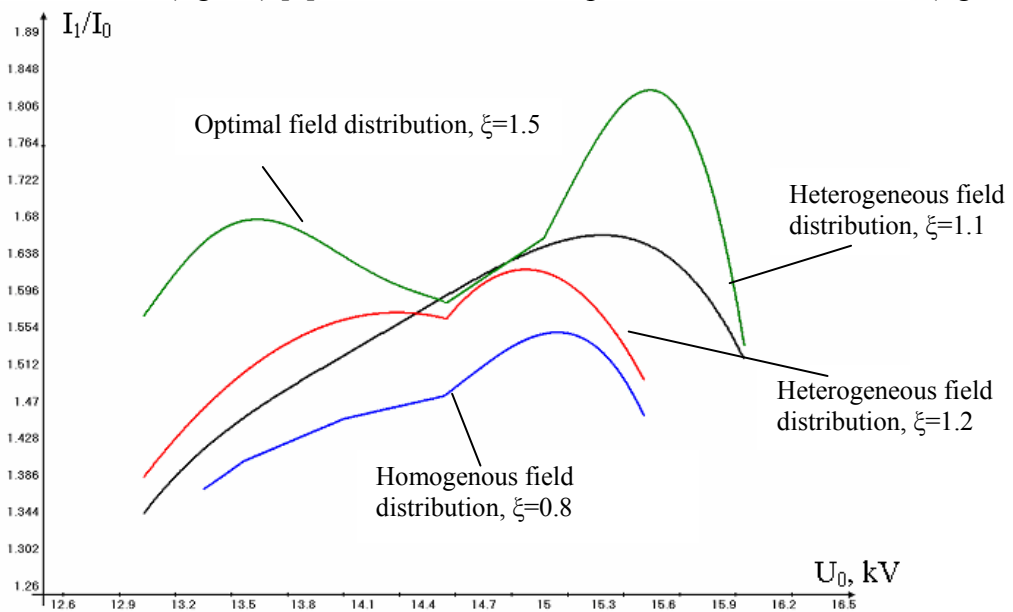
Fig.4. The dependences of first harmonic normalized amplitude of convection current as function of the accelerating voltage

The results of investigations shown that for homogenous field a maximum of a convection current $I_{1max}/I_0 = 1.55$ is reached for $U_0=15$ Kv at $\xi=0.8$; with increasing ξ ($\xi>0.8$) a regrouping of electron beam is occurred accordingly maximum of convection

current shifts in side of third gap and extraction of energy occurred in the third gap. Therefore such field distribution is not effective.

For heterogeneous field (Fig.2) a maximum of convection current $I_{1max}/I_0 = 1.6$ is reached at $U_0 = 15.3$ Kv, $\xi = 1.1$; at $\xi > 1.2$ and extraction of energy occurred in third gap.

For optimal distribution function (Fig.3), maximum of convection current $I_{1max}/I_0 = 1.8$ is reached at $U_0 = 15.5$ Kv, $\xi = 1.5$; at $\xi > 1.5$ and extraction of energy occurred in third gap.

Therefore a numerical experiments shown that an optimal operating condition for this device is where additional grouping and energy extracting combine in two last gaps. The evidence of this supposition is dependence of normalized amplitude of first harmonic convection current (Fig.4).
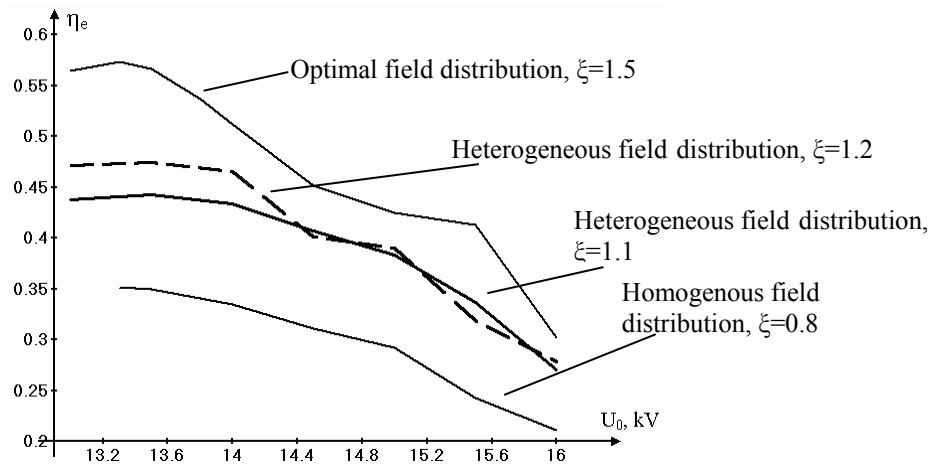
Fig. 5. Dependence of electron efficiency against accelerating voltage

The maximum value of a electron efficiency that can be reached in such a four-gap cavity structure operating at 2π-mode for homogenous field is approximately 35% and 48% for heterogeneous field at $U_1/U_4 = 0.52$, $U_2/U_4 = 0.47$, $U_3/U_4 = 0.68$. For optimal field distribution with a relative voltage amplitude $U_1/U_4 = 0.22$, $U_2/U_4 = 0.6$, $U_3/U_4 = 0.89$ efficiency is 60%.

3. Conclusions

The quality of investigated electrodynamic system is high efficiency that reached on condition that electrical strength of cavity doesn't disturb. More cavity output power can be reached with using annular or a multibeam electron-optical system with a high summary perveance that allowed decreasing accelerating voltage, overall dimensions and mass of device. Utilizing one cavity will allowed making adjusting of device at resonance frequency more easy in comparison with multiple-cavity klystron.

REFERENCES

1. Müller J.J., Rostas E. Un générateur à temps de transit utilisant un seul résonateur de volume // Helv. Phys. Acta. 1940. V. 13. No. 3. P. 435-450.

2. Barroso J.J. Design facts in the axial monotron // IEEE Trans. Plasma Sci. 2000. V. 28. No. 3. P. 652-656.

3. Fedyaev V.K., Gorlin O.A. Microwave generator with a double-gap cavity // Electronics and vacuum engineering. Devices and equipments. Technology: Proceedings of the conference. Saratov: Saratov State University, 2007. P. 73-74.

4. Grigoriev A.D., Silaev S.A. Calculation of the azimuthally-heterogeneous electromagnetic field modes for axially symmetric cavities with a random form of generating line // Sov. Electron Tech. Microw. Electron. 1981. No. 2. P. 62-65.

5. Teryaev V.E. DISKLY code for calculation and optimization of klystrons // Proc. Int. Workshop on Pulsed RF Power Sources for Linear Colliders (RF-93).1993. P. 161-166.

ENVELOPEE SOLITONS IN PERIODIC FERROMAGNETIC STRUCTURES AT EXCITATION OF MAGNETOSTOTIC WAVES NEAR THE BAND-GAP

M.A. Morozova, *Member IEEE*, Yu.P. Sharaevskii, *Member IEEE,* S.E. Sheshukova

Saratov State University, Saratov, 410012, Russia
E-mail: *SheshukovaSE@yandex.ru*

Abstract — The features of envelope solitons formation in one-dimensional periodic ferromagnetic structure were considered. The model based on the coupled nonlinear Schrodinger equations was used for investigation. The parameter space showing the region, in which the solitons similar to Bragg solitons with different features can form, was calculated. The mechanisms of the formation of the solitons localized on the limited length of the structure were considered.

1. Introduction

At the present time investigation of the envelope solitons (localized wave packets) are of a great interest. This type of solitons can be formed from a pulses propagating in different medium with nonlinearity and dispersion [1]. A new type of solitons, called Bragg soliton, or the gap solitons can be formed in nonlinear media whose properties vary periodically in the definite direction with length [2]. The photonic crystals are an example of such media in optics. In this structure the refractive index is a periodic function of spatial coordinates [3]. The investigation of Bragg solitons are of interest not only from a fundamental point of view, but also have great potential for practical use of such structures in telecommunications systems, in optical communication lines [4].

In recent years, due to advances in the technology of thin-film magnetic materials raising and a new approaches to obtain periodic structures the production of crystals, based on the magnetic materials — magnon crystals (such as photonic crystal) represent a great interest. The magnon crystals where spin waves propagate are similar to the photonic crystal [5,6].The magnon crystals have a number of significant advantages compared to the photonic crystals: the ability to manage their properties by an external magnetic field and to use a planar technology, and moreover crystals creation with magnon band gap at microwave frequencies (the order of several millimeters). The nonlinear effects in ferromagnetic films appear at relatively low power levels [6].

The magnon crystals by analogy with the photonic crystals demonstrate more interesting nonlinear phenomena in comparison with the effects observed in homogeneous ferromagnetic films. However, we can conclude that the nonlinear processes in such periodic structures, including those associated with the peculiarities of formation of solitons are investigated insufficiently. You can specify only some work in this direction [7-9], which shows the experimental and numerical simulation results based on a one-dimensional nonlinear Schrödinger equation (NSE). The coefficients of dispersion and nonlinearity, which were calculated based on the assumption that only
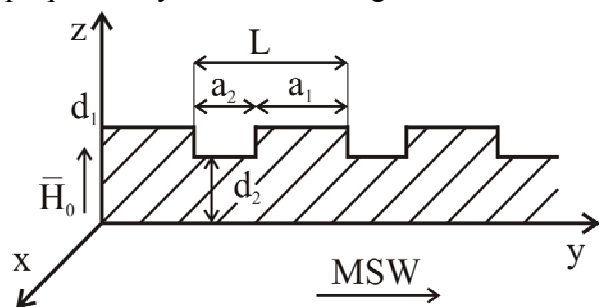

Fig.1. The scheme of periodic ferromagnetic structure with the geometrical sizes: L – period; d_1 – thickness of a film; $\Delta d = d_1 - d_2$ – depth of a groove; $a_2 = L - a_1$ – width of a groove

one magnetostatic wave propagates in the ferromagnetic film. The dispersion of this wave depends on the parameters of the periodic structure.

The coupled-mode theory was used for investigation fiber-optic gratings [3]. The essence of this method lies in the fact that the nonlinear wave processes in such structures, mainly due to a superposition of incident and reflected waves. The system of coupled NSE was used to describe this structure. In this case the use of one NLS is a simplified approach to describe a nonlinear dynamics of periodic structures.

The aim of this work was to investigate the features of formation the solitons are similar to a Bragg solitons in the ferromagnetic one-dimensional periodic structure. The system of coupled nonlinear Schrödinger equations for the amplitude envelopee of the forward and backward waves was used for numerical simulation. We pay great attention to the conditions of formation of solitons, such as Bragg or gap solitons.

2. Theoretical model

A one-dimensional periodic ferromagnetic structure (magnon crystal) was considered. The structure is infinite in the direction of the x and y (Fig.1). The constant magnetic field is applied perpendicular to the film plane. The value of this field $\vec{H}_0$ was chosen in such a way that the forward volume MSW (FVMSW) propagated in the y direction. The dispersion equation for FVMSW in a homogeneous ferromagnetic film, loaded with the two semi-infinite dielectric layers, can be written as [10]:

$$\text{tg}\left(\xi k d\right) = \frac{2\xi}{\xi^2 - 1}, \tag{1}$$

where $\xi^2 = \dfrac{\omega^2 - \omega_H\left(\omega_H + \omega_M\right)}{\omega_H^2 - \omega^2}$, ω is a frequency of the signal, $\omega_H = \gamma H_0$, $\omega_M = 4\pi\gamma M_0$, M_0 — saturation magnetization, γ — gyromagnetic ratio, k — propagation constant for a FVMSW, d — film thickness.

Fig.2. The dispersive diagram ($\text{Re}\left(\Omega(KL)\right)$ - curves 1, $\text{Im}\left(\Omega(KL)\right)$ - curves 2, $\Omega = \omega/\omega_H$) of a periodic structure at $\Omega_M = 2$, $a_1 = 0.5$, $d_1 = 0.1$, $d_2 = 0.08$

Following to [6,11], a dispersion relation for the one-dimensional system consisting of alternating layers of two media with different velocities of wave propagation can be written as:

$$\cos\left(KL\right) = \cos\left(k_1\left(\omega\right)a_1\right)\cos\left(k_2\left(\omega\right)a_2\right) - \frac{k_1^2\left(\omega\right) + k_2^2\left(\omega\right)}{2k_1\left(\omega\right)k_2\left(\omega\right)}\sin\left(k_1\left(\omega\right)a_1\right)\sin\left(k_2\left(\omega\right)a_2\right), \tag{2}$$

where k is wavenumber for a wave propagating in the structure with the period $L = a_1 + a_2$, a_2 — width of the groove, functions $k_1\left(\omega\right)$, $k_2\left(\omega\right)$ is dispersion relations of FVMSW for films thicknesses d_1 and d_2, correspondingly. These functions were determined by the ratio (1).

The results of numerical solution of equations (1) and (2) were shown in Fig. 2 (with determinate geometric dimensions of the one-dimensional periodic structure). It shows the behavior of the real and imaginary parts of KL in the FVMSW pass band with varying frequency $\Omega = \omega/\omega_H$. The geometric dimensions of the structure are normalized to the
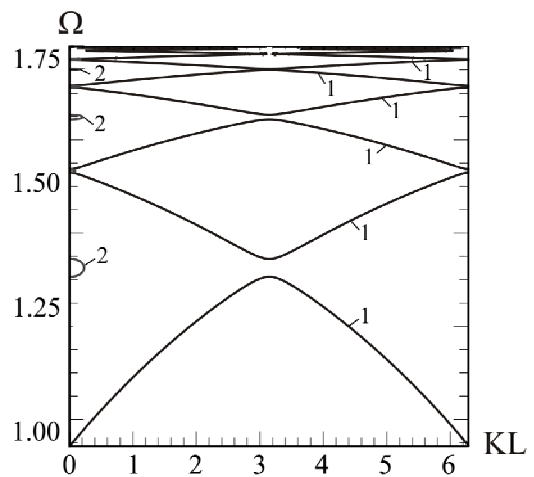
period of the structure $L=1$. As seen in Fig. 2, the periodicity of the structure leads to the appearance of a band gaps on the dispersion characteristics for $KL = \pi$. From the last condition (Bragg condition) follow that $K_B = \dfrac{\pi}{L} = \dfrac{2\pi}{\lambda_B}$, where K_B and λ_B are the Bragg propagation constant and the wavelength, respectively.

The Bragg condition provides the addition of a weak reflected wave on a phase along the entire length of the lattice. It leads to an effective reflection of the incident wave. To construct a nonlinear model of the periodic structure of the ferromagnetic use, similar to optical systems [3,4], coupled-wave approximation and represent the distribution of the magnetostatic potential near the gap as the sum of forward and backward waves:

$$\psi(y,t) = \varphi_f(y,t)\exp\big(i(\omega t - K_B y)\big) + \varphi_b(y,t)\exp\big(i(\omega t + K_B y)\big), \qquad (3)$$

where $\varphi_f(y,t)$, $\varphi_b(y,t)$ are slowly varying complex envelopes of the forward (incident) and backward (reflected) waves, respectively.

Taking into account [3] in the approximation of weak nonlinearity the nonlinear equations for the envelopes of direct and reflected waves can be represented as:

$$\begin{cases} i\left(\dfrac{\partial \varphi_f}{\partial t} + V_g \dfrac{\partial \varphi_f}{\partial y}\right) - \beta \dfrac{\partial^2 \varphi_f}{\partial y^2} + \eta\varphi_f + \chi\varphi_b + \gamma\left(\left|\varphi_f\right|^2 + 2\left|\varphi_b\right|^2\right)\varphi_f = 0 \\[4mm] i\left(\dfrac{\partial \varphi_b}{\partial t} - V_g \dfrac{\partial \varphi_b}{\partial y}\right) - \beta \dfrac{\partial^2 \varphi_b}{\partial y^2} + \eta\varphi_b + \chi\varphi_f + \gamma\left(\left|\varphi_b\right|^2 + 2\left|\varphi_f\right|^2\right)\varphi_b = 0 \end{cases}, \qquad (3)$$

where V_g — group velocity, $\eta = \omega_0 - \omega_B$ — detuning ($\omega_B = K_B V_{ph}$, V_{ph} — MSW phase velocity in homogenous structure), β — coefficient of dispersion, χ — coefficient of coupling, γ — nonlinear coefficient.

Equations (4) are similar to the system of two coupled nonlinear Schrödinger equations describing the propagation of the direct and reflected waves in Bragg optical lattices [2-4]. It should be noted that the system (4) without taking into account the dispersion ($\beta = 0$), as shown in the [3], may have soliton solutions — the family of Bragg solitons. This type of soliton represents a combination of two waves moving together or remaining in place. If $\varphi_f(y,t) = \varphi_b(y,t)$ soliton does not move — a stationary gap soliton.

In the case of excitation of magnetostatic waves with a carrier frequency near to the band gap, the dispersion medium plays more important role than the dispersion caused by the structure's periodicity. Moreover, the coupling parameter, the coefficient of dispersion and nonlinearity depend on the type of MSW excited in a ferromagnetic film (on the direction of the external magnetic field $\vec{H}_0$) significantly.

When FVMSW was excited in a periodic structure the coefficient $\beta = \partial^2\omega/\partial k^2$ and the group velocity $V_g = \partial\omega/\partial k$ were calculated if the thickness of the lattice $d = d_0 = \dfrac{a_1 d_1 + a_2 d_2}{L}$ is the effective thickness. The nonlinear coefficient for FVMSW at $kd <<< 1$ is $\gamma = -\dfrac{1}{4}\left(1 + \dfrac{\omega^2}{\omega_H^2}\right)\left(\dfrac{kd}{2}\right)^2$ [10].

To calculate the coupling coefficient, we assume that the thickness of the film in the direction of wave propagation in periodic structure is described by the expression:

$$d = d_2 + \delta(y), \qquad (5)$$

where $\delta(y) = \delta(y+L) = \begin{cases} \Delta d = d_1 - d_2, & 0 \le y \le a_1, \\ 0, & a_1 \le y \le L, \ L = a_1 + a_2. \end{cases}$

74

The function $\delta(y)$ was expanded in a Fourier series and **restricting the expansion** coefficients with $n = 0, \pm 1,$ the relation (5) can be represented as:

$$d = d_0 \left[1 + \delta d \, \cos\left(\frac{2\pi}{L} y \right) \right],$$ (6)

where $\delta d = \dfrac{2\Delta d}{\pi d_0} \sin \dfrac{\pi a_1}{L}$.

Taking into account the relation (6) the coupling parameter for a one-dimensional periodic lattice of 1-th order for $kd_0 \ll 1$ can be written as:

$$\chi = \frac{\pi V_g}{\lambda} \delta d \,,$$ (7)

where λ is a wavelength of FVMSW at the frequency ω.

3. Simulation results

The results relating to the formation of solitons in this system were obtained based on the numerical solution of the coupled system of the NSE (4) using a SSFM method [3]. The coefficients in (4) were calculated taking into account the relations (1), (7) and were accepted as $\beta = -2 \cdot 10^4 \ cm^2 \cdot s^{-1}$, $\gamma = 3 \cdot 10^{10} \ s^{-1}$, $\delta = 1 \cdot 10^6 \ s^{-1}$. The pulse was specified only on a forward wave as the initial conditions $\varphi_{0f} = \varphi_0 \exp\left(-y^2 / y_{imp}^2 \right)$, $\varphi_{0b} = 0$, where y_{imp} - pulse width, φ_0 — dimensionless pulse amplitude during the initial moment of time which got out above a soliton threshold [3].

We consider the features of the wave evolution at a fixed value V_g depending on the parameter χ. This parameter characterizes the geometrical parameters of the periodic structure and the relationship between the forward and backward waves, accordingly. The extreme case (when $\chi = 0$) corresponds to a homogeneous film ($a_1 = 0$) and the backward wave is not excited in the structure. When $\chi \neq 0$, a linear relationship leads to the exchange of power between the waves. In this case the backward wave is excited and the solitons are formed, such as Bragg solitons. The parameter space (V_g, χ) corresponding to the solitons formation with a different features is shown in Fig. 3. The parameter space corresponding to solitons, which move with some velocity $V_c < V_g$, is shown in white color. The parameter space corresponding to the solitons remained localized on the limited length of structure is shown in gray color on the Fig. 3. Figure 4 demonstrate the dynamic of the solitons formation for parameters values conformable to the point 1 on the Fig. 3. For small values χ there
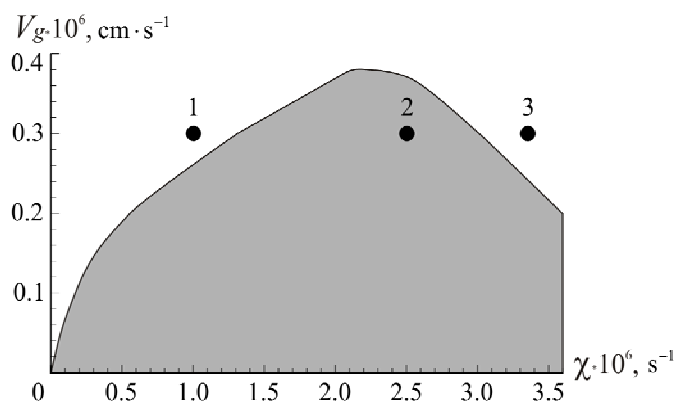

Fig.3. The parameter space (χ, V_g), corresponding to envelope soliton formation

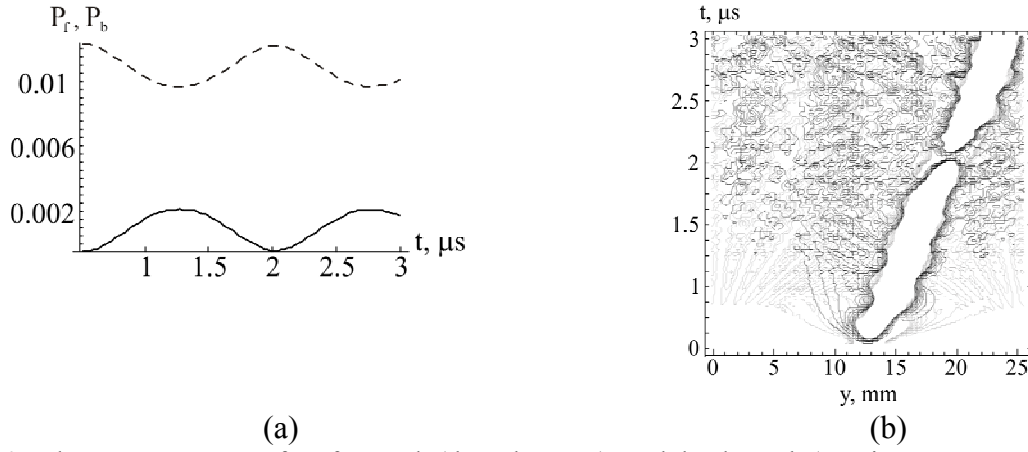(a)   (b)

Fig. 4. The power swap of a forward (dotted curve) and backward (continuous curve) waves eventually (a); lines of equal level of envelope amplitudes for φ_f (it is shown by grey color) and φ_b (is shown by black) (b) at $\chi = 1\ 10^6\,\text{s}^{-1}$ ($V_g = 0.3\ 10^6\,\text{cm/s}$)

is incomplete transfer of power of the forward wave $P_f = \int_0^l |\varphi_f|^2\, dy$ into the backward wave

$P_b = \int_0^l |\varphi_b|^2\, dy$, where l — length of a structure (Fig. 4 a). The forward wave dominates and solitons are moving in the positive direction of axe y at a velocity $V_c < V_g$ (Fig. 4 b). Figure 5 demonstrate the dynamic of the solitons formation for parameters values conformable to the point 2 on the Fig. 3. The complete power swap between waves with period T was observed (Fig. 5a). Thus on a forward wave it is formed soliton, moving in a positive direction of axe y (Fig. 5c). Figure 5d demonstrates that its power proceed to the soliton on the forward wave, traveling to the same direction. After the time cell $T/2$ the power of these solitons turns equal and solitons moving decease. Thus the solitons change its propagation direction periodically in time, and move to the direction of the major power wave. Ones can notice some «kinking» of the solitons, but nevertheless it remains to be localized on the certain limited structure length. The period T decreases and «zigzags» become smooth with the increasing of χ, and solitons can exist without moving ($V_c = 0$). In the parameter space situated on the right of the gray area (point 3 on the Fig. 3), solitons are not also localized in space and travels with the some velocity. This phenomenon can be explained by that the period T get minor in comparison with soliton period $T_c \approx 1/\varphi_o$ [4], it leads to the power swap periodicity disturb, and provokes the solitons moving.

At increase in V_g power swapping V_g becomes less effective (period T decreases and swapping becomes incomplete), that leads to a pulling down of pulses at increase in V_g.

4. Conclusion

In this paper with use of model in the form of coupled nonlinear Schrodinger equations for the envelope amplitude forward and backward waves are calculated the parameter spaces of periodic ferromagnetic structure corresponding to solitons, similar Bragg solitons, with different properties. In particular, the basic mechanism of formation of soliton, similar Bragg soliton, and localized on the limited length of structure, is mutual capture of pulses on forward and backward waves, which move with the cumulative velocity (velocity, in turn, it is defined by relative power of two waves), and presence of power swapping between forward
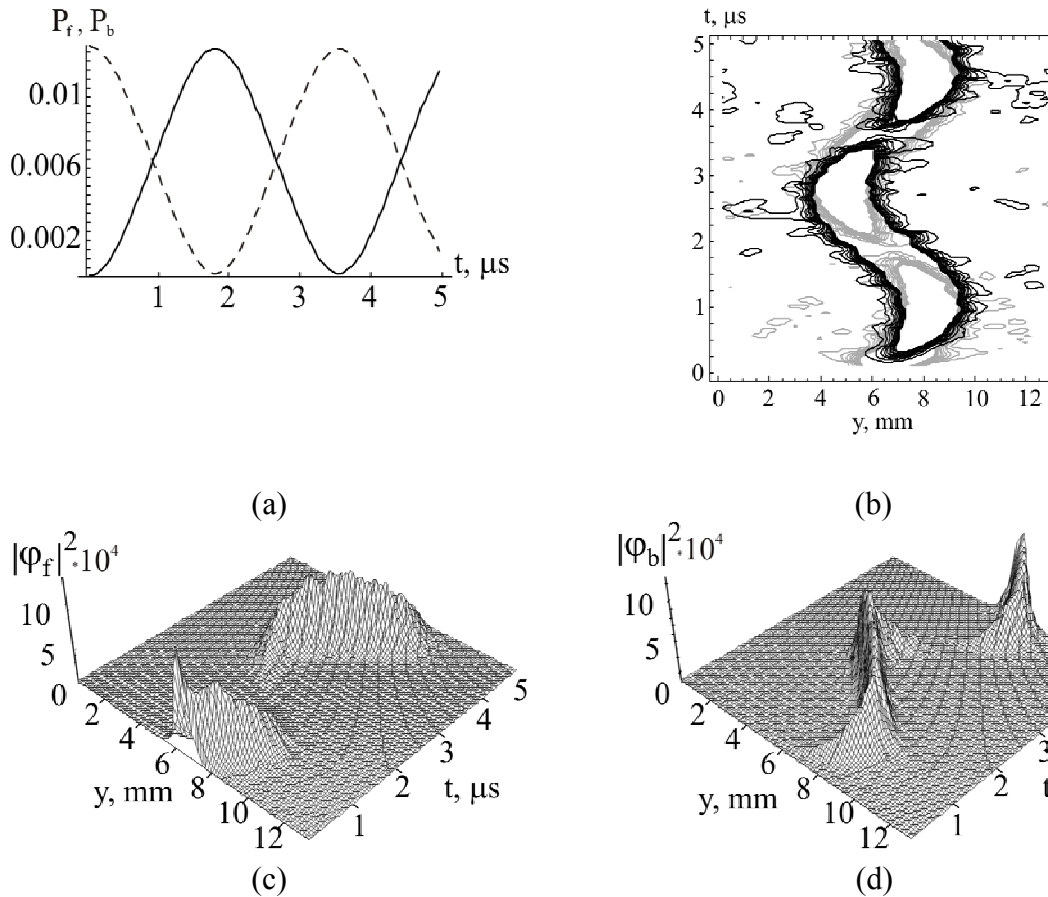
(a)

(b)

(c)

(d)

Fig.5. The power swap of a forward (dotted curve) and backward (continuous curve) waves eventually (a); lines of equal level of envelope amplitudes for φ_f (shown by grey color) and φ_b (shown by black) (b); the space-time evolution envelope amplitude φ_f (c) and φ_b (d) at $\chi = 2.5$ $10^6 \, s^{-1}$ ($V_g = 0.3 \, 10^6 \, cm/s$)

and backward waves which is defined by value coupling between waves. Features of wave evolution depending on coupling parameter and group velocity and the areas of parameters corresponding to formation of pulses, similar to Bragg solitons and localized on the limited length of structure, are investigated.

REFERENCES

1. Akhmediev N.N., Ankevich A. Solitons. Nonlinear pulses and beams. M.: Fizmatlit. 2003. 299 p.
2. Malomed B.A. Soliton management in periodic systems. M.: Fizmatlit. 2009. 192 p.
3. Kivshar J.S., Agrawal G.P. Optical solitons. From fibers to photonic crystals. M.: Fizmatlit. 2005. 648 p.
4. Agrawal G.P. Lightwave Technology. Telecommunication. New Jersey: John Wiley and Sons. 2005. 461 p.

5. Lyubchanskii I.L., Dadoenkova N.N., Lyubchanskii M.I., Shapovalov E.A. and Rasing Th. // J. Phys. D: Appl. Phys. 2003. V. 26. P. 277-287.
6. Guljaev J.V., Nikitov S.A., Zhivotovskii L.V. // JETP Lett. 2003. V. 77. No. 10. P. 670-674.
7. Niu-Niu Chen, Slavin A.N., Cottam M.G. // Phys. Rev. B. 1993. V. 47. P.8667.
8. Ustinov A.B., Grigoreva N.J., Kalinikos B.A. // JETP Lett. 2008. V. 88. No. P. 34-39.
9. Drozdovskij A.V., Cherkasskii M.A., Ustinov A.B., Kovshikov N.G., Kalinikos B.A. // JETP Lett. 2010. V. 91. No. 1. P. 17-22.
10. Vashkovskii A.V., Stalmakhov V.S., Sharaevskii Yu.P. Magnetostatic waves in microwave electronics. Saratov: SSU. 1993. 312 p.
11. Vinogradova M.B, Rudenko O.V, Sukhorukov A.P. Wave theory. M.: Nauka. 1979. 383 p.

METALLIC WIRE PHOTINIC CRYSTALS: ANALYSIS OF ELECTROPHYSICAL PROPERTIES

M.V. Davidovich, *Senior Member IEEE,* J.V.Stephuk, P.A. Shilovsky

Saratov State University, 410012, Saratov, Russia
E-mail *DavidovichMV@info.sgu.ru*

Abstract – The simplest wire metallic photonic crystals have been investigated using the electromagnetic simulations based on the periodic Green's function and integral equation approach. The permittivity tensor has been obtained and explored by using the homogenization for the solutions which correspond to lowest dispersion branches.

Introduction

The wire metallic photonic crystals (MPC) are widely investigated during recent three decades in connection with the availability of several their specific and unusual for natural media properties, in connection with the possibility to get the artificial media (metamaterials) with magnetic characteristics, with negative real part of permittivity or both permittivity and permeability, and also because of creation on its usage some filtering. waveguide, focusing, matching and others devices [1-28]. There are following unusual MPC properties: the strong spatial and time (frequency) dispersions, the negative refraction, bianisotropy. These properties take place from microwaves to optical waves. We understand any periodically located metallic objects or such objects periodically embedded into dielectric matrix (background) when we say about MPC. We assume for simplicity that the background is the homogeneous dispersionless (so, the lossless) and with real scalar permittivity ε. From numerous objects of research, which were earlier have been considered in a great number of works devoted to MPC, we choose the elementary simplest linear noncontacting wire inclusions. Such MPC are anisotropic, but they have not bianisotropy and the magnetic properties (in thin wire approach). The similar choice is caused by the fact that the rigorous electrodynamic analysis of similar structures is highly not simple. Most investigations of MPC are based on different approximate models, or by several software tools (which usually are constructed on finite difference or finite-elements methods).

We have used the approach based on the periodic Green's function (GF) and integrodifferential or integral equation methods (IE) (see [29,30]). We also use the thin wire approximation. This means that their radius r much smaller of all structure dimensions. And, at the same time, the transverse (or azimuthal) current components (and correspondingly the magnetic properties) may be neglected and the problem may be reduced to one-dimensional IE. The one out from three homogenization methods earlier developed in [31-36] has been applied, that allows one to get the effective electrophysical parameters of structures. It is the effective permittivity tensor (EPT) in our case. The accent here has been made to receive the analytical results. The rigorous numerical models for any prescribed accuracy are also were considered. The paper results have been compared with the data of similar publications.

1. Problem statement

Let's consider the three-dimensional (3-D) periodic MPC consisting from thin metallic wires of length l and radius r, which are periodically embedded in dielectric background with permittivity ε and located in Cartesian system x, y, z with

corresponded periods a, b and c (fig. 1). The wires are thin, so $r \ll l$, $r \ll \min(a,b,c)$. As the particular case let us also consider the two-periodic (2-D) such MPC with infinitely long wires (with infinitely large period $c \to \infty$). This case is realizing in reality from the considered above when the wire length l and the period dimension c are much lager the remaining dimensions a and b, or we have only one long sell in z-direction. In such case one may take into consideration the infinite l. Then there are the traveling current waves along the wires with the dependence $\exp(i\omega t - i\mathbf{kr})$ and some phase shifts, in which connection the current density for wire 1 in the zero number cell is

$$\mathbf{J} = \mathbf{z_0}I\delta(x)\delta(y)\exp(-ik_z z) \ . \tag{1}$$
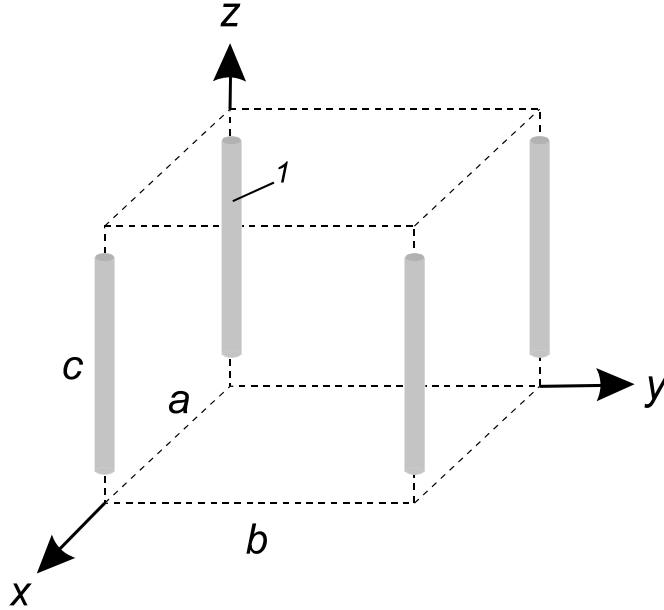
Fig.1. The MPC in the form of 3-D periodic cells with one linear wire inclusion per sell

Here $\mathbf{z_0}$ denotes the unit normal vector of z-axis. Further for MPC we will use the scalar GF of periodically located and phased sources (the periodic GF) [29,30]. The free waves (eigenwaves) of MPC creates on the metallic wires the phase shifted currents, which for one's turn support (excite) the wave. In accordance with based on the GF and IE approach it is sufficient to solve the IE in one (zero number) cell of periodicity using only the objects in this cell. In our case it is only the wire 1 (fig. 1). The current density (1) creates only one z-component of electric vector potential A_z, through which one can express the electric and magnetic fields. For electric field we have

$$\mathbf{E} = \frac{grad(div) + k_0^2\varepsilon}{i\omega\varepsilon_0\varepsilon}\mathbf{z_0}A_z \ . \tag{2}$$

Further we will need only the lectric field E_z component as only it is present in the boundary conditions owing to small r. After the integration of (1) with the GF we get the A_z, that according to (2) gives

$$E_z = I\frac{k_0^2\varepsilon - k_z^2}{i\omega\varepsilon_0\varepsilon ab}\sum_{m=-\infty}^{\infty}\sum_{n=-\infty}^{\infty}\frac{\exp(-ik_{xm}x - ik_{yn}y - ik_z z)}{k_{xm}^2 + k_{yn}^2 + k_z^2 - k_0^2\varepsilon} \ . \tag{3}$$

Here $k_{xm} = k_x + 2m\pi/a$ and $k_{yn} = k_y + 2n\pi/b$ correspond to spatial harmonics, the time exponent is omitted (there and everywhere). Let us note that instead of surface current density on the wire we have used the linear axes current owing to small r, so we transfer from surface IE to linear one. If the wire impedance is finite, and frequencies are high enough, it is necessary to use the volume distribution of current density of type (1). It, in

80

particular, concerns infra-red and optical ranges where the nanodimensional metallic wires should be modeled as plasma. To the dispersion equation (DE) from (3), it is enough to impose the boundary condition on any line on wire surface, for example, for $x = r$, $y = 0$. In general case we must write

$$E_z(x,y,z) = Z_S J_S(x,y,z) \ . \tag{4}$$

Here the points x, y belong to the surface, Z_S is the surface impedance, J_S is the surface current density. In our case it is necessary to consider the surface current density as uniform $J_S = I / (2\pi r) \exp(-ik_z z)$ and connected with a linear current I. It is possible to take the surface impedance in the Leontovich form or zero (in approach of ideally conducting wires). It is convenient to put $z = 0$ in the equation (4). Then the boundary condition (4) may be taken as averaged electric field on four symmetric points of the circle, or as the condition averaged on an azimuthal angle in the cylindrical system connected with a wire. In both cases we get the analytical DE in which one of the sums can be calculated obviously [29,30].

So, we have the DE of the type

$$F(k_0, \mathbf{k}) = 0 \ , \tag{5}$$

which (at the given k_z) defines the relation of wavenumber k_0 and transverse wavevector components k_x and k_y. Let us notice, that it really depends on a square of wave number. Setting the specified values of wave vectors, it is possible to construct a dispersive surface $k_0 = f(k_x, k_y)$ for everyone k_z [29,30]. Generally, the DE defines a three-dimensional hypersurface in four-dimensional space. It is multisheeted surface for ideally conducting wires which also consists of not connected each other sheets. Accordingly, there are the forbidden zones for k_0 (bandgaps). The periodicity is broken, and the specified surfaces incorporate in case of a photon crystal (PC) with losses [29].

To receive the electrophysical parameters we will take advantage of one of homogenization methods, described in [31-36] and based on calculation of the dipole and the higher multipole moments. As electrophysical parameters it is understood the permittivity and the permeability defined on the basis of strict electrodynamic model, depending from k_0 and $\mathbf{k}$.

It means the account of time and spatial dispersions. Further, we will define only the dipole contributions to polarization $\mathbf{P}$. It is known that the metallic inclusions can lead to presence of magnetic properties [5]. They appear if to consider the finiteness of r and the presence of azimuthal currents on the wire inclusions. In our case of thin wires always $\mu = 1$, and the EPT may be written as

$$\hat{\varepsilon}(k_0, \mathbf{k}) = \begin{bmatrix} \varepsilon & 0 & 0 \\ 0 & \varepsilon & 0 \\ 0 & 0 & \varepsilon_{zz} \end{bmatrix}. \tag{6}$$

The required component is connected with unique z-component of polarization vector

$$\varepsilon_{zz}(k_0, \mathbf{k}) = 1 + \frac{P_z}{\varepsilon_0 \langle E_z \rangle} \ , \tag{7}$$

where the Dirac bracket means the averaging on a cell of electric field z-component (3).

The Homogenization procedure assumes the averaging, i.e. the replacement quickly oscillated fields like (3) on their certain effective values. As ways of averaging can be much, the homogenization is ambiguous procedure. In particular, it is necessary for us to average some functions of type $\exp(-ik_{xm}x)$. As an averaging interval it is possible to take

$(0, a)$, and the complex values thus turn out. We will take these intervals symmetrically: $(-a/2, a/2)$. Then the average exponent value is

$$e_{xm}(k_x, a) = \langle \exp(-ik_{xm}x) \rangle = \frac{1}{a} \int_{-a/2}^{a/2} \exp\left(-i\left[k_x + \frac{2m\pi}{a}\right]x\right)dx = \frac{2}{a} \frac{(-1)^m \sin(k_x a/2)}{k_x + 2m\pi/a} \ . \tag{8}$$

Averaging on z we will fulfill so:

$$e_z(k_z, L) = \langle \exp(-ik_z z) \rangle = \frac{1}{2L} \int_{-L}^{L} \exp(-ik_z z)dz = \frac{\sin(k_z L)}{k_z L} \ .$$

This quantity as function of L decreases and oscillates with the period $2\pi/k_z$. Therefore, we will average it on the specified period:

$$e_z(k_z) = \langle e_z(k_z, L) \rangle = \frac{k_z}{2\pi} \int_{-\pi/k_z}^{\pi/k_z} \frac{\sin(k_z L)}{k_z L} dL = \frac{1}{\pi} si(\pi). \tag{9}$$

Let's notice that it does not depend from L. Taking divergence of (1), we will find the charge density

$$\rho = -k_z I \delta(x)\delta(y)\exp(-ik_z z)/\omega \ . \tag{10}$$

The delta-functions presence says that actually we have a linear charge and a linear current. The polarization vector has only one z-component

$$P_z(k_z, L) = \frac{Ik_z}{2\omega ab L} \int_{-L}^{L} z \exp(-ik_z z)dz = \frac{-iI}{\omega ab}\left\{-\cos(k_z L) + \frac{\sin(k_z L)}{k_z L}\right\} \ . \tag{11}$$

The terms in (11) as functions of L are even, the first term oscillates with the period $2\pi/k_z$, and the second one oscillates and also damps at the big lengths. Therefore, we will average the result on the oscillation period:

$$\langle P_z \rangle = \frac{k_z}{\pi} \int_{0}^{\pi/k_z} P_z(k_z, L)dL = \frac{-iI}{\pi\omega ab} si(\pi). \tag{12}$$

We have received the result, which is not dependent on k_z. At the conclusion of (12), however, the length L was assumed big, i.e. the $k_z = 2\pi/L$ is sufficiently small. So, we have

$$\langle E_z \rangle = I \frac{(k_0^2\varepsilon - k_z^2)e_z(k_z)}{i\omega\varepsilon_0\varepsilon ab} \sum_{m=-\infty}^{\infty} \sum_{n=-\infty}^{\infty} \frac{e_{xm}(k_x, a)e_{yn}(k_y, b)}{k_{xm}^2 + k_{yn}^2 + k_z^2 - k_0^2\varepsilon} \ . \tag{13}$$

Now the permittivity is defined by the formula (7) in which it is necessary to replace the polarization with its average value (12). Let us notice that we averaged the polarization and a field by the identical method. We will result the received form:

$$\varepsilon_{zz}(k_0, \mathbf{k}) = 1 + \frac{\varepsilon ab\left[\sin(k_x a/2)\sin(k_y b/2)\right]^{-1}}{4(k_0^2\varepsilon - k_z^2)\sum_{m,n=-\infty}^{\infty} \dfrac{(-1)^{m+n}}{(k_{xm}^2 + k_{xn}^2 + k_z^2 - k_0^2\varepsilon)k_{xm}k_{yn}}} \ . \tag{14}$$

It is necessary to notice that at averaging of a field we integrated on all cell volume. For ideally conduction wires the field inside them is absent, and their own volume can be excluded. Corresponding specifications, however, are insignificant, as the field satisfies the approached boundary condition (4), i.e. it is negligible small both on a surface, and inside a wire. The error thus turns out the second order on r/a. We will make one more important remark. The terms are entering into (14) are not independent. They are connected by means of DE (5). For example, setting k_0, we choose the dispersion surface. If the wave number gets to a bandgap, the permittivity is not defined, as there are no any real solutions of DE. It is possible to consider its big negative that corresponds to absence of propagation of a wave

(attenuation). Further we will specify, how it to define and in this case. Having set k_0, k_z and one of tangential component of wave vector, we find another from (5). Then their substitution in (15) defines EPT (6). It is different for different dispersion surfaces, and also depends at given $k_0 = \omega / c$, generally speaking, on two transversal wave vector components (if k_z is set). The DE (5) is periodical on k_x and k_y with the periods of a return lattice $2\pi / a$ and $2\pi / b$ accordingly. That also concerns to (14). This formula may be rewritten down in the form:

$$\varepsilon_{zz}(k_0, \mathbf{k}) = 1 - \frac{k_p^2(\omega, k_x, k_y, k_z)\varepsilon}{k_0^2 \varepsilon - k_z^2} \quad . \tag{15}$$

The expressions like (15) have been received in a number of works from various qualitative and modelling reasons [1-3,5,11,12,14,18,20-22,28], including its kind was considered at $k_z = 0$ [11,12]. In this case the PC behaves as plasma with cutoff on plasma frequency $\omega_p = ck_p(\omega_p, k_x, k_y, k_z)$. This frequency usually is displaced into high-frequency region with growth of k_z^2: $\omega = c\sqrt{k_p^2(\omega, k_x, k_y, k_z) + k_z^2 / \varepsilon}$ [29]. Let us analyze the relation (14). The series converges rather quickly, and its sum (at small $k_0, |\mathbf{k}|$) is defined basically by a zero term. At $k_x \to 0$, $k_y \to 0$ we have $\varepsilon_{zz}(k_0, \mathbf{k}) \to 0$ that corresponds to low-frequency cutoff. And the cutoff frequency increases when k_z is increasing. The same concerns to the case $k_x = 2\pi / a$, $k_y = 2\pi / b$, and to similar points owing to periodicity of (14) on transverse wave vectors components. At small k_x, k_y, as it is easy to see $0 < \varepsilon_{zz}(k_0, \mathbf{k}) < 1$. For MPC configuration $a = b = c$, $r / a = 0.001$, $\varepsilon = 1$ we have the estimation $k_p a = 1.43$. On lower frequencies according to model (15) the ε_{zz} is negative and can aspire to enough big negative values at $k_0 \to 0$ (it is supposed that $k_z = 0$). If $k_0 \sqrt{\varepsilon} = k_z$ and $k_x^2 + k_y^2 > 0$ that the expression (14) aspires to infinity. It corresponds to that the free wave cannot propagate along the wires. The flat wave excites by a incident source passes through finite such MPC structure almost without reflections as its electric field is perpendicular to the wires and does not induce at them any currents. However, free eigenwaves in infinite structure should induce such currents, which support them. It cannot be carried out in this case. The value k_z is real in the absence of losses and defines a wave of a current (1). If $k_0 \sqrt{\varepsilon} > k_z$, this wave fast, and at $k_0 \sqrt{\varepsilon} < k_z$ it is slow. If $k_x^2 + k_y^2 > 0$, that the current wave can be only fast, i.e. $k_z < k_0 \sqrt{\varepsilon}$. The definition of effective permeability at $k_0 < k_p$ or in the next bandgap also can be received by the specified method. It is necessary for this purpose to search the imaginary roots k_x and k_y, or, setting their values imaginary, to define k_0, and further to spend the considered averagings at the calculation of dipole moment.

2. Uniaxial, biaxial и triaxial MPC with non-connected wires

From stated above it is clear that the wire orientations defines its contribution into the electric dipole moment in a corresponding direction. Further, we will consider non-connected wires of finite length. Connected (contacting) wire PC demand the account of a continuity of a current (under the Kirchhoff's law) that complicates the consideration [18] and makes a subject of separate research. We will consider the elementary structure fig. 1. Now the current density we will write down as

$$\mathbf{J} = \mathbf{z_0}\delta(x)\delta(y)\sum_{s=1}^{N_s} I_s \cos(k_s z). \qquad (16)$$

Here $k_s = (2s-1)\pi/l$, and the coordinate system zero in comparison with fig. 1 is shifted in the wire centre so on its ends the current is zero. Using the approach stated above, we will find

$$E_z = \frac{2}{i\omega\varepsilon_0\varepsilon ab}\sum_{s=1}^{N_s}(-1)^s k_s I_s \sum_{m,n,k=-\infty}^{\infty}\cos\left(\frac{k_{zk}l}{2}\right)\frac{\left(k_0^2\varepsilon - k_{zk}^2\right)\exp\left(-i[k_{xm}x + k_{yn}y + k_{zk}z]\right)}{\left(k_{zk}^2 - k_s^2\right)\left[k_{xm}^2 + k_{yn}^2 + k_{zk}^2 - k_0^2\varepsilon\right]}. \qquad (17)$$

The component (17) should turn in zero on the wire surface. Applying the Galerkin method, we have

$$\int_{-l}^{l} E_z(x,y,z)\cos(k_{s'}z)dz = 0. \qquad (18)$$

In the relation (18) the point (x,y) belongs to the circle: $x^2 + y^2 = r^2$. It is possible to take any point of this circle. Then the relations (17) and (18) lead to system of the linear algebraic equations (SlAE) which determinant Δ should be equal to zero. Actually $F(k_0,\mathbf{k}) = \Delta = 0$ is the required DE. It poorly varies at movement of the chosen point on a circle. It is convenient to impose boundary conditions in four symmetric points $x = \pm r, y = 0$ and $x = 0, y = \pm r$. Thus instead of exponent in (17) we receive $\alpha_{mn}(k_x,k_x) = \cos([k_{xm} + k_{yn}]r/2)\cos([k_{xm} - k_{yn}]r/2)$, and the component (17) depends only on coordinate z and has decomposition

$$E_z(z) = \sum_{s=1}^{N_s} I_s \widetilde{E}_{zs}(z). $$

Now the matrix elements according to (18) can be written down so:

$$E_{ss'} = \int_{-l/2}^{l/2}\widetilde{E}_{zs}(z)\cos(k_s z)dz = \frac{4k_s k_{s'}}{i\omega\varepsilon_0\varepsilon ab}(-1)^{s+s'}\sum_{m,n,k=-\infty}^{\infty}\cos^2\left(\frac{k_{zk}l}{2}\right)\frac{\left(k_0^2\varepsilon - k_{zk}^2\right)\alpha_{mn}(k_x,k_y)}{\left(k_{zk}^2 - k_s^2\right)\left[k_{xm}^2 + k_{yn}^2 + k_{zk}^2 - k_0^2\varepsilon\right]}. $$

We, however, will average on all points of a circle, having written down $x = r\cos(\varphi)$, $y = r\sin(\varphi)$, and having integrated on the angle. Thus the Bessel functions appear owing to the formula [30]

$$\frac{1}{2\pi}\int_0^{2\pi}\exp(\pm ir(k_{xm}\cos(\varphi) + k_{ym}\sin(\varphi)))d\varphi = J_0\left(r\sqrt{k_{xm}^2 + k_{yn}^2}\right).$$

It corresponds to change the entered before term so: $\alpha_{mn}(k_x,k_y) = J_0\left(r\sqrt{k_{xm}^2 + k_{yn}^2}\right)$. As the series converge enough quickly, the difference of both terms at small r and for low numbers of indexes is insignificant. However, such averaging leads to improvement of series convergence. It is seen that the singularity at $k_{zk} = \pm k_s$ is removable. However when the square bracket in the denominator of (17) makes vanish, the matrix elements have poles. Often the specified poles are near to DE roots that complicates a finding of the last. The elimination of poles is possible by the addition of a small imaginary part to wave number: $k_0 \to k_0 - i\delta$. However, such addition leads to false roots. We will notice that the specified way at $\delta \to +0$ in case of free space GF allocates its demanded kind, satisfying to the radiation condition [37]. In case of PC it is not necessary to impose a radiation condition: in the exponent of periodic GF it is possible to take both signs: $\exp(\pm i\mathbf{k}_{mnk}(\mathbf{r} - \mathbf{r}'))$ as there is no allocated direction of radiation. Eigen direct (forward) and return (backward) waves (without a source) are indiscernible [29]. The specified poles correspond to conditions $k_0^2\varepsilon = k_{xm}^2 + k_{yn}^2 + k_{zk}^2$ which divide the dispersion branches. In

particular, at $m = n = k = 0$ we have $\sqrt{k_x^2 + k_y^2 + k_z^2} = \pm k_0 \sqrt{\varepsilon}$. For a wave with $k_y = k_z = 0$ the straight lines separate the branches of slow and fast waves of the first zone. We will notice that for the series with $\alpha_{mn}(k_x, k_y)$ in form of cosines it is possible to sum up asymptotically on two indexes at their big values. However, such summation is rather intricate and leads to inconvenient relations. The initial relations are convenient for code parallelization, as it has been made in the calculations.

The dipole moment of unit volume is

$$P_z = \frac{i}{abc\omega} \int_{-a/2}^{a/2} \int_{-b/2}^{b/2} \int_{-c/2}^{c/2} z \frac{dJ_z}{dz} dx\, dy\, dz \ . \tag{19}$$

Calculating it, we will receive

$$P_z = \frac{-2i}{abc\omega} \sum_{s=1}^{N} I_s \left\{ -l\cos(k_s l) + \sin(k_s l)/k_s \right\} .$$

The averaging is not required for this, as there is one wire per a cell. Averaging a component of electric field (17), one can find

$$\langle E_z \rangle = \frac{2}{i\omega\varepsilon_0 \varepsilon ab} \sum_{s=1}^{N_s} (-1)^s k_s I_s \sum_{m,n,k=-\infty}^{\infty} \cos\left(\frac{k_{zk}l}{2}\right) \frac{\left(k_0^2 \varepsilon - k_{zk}^2\right) e_{xm}(k_x, a) e_{yn}(k_y, b) e_{zk}(k_z, c)}{\left(k_{zk}^2 - k_s^2\right)\left[k_{xm}^2 + k_{yn}^2 + k_{zk}^2 - k_0^2 \varepsilon\right]} \ . \tag{20}$$

Accordingly, zz-component of tensor (6) is defined under the formula (7). Thus, at first it follows, having the set k_x, k_y. k_z, to define the k_0 from the DE. There may be several values at finite number of basic functions in (16). It is necessary to choose that is need, for example, the lowest from them. Further we set the amplitude $I_1 = 1$ (a wave is defined accurate within any amplitude), and then we will express through it the remained amplitudes of harmonics of a current as the solutions of SLAE which order is smaller on unit. Then all defined terms we substitute into (20), and then we define the permittivity.

The triaxial MPC has three wires per on a cell of periodicity in the form of a parallelepiped with the edges a, b, c . The wires lengths are l_1, l_2, l_3, Such MPC is characterized by the diagonal tensor of effective permittivity:

$$\hat{\varepsilon}(k_0, \mathbf{k}) = \begin{bmatrix} \varepsilon_{xx} & 0 & 0 \\ 0 & \varepsilon_{xx} & 0 \\ 0 & 0 & \varepsilon_{zz} \end{bmatrix} . \tag{21}$$

Basically, the wires can be located asymmetrically. Besides, such wires are possible on the edges (sides) of a cell and inside it, thus their orientation may be any. It leads to nondiagonal tensor like (21) as arbitrary oriented wire gives the contribution to all dipole moment components. However owing to the Onsager-Cazimir theorem under the absence of dissipation and because of self-conjugacy it is had $\varepsilon_{mn}(k_0, \mathbf{k}) = \varepsilon_{nm}^*(k_0, \mathbf{k})$. It is symmetric with all real tensor components if losses in dielectric background and in wires are absent. However for loss structures the tensors like (2) are already non-Hermitian, and the Onsager-Cazimir condition should be altered so: $\varepsilon_{mn}(k_0, \mathbf{k}) = \varepsilon_{nm}'(k_0, \mathbf{k}) - i\varepsilon_{nm}''(k_0, \mathbf{k})$. The presence of N_0 wires per a cell leads to the system of coupled one-dimensional IEs and to DE in the form of equality to zero of a determinant of SLAE, corresponding to discretization of the equations. The determinant order under the account of several current harmonics on each wire at $N_s > 3$ is already enough essential factor, which is worsening the search of its complex roots in three-dimensional complex area $\mathbf{k}$ that becomes rather not trivial problem. The dispersion is defined then by a hypersurface in six-dimensional area. The loss are very essential for microstructured and nanostructured MPCs in terahertz, infra-red and optical bands. Such MPCs have no sharply expressed bandgaps, therefore the

tensor $\hat{\varepsilon}(k_0, \mathbf{k})$ is possible to define in all necessary area of frequencies and wave vectors. The corresponding components of EPT are zero on the borders of bandgaps for lossless systems. In the bandgap the vector $\mathbf{k}$ is purely imaginary (for 3-D structures), or has imaginary some from its component (for 1-D and 2-D structures) [29]. Accordingly, the wave in the specified directions fades. Such attenuation has the reactive (nondissipative) character, thus the periodicity is not violated. Once again, we will notice that in periodic and dissipative photonic crystals (PC) the periodicity in electrodynamic sense is broken: the wave propagates with attenuation. This is basic PC difference from usual solid-state crystals for which the local probability density is conserved, as the global probability, i.e. the number of particles, are also under the conservation. As consequence of it we have the periodicity (to within phase factor) of Bloch waves of probability density and the self-adjoint problem. The violation of periodicity here is possible only by dislocations and finiteness of structure, thus a problem again self-interfaced. There is the radiation in finite PCs, therefore eigenfrequencies of resonators based on such PC are complex (like the frequencies of open dielectric resonators).
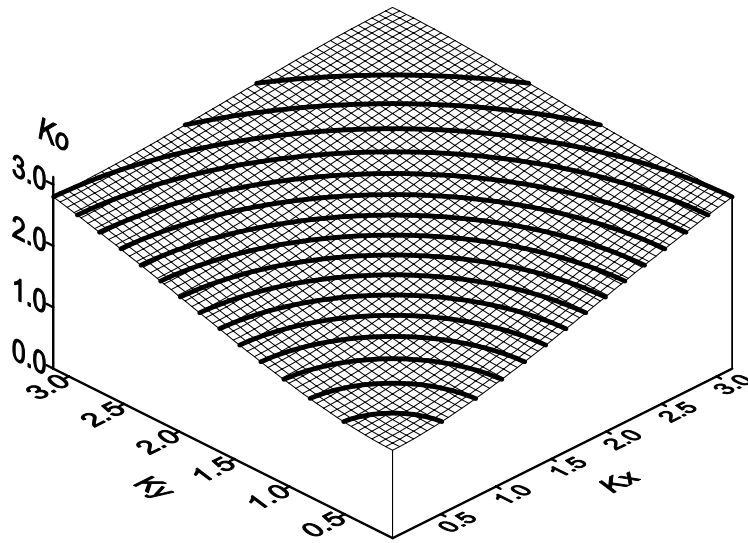
Fig. 2. Dispersion approximation of 2-D-P WPC according to the simulation results for DE
($a = b = 1$, $k_z = 0$, $r/a = 0.001$, $\varepsilon = 1$)

3. Numerical results

Further everywhere the following configuration is considered $a = b = c$, $\varepsilon = 1$. The dispersion for MPC in the form of infinitely long and parallel located 2-D periodic wires has been received in the works [29,30]. On the basis of DE solutions the approximations of two-dimensional surfaces $k_0 = f(k_x, k_y)$ are executed at the value $k_z = 0$. For the case $a = b = 1$, $r/a = 0.001$, $\varepsilon = 1$, and for site of the first sheet of the dispersive surface with forward wave such approximation is presented in the fig. 2. In the fig. 3 the calculations under the formula (14) are resulted for the same case when the k_0 is defined by the surface of fig. 2. It is visible that, in the field of small wave vectors, the component ε_{zz} is essentially less than the unit, and the wave is fast. It is confirmed also by the dispersive characteristic as for small values $|\mathbf{k}|$ the wave number always has finite value which greater than k_p.
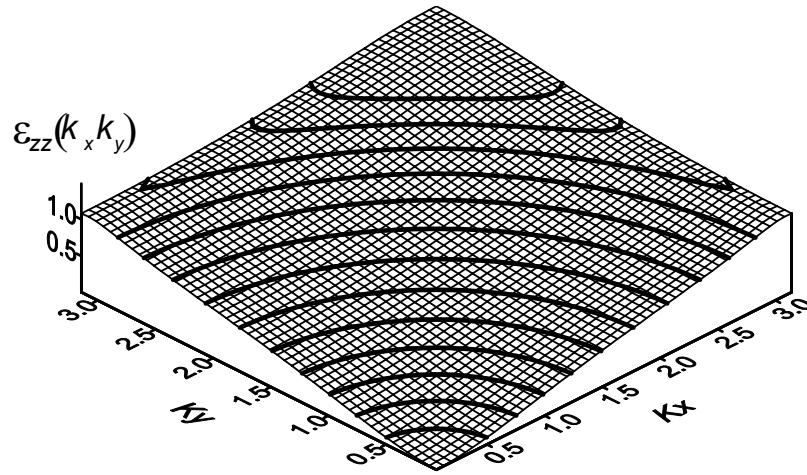
Fig. 3. The component ε_{zz} versus wave vector components in the main sector of first propagation band at $k_z = 0$ (the results correspond to fig. 2)
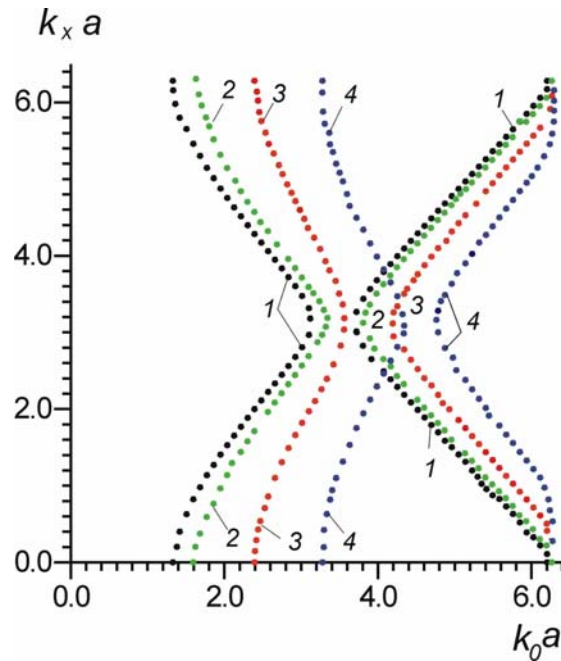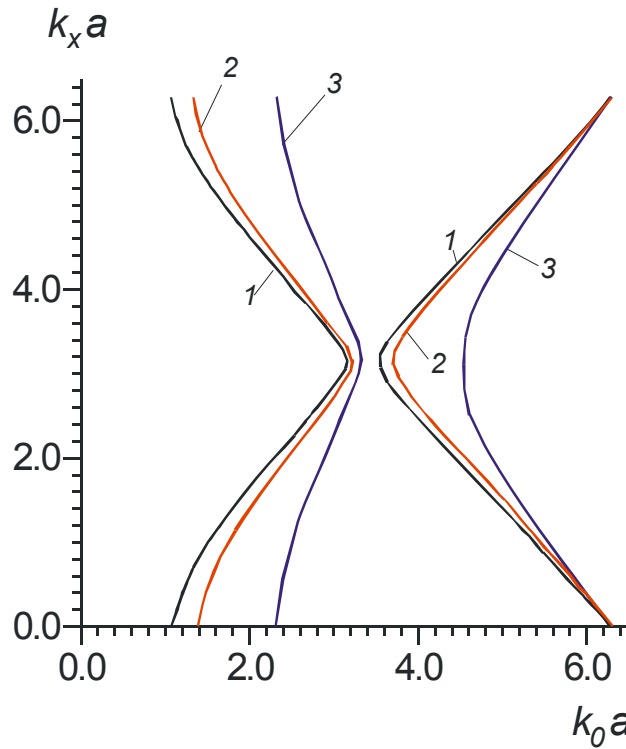

Fig. 4. The dependence of normalized wave vector component from normalized frequency for 2-D-P MPC with the lattice $a = b$ for $r/a = 0.005$, $k_y = 0$ and different $k_z a$ values: 0 (curve 1); 1 (2); 2 (3); 3 (4)

With increase of $|\mathbf{k}|$ the wave becomes slow with small retardation $n = \sqrt{\varepsilon_{zz}} \sim 1.2$ that corresponds to the permittivity component a little more than unit. Naturally, owing to periodicity in the space of wave vectors the same periodicity takes place for EPT. In the bottom forbidden zone $k_0 < k_p$ the components k_x and k_x are imaginary, therefore the sign before the sum in the formula (14) changes and the component ε_{zz} becomes negative. The same is for the next top forbidden zone (bandgap) which in our case is $2.93 < k_0 a < 3.4$. Accordingly, for each of k_0 values in these areas it is possible to construct the surfaces ε_{zz} as functions of imaginary components of wave vector, using the relation (14). Thus the minimum (maximum on the module) value in the lowest bandgap in the considered case has been obtained as $\varepsilon_{zz} = -1.045$.

Fig. 5. The dependence of normalized wave vector component from normalized frequency for 2-D-P MPC with the lattice $a = b$ for $k_y = k_z = 0$ various r/a values: 0.001 (line 1); 0.005 (2); 0.05 (3)

In the fig. 4 the dependences of influence on dispersion data from k_z value are resulted. The dependence of dispersion on a thickness of wires is given in the fig. 5. The dispersion results (band structure) of MPC with finite length are resulted in fig. 6 for two r values. This problem already demands the big computing resources, especially if $l \sim c$ (for what the account of a great number of harmonics in (16)is necessary), and can lead to a determinant of a high order. In the presented results with $l/a = 0.6$ it is enough to consider 1-3 harmonics, and the difference on accuracy for 1 and 3 harmonics makes less than 1 %, and the computing times differ in 6 times. Strong truncation of three-dimensional series brings errors, which can lead to the admission of roots or to their essential change. Numerical research has shown that these effects vanish at $N = M = K > 20$ (N, M, K - the numbers of terms with positive indexes in the sums). All calculations have been executed at $N = M = K = 30$, i.e. the $61^3 = 226981$ flat waves have been taken into consideration. The calculation with $N = M = K = 10$ increases speed more than in 200 times, thus accuracy of roots definition worsens on 2-3 %. Let us notice that the series truncation brings effect of radiating losses, as the finite PC structure with eigenmodes is radiating one. The presence of the poles, sometimes very close approaching to roots, complicates search of the last. The procedure of smoothing of poles (by introduction of infinitesimal losses) and of false roots avoidance has been developed.

For the first dispersive branch fig. 6 also has been calculated the component ε_{zz} (fig. 7). It changes from 1 at $k_x = k_y = 0$ (the wave propagates with a velocity of light) to values 1.2 (fig. 6,) and 1.3 (fig. 6,) at $k_x a = k_y a = \pi$ of cutoff frequency. In the first bandgap it is negative. The Fig. 7 shows its dependence from k_0 at $k_y = 0$. It is necessary to have in view of that in this case k_0 and k_x are unequivocally connected by a dispersive curve up to the beginning bandgap point $k_x a = \pi$. As it is shown in the works [28,30], the introduction of losses (even infinitesimal) deforms dispersive branches as follows. The

direct (forward) and return (backward) branches in the lowest propagation band are disconnected, the bandgap vanish, and in them the forward lines of lowest frequency branch close up with the forward higher branches and accordingly the backward higher branches close up with the backward lowest ones. There is a small attenuation in the propagation bands, and in the former bangaps there is the wave propagation with small phase velocity, large group velocity and strong attenuation. Under the infinitesimal attenuation, the group velocity in the bandgaps becomes infinite. It is connected by that zero interval of wave vectors corresponds to finite band interval Δk_0 (in our case $k_x a = \pi$, $\Delta k_x = 0$, and Δk_0 is finite). Therefore the transition from one branch to another goes on a vertical line $k_x a = \pi$ (see fig. 6), thus k_0 changes within the bandgap strip. Accordingly, the normalized group velocity is the tangent of tangential line angle to this line, i.e. $v_g = c \cdot \tan(\pi/2)$. Actually at such movement along one of dispersion curves fig. 6 the dependences 1 and 2 in the fig. 7 are constructed, thus for the first one the component k_x is imaginary (see fig. 6), and the ε_{zz} is negative (for the second curve accordingly in the region $2.66 < k_0 a < 3.16$).

The transition to the following branch in propagation band ($k_0 a = 3.21$) becomes ambiguous. The presence of losses removes this ambiguity: movement always goes along the direct of return branch either a forward wave, or backward. It and the attenuation connected with it break periodicity of fields, which cause the described effect.
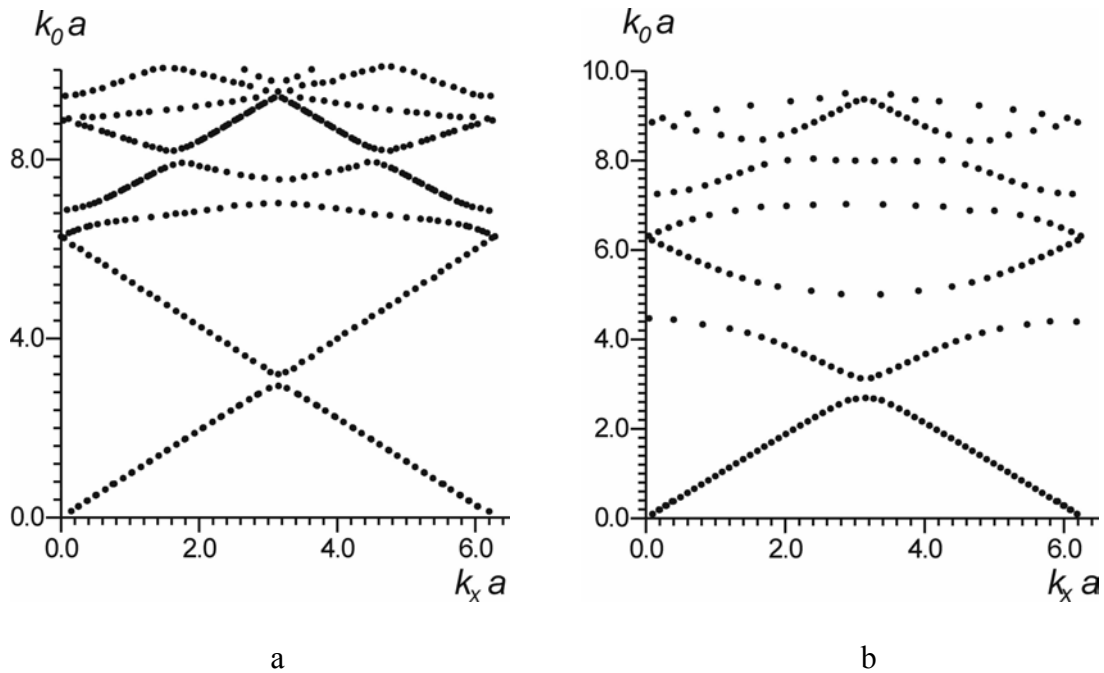

a   b

Fig. 6. Band structure of 3-D-P wire MPC at $k_z = k_y = 0$, $l/a = 0.6$ for $r/a = 0.01$ (a) и $r/a = 0.06$ (b)
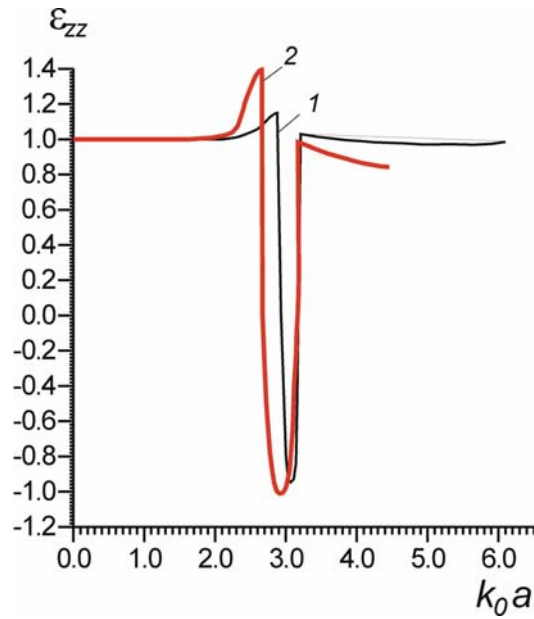
Fig. 7. The component ε_{zz} versus normalized frequency for lowest dispersion branches of fig. 6: a – line 1, b – line 2

Conclusions

The electrophysical parameters of the elementary wire MPC in the form of linear wires of infinite and finite lengths have been obtained by the method of the integral equations formulated on the basis of GF of periodically located sources. The case of thin ideally conducting and not contacting wires is considered. One of the homogenization methods, using the calculation of averaged on a cell multipole moments and the averaging of fields is applied. It is shown, that except of homogenization ambiguities the construction of effective permittivities in the absence of losses is also ambiguously in connection with necessity of a choice of a corresponding dispersion branch. This ambiguity disappears under the wave diffraction on the finite (i.e. quasiperiodic) structures when at a falling wave have the set k_0 and $\mathbf{k}$. The results of plasma frequency estimation in the formula (15) are in good conformity with earlier published models. This also corresponds to the wave retardation, which is defined from the dispersive curves (surfaces). The case $l \approx c$ demands taking into account of a great number of current harmonics in the (16) that simulates the capacities of corresponding gaps between wires. Such MPC at high frequencies with finite wires length l is similar to PC with the infinite ones. Accordingly, the dispersive curve is bent in high-frequency range, however the low-frequency cutoff is absent. It is not real to use the resulted algorithm for a limiting case of wires with infinitesimal gaps (i.e. for transition to the first of the considered problems). It is easily to take big c and l values. The method can be extended to any wire configurations of MPC structures, including ring, spiral, helix, Ω elements etc., and also on dielectric and magnetic PC. Owing to symmetry to the centre of wires we took the ymmetric distribution of a current (16) in the form of decomposition on cosine. Thus, the plane $z = 0$ is the electric wall (as well as the planes periodically displaced on c). It is possible to use the decomposition also on sine that will give the magnetic walls. The currents should be decomposed in the absence of the symmetry in a general Fourier series taking into account the boundary conditions on the wires ends. The account of losses will lead effective complex permittivities and permeabilities. However, it does not mean the conductivity presence: specified dissipation

is connected with a phase shifts between the polarization (electric and magnetic) currents and the fields. The conductivity should exist in physical structures of MPC with nanowires, and its mechanism is connected with quantum effects, and may have the jump character.

REFERENCES

14. Pendry J.B., Holden A. J., Stewart W. J. Youngs I. Extremely low frequency plasmons in metallic meso structures // Phys. Rev. Lett. 1996. Vol. 76. P. 4773–4776.
15. Sievenpiper D.F., Sickmiller M.E. Yablonovitch E. 3D wire mesh photonic crystals // Phys. Rev. Lett. 1996, Vol. 76. P. 2480–2483.
16. Pendry J.B., Holden A.J., Robbins D.J., Stewart W.J. Low frequency plasmons in thin wire structures // J. Phys. Condens. Matter. 1998. Vol. 10, pp. 4785–4809.
17. Sievenpiper D.F., Yablonovitch E., Winn J.N., Fan S., Villeneuve P.R., Joannopoulos J.D. 3D metallo-dielectric photonic crystals with strong capacitive coupling between metallic islands // Phys. Rev. Lett. 1998. Vol. 80. P. 2829–2832.
18. Pendry J.B., Holden A.J., Robbins D.J., Stewart W.J. Magnetism from conductors and enhanced nonlinear phenomena // IEEE Trans. 1999. V. MTT- 47. No. 11. P. 2075–2084.
19. Smith D.R., Padilla W.J., Vier D.C., Nemat-Nasser S.C., Schultz S. Composite medium with simultaneously negative permeability and permittivity // Phys. Rev. Lett. 2000. Vol. 84. P. 4184.
20. Smith D.R., Knoll N. Negative refractive index in left-handed materials // Phys. Rev. Lett. 2000. Vol. 85. P. 2933–2936.
21. Shelby R., Smith D., Schultz S. Experimental verification of a negative index of refraction. Science. 2001. Vol. 292. P. 77–79.
22. Pokrovsky A.L., Efros A.L. Lens based on metallic photonic crystals and the problem of left-handed materials // Phys. Rev. Lett. 2002. Vol. 89. P. 093901(1–4).
23. Luo C., Johnson S.G., Joannopoulos J.D., Pendry J.B. All-angle negative refraction without negative effective index // Phys. Rev. B. 2002. Vol. 65. P. 201104(1–4).
24. Maslovski S.I., Tretyakov S.A., Belov P.A. Wire media with negative effective permittivity: a quasistatic model // Microwave Opt. Technol. Lett. 2002. Vol. 35. 47–51.
25. Belov P.A., Marque R., Maslovski S.I., Nefedov I.S., Silveirinha M., Simovski R., Tretyakov S.A. Strong spatial dispersion in wire media in the very large wavelength limit // Phys. Rev. B 67. 2003. P. 113103(1–4).
26. Luo C., Johnson S.G., Joannopoulos J.D., Pendry J.B. Subwavelength imaging in photonic crystals // Phys. Rev. B. 2003. Vol. 68. P. 045115(1–15).
27. Pokrovsky A.L. Analytical and numerical studies of wire-mesh metallic photonic crystals // Phys. Rev. B. 2004. Vol. 69. P. 195108(1–7).
28. Simovski C.R., Belov P.A. Low-frequency spatial dispersion in wire media, Phys. Rev. E. 2004. Vol. 70. P. 046616.
29. Smith D.R., Pendry J.B., Wiltshire M.C.K. Metamaterials and negative refractive index // Science. 2004. Vol. 305. P. 788–782.
30. Shen J.T., Catrysse P.B., Fan S. Mechanism for designing metallic metamaterials with a high index of refraction. Phys. Rev. Lett. 2005. Vol. 94, P. 197401.
31. Silveirinha M.G., Fernandes C.A. Homogenization of 3D- connected and non-connected wire metamaterials // IEEE Trans. 2005. Vol. MTT-53. P. 1418–1430.
32. Belov P.A., Simovski C.R., Ikonen P. Canalization of subwavelength images in layers by electromagnetic crystals // Phys. Rev. B. 2005. Vol. 71. P. 193105(1–4).
33. Nefedov I.S., Viitanen A.J., Tretyakov S.A. Electromagnetic wave refraction at an interface of a double wire medium // Phys. Rev. B. 2005. Vol. 72. P. 245113.

34. Nefedov I.S., Viitanen A.J., Tretyakov S.A. Electromagnetic wave reflection from an interface with a 2D wire medium // Proc. of Joint 9th Intern. Conf. on Electromagnetics in Advanced Applications and 11th European Electromagnetic Structures Conference. 2005. Torino, Italy. P. 571–574.

35. Nefedov I.S., Simovski C.R., Belov P.A., Viitanen A.J. Tretyakov S.A. Negative refraction at the interface of double wire media // EPFL Latsis Symposium 2005. Programme & abstracts. Lausanne. 2005. P. 117.

36. Belov P.A., Simovski C.R., Nefedov I.S., Tretyakov S.A., Low-frequency superprism effect and hybridization of transmission-line modes in two- and three-dimensional wire media // PIERS 2005. Progress In Electromagnetic Research Symposium, Proceedings. 2005. Hangzhou, China. P. 285–289.

37. Nefedov I.S., Viitanen A.J., Tretyakov S.A. Propagating a dimensional wire media // Phys. Rev. E. 2005. Vol. 71. P. 046612(1–10).

38. Belov P.A., Hao Y., Sudhakaran S. Subwavelength microwave imaging using an array of parallel conducting wires as a lens // Phys. Rev. B-73. 2006. P. 033108(1–4).

39. Zhao Y., Belov P.A., Hao Y. Modelling of wave propagation in wire media using spatially dispersive finite-difference time-domain method: numerical aspects // IEEE Trans. 2007. Vol. AP-55. No. 6. P. 1506–1513.

40. Silveirinha M.G., Fernandes C. A., Costa J.R. Superlens made of a metamaterial with extreme effective parameters, Phys. Rev. B. 2008. Vol. 78. P. 195121.

41. Silveirinha M.G., Fernandes C.A., Costa J.R. An array of crossed metallic wires as a metamaterial with extreme index of refraction // 3rd International Congress on Advanced Electromagnetic Materials in Microwaves and Optics (Metamorphose-VI). 2009. P. 175–177.

42. Davidovich M.V. Photonic crystals: Green's functions, integro-differential equations, and simulation results // Radiophysics and Quantum Electronics, 2006. Vol. 49, No. 2. P. 134-146.

43. Davidovich M.V. Photonic crystals: Green's functions, integro-differential equations, and results. Saratov, Saratov University Press, 2005. 40 pp.

44. Davidovich M.V., J.V. Stephuk. Homogenization of periodic artificial media // Modeling in Applied Electromagnetics and Electronics. Saratov University Press. 2007. Issue 8. P. 67–75.

45. Davidovich M.V., J.V. Stephuk. Homogenization of periodic metamaterials // Mathematical Methods in Electromagnetic Theory. Proceedings of 12-th International Conference (MMET'2008). Odessa, Ukraine. 2008. P. 527–529.

46. Davidovich M.V., Stephuk J.V. Homogenization of periodic wire and dielectric metamaterials // 2008 International Workshop on Metamaterials, Meta08. Nov. 9-12, Nanjing, China. 2008. P. 251–254.

47. Davidovich M.V. Homogenization of periodic artificial media // Problems of Optical Physics. Proceedings of 11-th International Youth Scientific Shool on Optics, Laser Physics and Biophotonics. Saratov, Novyi Veter, 2008. P. 99–106. (In Russian).

48. Davidovich M.V., Savin A.N., Stephuk J.V. Homogenization of periodic metamaterials in form of wire inclusions // Radiation and Sacttering of Electromagnetic Waves. Proceedig of International Conference, Taganrog, TRTU. 2009. P. 370–375. (In Russian).

49. Davidovich M.V. Homogenization of periodic metamaterials // Abstracts of XIII-th Winter Scool on Microwave electronics and Radio Physuics. Saratov, GosUSC-College, 2006. P.80. (In Russian).

50. Markov G.T., Chaplin A.F. Excitation of electromagnetic waves. Moscow, Radio i Svyaz, 1983. 296 p. (In Russian).

CONTENTS

Научное издание

МОДЕЛИРОВАНИЕ В ПРИКЛАДНОЙ ЭЛЕКТРОДИНАМИКЕ И ЭЛЕКТРОНИКЕ

Сборник научных трудов

Выпуск 10

Ответственный за выпуск *М.В. Давидович*

Технический редактор *Л.В.Агальцова*

Оригинал-макет подготовлен *М.В. Давидовичем*

_____